MARS
The International Journal of Mars Science and Exploration

MARS INFORMATICS
Open Access Journals

Science

Geologic mapping and characterization of Gale Crater and implications for its potential as a Mars Science Laboratory landing site

Ryan B. Anderson and James F. Bell III

Department of Astronomy, Cornell University, Ithaca, NY 14853, USA, randerson@astro.cornell.edu

Citation: Mars 5, 76-128, 2010; doi:10.1555/mars.2010.0004
History: Submitted: November 15, 2009; Reviewed: April 30, 2010 Revised: June 1, 2010; Accepted: July 13, 2010; Published: September 14, 2010
Editor: Jeffrey B. Plescia, Applied Physics Laboratory, Johns Hopkins University
Reviewers: Nathan T. Bridges, Applied Physics Laboratory, Johns Hopkins University; Simome Silvestro, International Research School of Planetary Sciences

Abstract

Background: Gale Crater is located at 5.3°S, 222.3°W (137.7°E) and has a diameter of ~155 km. It has been a target of particular interest due to the > 5 km tall mound of layered material that occupies the center of the crater. Gale Crater is currently one of four finalist landing sites for the Mars Science Laboratory rover.

Method: We used visible (CTX, HiRISE, MOC), infrared (THEMIS, CRISM, OMEGA) and topographic (MOLA, HRSC, CTX) datasets and data products to conduct a study of Gale Crater, with a particular focus on the region near the proposed Mars Science Laboratory (MSL) landing site and traverse.

Conclusion: The rim of Gale Crater is dissected by fluvial channels, all of which flow into the crater with no obvious outlet. Sinuous ridges are common on the crater floor, including within the proposed MSL ellipse, and are interpreted to be inverted channels. Erosion-resistant polygonal ridges on the mound are common and are interpreted as fractures that have been altered or cemented by fluid. We identified key geomorphic units on the northwestern crater floor and mound, and present a simplified stratigraphy of these units, discussing their properties and potential origins. Some layers in the mound are traceable for >10 km, suggesting that a spring mound origin is unlikely. We were unable to rule out a lacustrine or aeolian origin for the lower mound using presently-available data. Pyroclastic processes likely have contributed to the layers of the Gale mound, but were probably not the dominant depositional processes. The upper part of the mound exhibits a pattern that could be cross-bedding, which would suggest an aeolian dune-field origin for that unit. Aeolian transport appears to be the most plausible mechanism for removal of material from the crater without breaching the rim; however, fluvial, mass-wasting, or periglacial processes could have contributed to the breakdown of material into fine grains susceptible to aeolian transport. We have identified two potential traverses for MSL that provide access to the diverse features on the crater floor and the mound. We discuss the suitability of Gale Crater as a landing site for MSL in terms of diversity, context, habitability and biomarker preservation and conclude that Gale Crater would be a scientifically rewarding and publicly engaging landing site.

Introduction and previous work

Gale Crater is located at 5.3°S, 222.3°W (137.7°E) and has a diameter of ~155 km. It is situated in the northeastern portion of the Aeolis quadrangle on the boundary between the southern cratered highlands and the lowlands of Elysium Planitia (Figure 1), and the crater has been estimated to be Noachian in age (~3.5–3.8 Ga) (Greeley and Guest 1987; Cabrol et al. 1999; Bridges 2001). Gale has been a target of particular interest due to the mound of material that occupies the center of the crater, standing ~6 km higher than the lowest point on the floor. The age of the mound has been loosely constrained to the late Noachian/early Hesperian (Milliken et al.

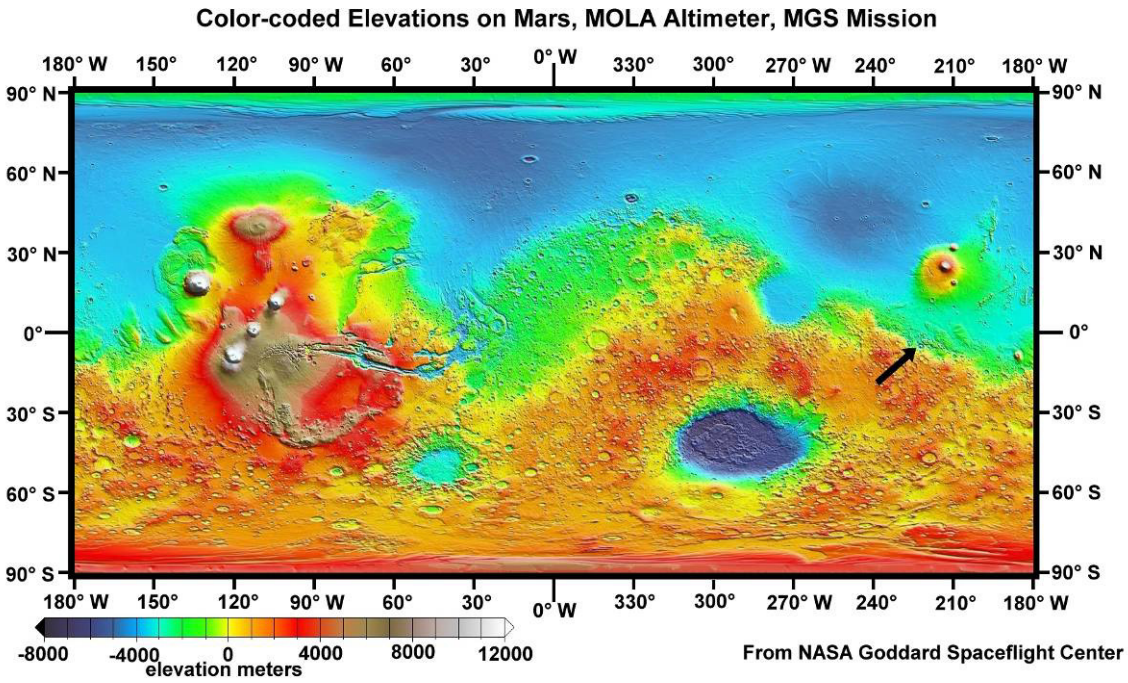

Figure 1. Global topographic map of Mars, based on MOLA data (Smith et al. 1999). The black arrow marks the location of Gale crater. (figure1.jpg)

2010). Gale Crater was considered as a potential landing site for the Mars Exploration Rovers (MER; Golombek et al. 2003) and is currently one of four finalist landing sites for the Mars Science Laboratory (MSL) rover (Golombek et al. 2009).

Early maps based on Viking data list a wide range of potential origins for the material in Gale Crater. Scott et al. (1978) interpreted the material as lava flows and aeolian deposits, Greeley and Guest (1987) suggested volcanic, aeolian or fluvial sedimentation, and Scott and Chapman (1995) invoked aeolian, pyroclastic, lava flow, fluvial and mass-wasted deposition. Cabrol et al. (1999) used Viking images, a Viking topographic map and several early Mars Orbiter Laser Altimeter (MOLA) profiles to suggest that Gale Crater may have hosted a lake intermittently from its formation in the Noachian until the early to middle Amazonian, and to speculate that it could have provided diverse environments for martian life, ranging from warm hydrothermal waters shortly after the crater-forming impact, to cold, ice-covered water at later times.

Malin and Edgett (2000) identified Gale Crater as one of a class of partially filled impact craters on Mars. They cited the fact that the peak of the Gale mound is higher in elevation than some portions of the crater rim to suggest that the entire crater was filled with layered material that was subsequently eroded. Malin and Edgett (2000) also identified an erosional unconformity on the mound, suggesting at least two episodes of net deposition and a significant amount of erosion.

Malin and Edgett (2000) also discussed a number of possible origins for the strata observed in Gale and other filled craters. Pyroclastic deposits were discussed but determined to be an unlikely source because terrestrial deposits thin very rapidly with distance from the source, and most of the layered rocks on Mars are far from potential volcanic vents. Impact ejecta was likewise ruled out because it rapidly thins with distance from the impact and therefore, to form thick deposits like the Gale Crater mound, would require "prodigious quantities" (Malin and Edgett 2000) of material. Aeolian deposition was considered a possible source if processes could be identified to explain the large volume of layered material and the apparent periodic nature of the layers in many deposits. Ultimately, Malin and Edgett (2000) favored a lacustrine origin for the layered material, citing the thickness and rhythmic nature of many layered deposits across the planet and their affinity for closed basins such as craters.

Pelkey and Jakosky (2002) conducted a study of Gale Crater using data from the Mars Global Surveyor (MGS) MOLA and the Thermal Emission Spectrometer (TES), as well as other Viking Orbiter and MGS Mars Orbiter Camera (MOC) data. They found evidence for a thermally thick dust layer on the upper mound which thins to reveal darker, higher thermal inertia material. They interpreted the northern crater floor as a dust-covered, cemented mantle, while the southern crater floor had little dust cover and variable terrain. They also found that the sand sheet in Gale Crater had a higher than expected thermal inertia and suggested some combination of coarse grain size, induration or inhomogeneities in the field of view as an explanation. They suggested that dark-toned material may be transported from the southeast into the southern

portion of Gale Crater and then northward around the mound. Pelkey and Jakosky (2002) concluded that interpreting the surface of Gale Crater is not straightforward, but that the surface layer varies considerably, likely due to multiple processes, and that aeolian processes have likely been important in shaping the surface.

In a subsequent paper, Pelkey et al. (2004) added Mars Odyssey Thermal Emission Imaging System (THEMIS) thermal inertia and visible observations to their analysis. They confirmed the observations of Pelkey and Jakosky (2002) that dust cover increases with altitude on the Gale mound and that aeolian processes have played a significant role in shaping the current surface of the crater and mound. They also noted that the numerous valleys in the crater wall and mound support hypotheses for aqueous processes in Gale Crater, and that the valleys likely postdate any deep lake in the crater because they extend down to the crater floor.

Thomson et al. (2008) interpreted ridges and fan-shaped mesas on the mound and crater rim as inverted fluvial channels and alluvial fans. They noted that there is no obvious change in slope to explain the transition from some inverted channels to fan-shaped features and suggested that this could be explained by a stream encountering a slower-moving body of water and depositing its sediment load as a fan. They also suggested that the upper mound material may be related to a widespread layered, yardang-forming unit known as the "Medusae Fossae Formation" (MFF). Recently, Zimbelman et al. (2010) have also mapped the Gale Crater mound as part of the MFF.

Rossi et al. (2008), citing unconformities in the mound, a relatively young crater retention age, and claiming that there is "no or little evidence of fluvial activity in the immediate surroundings of the craters hosting bulges and within their rim" have hypothesized that the Gale Crater mound has a local origin as a large spring deposit.

Rogers and Bandfield (2009) analyzed TES and THEMIS spectra of the dunes on the floor of Gale Crater and interpreted the results to indicate that they have a composition similar to olivine basalt, consistent with the Hamilton et al. (2007) decorrelation stretch mosaic of Gale Crater, in which mafic materials are displayed as magenta (Figure 2c). Analysis of OMEGA and CRISM observations confirm the presence of mafic minerals such as olivine and pyroxene in the dunes (Milliken et al. 2009).

Although it was not chosen as a MER landing site, Gale Crater has remained a high-interest location for a landed mission. It was proposed as a landing site for MSL at the first landing site workshop (Bell et al. 2006; Bridges 2006). The proposed MSL landing site is located on top of a large fan-shaped feature (Bell et al. 2006) which extends to the southeast from the end of a valley at the base of the northwestern crater wall. Numerous

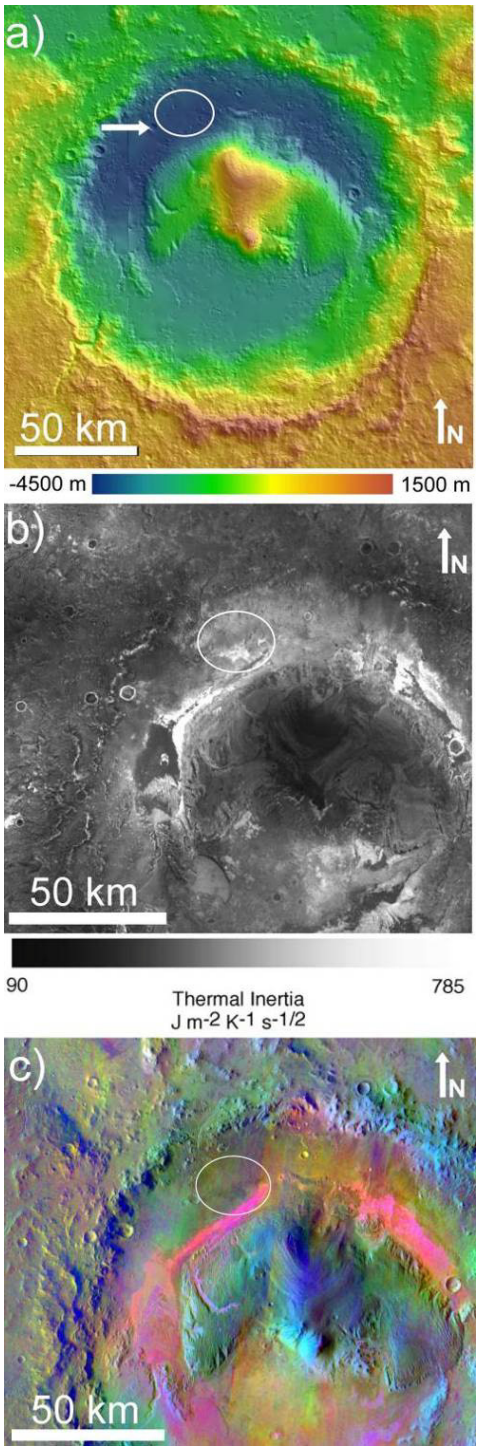

Figure 2. (a) HRSC shaded relief map of Gale crater, based on observations H1916_0000, H1927_0000, and H1938_0000. The proposed MSL landing ellipse is located in the NW crater floor. The lowest elevation in the crater is marked with an arrow. **(b)** THEMIS thermal inertia map of Gale crater (Fergason et al. 2006). **(c)** THEMIS decorrelation stretch map of Gale crater, using bands 8, 7 , and 5 for red, green and blue, respectively. (Hamilton et al. 2007) The THEMIS maps do not cover the eastern and southern rim of the crater. (figure2.jpg)

presentations at subsequent workshops have made a case for Gale Crater based on the exposure of a >5 km-thick sedimentary sequence, the numerous fluvial features on the mound and crater walls, and the detection of phyllosilicates and sulfates in the layered mound near the landing site (*e.g.*, Thomson et al. 2007; Thomson and Bridges 2008; Milliken et al. 2008).

Prior to the detection of hydrated minerals in Gale Crater, the site was interesting primarily for its geomorphology. However, the discovery of phyllosilicates and sulfates correlated to stratigraphic units in the northwestern mound, including the specific identification of the mineral nontronite (suggesting a moderate pH and possibly reducing conditions at the time of formation), have made Gale a more appealing site in terms of potential habitability and biomarker preservation (Milliken et al. 2009). In addition, the strata of the Gale mound appear to trend from phyllosilicate-bearing lower layers to sulfate and oxide-bearing middle layers to relatively unaltered upper layers (Milliken et al. 2010). Bibring et al. (2006) have proposed a global transition in climate and weathering on Mars that predicts a period of moderate pH and phyllosilicate production, followed by a period of acidic weathering with sulfate production and concluding with an era of superficial weathering to ferric oxides. It is possible that the layers of the Gale mound record this transition (Milliken et al. 2010) and can be used to test this hypothesis.

Despite interest in Gale Crater as a potential landing site, the origin of the mound remains enigmatic. We have made observations from multiple datasets in an attempt to evaluate mound-origin hypotheses and to better describe the geomorphic units that a) appear to be significant in the stratigraphic sequence and b) that MSL would be likely to encounter if Gale were chosen as the landing site. As we will show, Gale Crater exposes a rich and diverse Martian history, and it is likely that a combination of depositional and erosional environments must be invoked to explain the features that are visible today.

Data & methods

Visible data

We used radiometrically calibrated data from the Mars Reconnaissance Orbiter (MRO) Context Camera (CTX) (Malin et al. 2007) to generate a 6 m/pixel mosaic of the entire crater to use as the primary base map for this study. The list of individual images in the mosaic is given in Table 1. The extensive coverage and high resolution of CTX makes it ideal for mapping geomorphic units. We estimated the CTX Lambert albedo values given in the following sections by dividing calibrated radiance factor values by the cosine of the average incidence angle for the observation of interest.

The second visible imaging dataset used for this study was ~0.27 m/pixel data from the High Resolution Imaging Science Experiment (HiRISE) instrument (McEwen et al. 2007) on MRO. Because Gale Crater is one of the four finalist MSL landing sites (Golombek et al. 2009), it has been targeted repeatedly by HiRISE, both in the proposed landing ellipse and in other locations on the mound and crater floor. For this study, we focused primarily on the images of the landing site and the nearby mound units where there is very good HiRISE coverage. However, we also examined HiRISE images of other portions of the mound to better understand the complete stratigraphic section. Table 2 lists the HiRISE images used in this work.

The Gale Crater mound has also been extensively imaged at ~1.5 m/pixel resolution by the MGS MOC (Malin and Edgett 2010). In locations that lack HiRISE coverage, we have used MOC images to study small-scale features that are beyond the CTX resolution limit. Table 3 lists the MOC images used in the mosaic. CTX and MOC data were mosaicked using spacecraft position and pointing (SPICE) data, and using MOLA data to correct for topographic distortions. Note that in figures using high-resolution data such as HiRISE and MOC, the planetocentric latitude and longitude are provided to aid in locating the features discussed.

Infrared data

Near-infrared. In addition to visible images, we used data products from the Compact Reconnaissance Imaging Spectrometer for Mars (CRISM) (Murchie et al. 2007), a hyperspectral visible-near infrared imaging spectrometer on MRO. CRISM's high spatial and spectral resolution (15–19 m/pixel, 362–3920 nm at 6.55 nm/channel) allowed us to use spectral parameter maps created by Milliken et al. (2009) to correlate the geomorphology of the units at the proposed landing site with the inferred composition.

We also used data from the Observatoire pour la Mineralogie, l'Eau, les Glaces et l'Activité (OMEGA) visible-near infrared mapping spectrometer on the Mars Express orbiter (Bibring et al. 2004). OMEGA has an angular resolution of 1.2 mrad, resulting in a spatial resolution varying from ~350 m/pixel to >8 km/pixel, depending on where the spacecraft was in its elliptical orbit when the data were collected. We generated a mosaic of six OMEGA observations over Gale Crater. These observations are listed in Table 4. Unfortunately, the proposed landing site and western mound had only very low (~7.2 km/pixel) resolution OMEGA coverage. We adapted the CRISM spectral parameters described by Pelkey et al. (2007) to OMEGA wavelengths by using the OMEGA band closest in wavelength to the corresponding CRISM band. The adapted parameters were applied to the OMEGA mosaic to generate spectral parameter maps.

Thermal infrared. We used thermal infrared data products to reveal additional details of the physical and compositional properties of the surface. In particular, we used 100 m/pix thermal inertia (Fergason et al. 2006) and decorrelation stretch data products (Hamilton et al. 2007)

Table 1. List of CTX images of Gale crater

Image ID	Figures 3 & 7	Figure 4	Figure 6	Figure 8	Figure 9	Figure 10	Figure 11	Figure 12	Figure 15	Figure 16	Figure 17	Figure 18	Figure 19	Figure 20	Figure 24	Figure 26	Figure 29	Figure 33	Figure 37	Figure 44	Figure 45	Figure 46	Figure 48	Figure 49
P01_001356_1747_XN_05S221W	X	X						X																
P01_001422_1747_XN_05S222W	X			X																				
P01_001488_1751_XI_04S222W	X																							
P01_001554_1745_XI_05S221W	X	X						X										X						
P01_001620_1749_XI_05S222W	X	X	X		X	X		X			X						X	X		X	X			X
P02_001752_1753_XI_04S222W	X																							
P03_002253_1746_XN_05S221W	X	X																						
P04_002464_1746_XI_05S221W	X	X	X		X			X	X	X							X	X		X		X		
P04_002530_1745_XI_05S223W	X	X		X																				
P04_002675_1746_XI_05S222W	X																							
P06_003453_1752_XI_04S222W	X																							
P13_005998_1746_XI_05S222W	X			X																				
P13_006143_1745_XN_05S223W	X	X		X											X			X						
P14_006644_1747_XI_05S222W	X	X		X		X	X	X			X						X	X					X	X
P15_006855_1746_XN_05S222W	X	X		X			X	X			X		X		X			X						X
P16_007356_1749_XI_05S222W	X	X		X		X	X	X			X	X	X	X		X	X	X	X				X	X

Table 2. List of HiRISE images of Gale Crater

Image ID	Figure 6	Figure 13	Figure 14	Figure 18	Figure 19	Figure 20	Figure 21	Figure 22	Figure 23	Figure 25	Figure 27	Figure 28	Figure 30	Figure 31	Figure 33	Figure 34	Figure 36	Figure 37	Figure 38	Figure 39	Figure 40	Figure 42	Figure 43
PSP_001488_1750				X											X		X			X			
PSP_001620_1750													X										
PSP_001752_1750								X															
PSP_002099_1720																							
PSP_003453_1750																	X	X					X
PSP_005998_1745															X								
PSP_006288_1740	X																						
PSP_007356_1750						X																	
PSP_008147_1750									X														
PSP_009149_1750				X							X												
PSP_009294_1750					X		X			X					X				X				
PSP_009571_1755		X	X															X					
PSP_009650_1755																X							
PSP_009716_1755					X																X	X	
PSP_009861_1755												X			X			X					
PSP_009927_1750														X									
PSP_010573_1755																					X		

Table 3. List of MOC images of Gale crater

Product ID			
E01-00067	E14-02234	M11-00989	R16-00139
E01-00538	E16-01112	M12-00231	R16-02163
E01-01026	E16-01641	M12-02852	R18-00974
E02-00942	E18-01261	M14-01617	R19-01648
E02-01579	E20-00143	R01-00210	R20-00784
E02-02493	E20-01495	R01-00595	S05-00434
E03-01733	E21-00160	R01-00946	S06-00098
E03-01915	E21-00428	R01-01335	S06-02328
E04-01829	E21-00521	R02-00546	S09-00404
E04-02461	E21-00833	R02-00913	S11-00421
E05-00772	E22-00419	R09-02667	S11-02858
E05-02541	E23-01009	R09-03892	S12-01881
E06-00143	M02-01391	R10-04983	S12-02067
E09-01039	M03-01521	R11-04327	S13-00501
E10-00863	M03-06805	R12-00567	S14-00576
E10-02079	M07-01419	R12-00762	S16-00680
E11-01254	M08-01028	R12-01498	S17-00627
E11-02505	M08-02542	R13-00776	S19-00656
E12-01615	M09-01696	R14-01644	S20-00585
E13-01884	M10-01253	R15-00805	S22-00845

Table 4. OMEGA data cubes used in Gale Crater mosaic

Product ID	Spacecraft-to-surface distance (km)	Resolution (km/pixel)
ORB0436_2	1149.6	1.4
ORB0436_3	1778.1	2.1
ORB0469_3	1833.4	2.2
ORB1002_6	292.0	0.4
ORB1339_1	1090.0	1.3
ORB1577_3	5971.5	7.2

derived from THEMIS measurements.

Thermal inertia is a measure of the resistance to temperature change of the upper several centimeters of the surface. It is determined by the thermal conductivity, heat capacity, and density of the material. On Mars, variations in the thermal conductivity, due primarily to changing particle size, are considerably more significant than variations in heat capacity and material density. (Fergason et al. 2006) Therefore, lower thermal inertia regions are interpreted as unconsolidated aeolian-deposited sand or dust, while higher thermal inertia regions are interpreted to have more abundant rocks or cemented materials, exposed bedrock, or some combination of those components. It should be emphasized that thermal inertia maps give information only about the upper few centimeters of Mars, and that mixing effects can be significant. For example, bedrock with small patches of fine-grained dust at scales smaller than the instrument resolution could have an intermediate observed thermal inertia that is quite different from the true thermal inertia of the rock and dust portions of the surface.

Decorrelation stretches are used to enhance variations in highly correlated data. The technique applies a principal component transformation to the data, followed by contrast-stretching and then re-projection back to the original display coordinates. In the case of images that have been assigned to a red, green and blue color space, this has the effect of exaggerating color variations without distorting the hues of the image. (Gillespie et al. 1986). Decorrelation stretched images cannot be used for quantitative measurements, but they give qualitative insight into the compositional variation of the surface. The decorrelation stretch used in this work is based on THEMIS bands 8 (11.79 μm), 7 (11.04 μm), and 5 (9.35 μm), which are displayed as red, green and blue, respectively. This results in mafic materials appearing as magenta, while more felsic and sulfate-bearing materials appear yellow and dusty surfaces appear blue. (Hamilton et al. 2007)

The THEMIS thermal inertia and decorrelation stretch maps for Gale Crater were generated by the THEMIS team, and made publicly available on the THEMIS website (Christensen et al. 2006) when Gale was announced as a potential landing site for MSL.

Topography

To provide the global context for Gale crater, we used a topographic map based on Mars Orbital Laser Altimeter (Zuber et al. 2002) data, shown in Figure 1.

We used three map-projected and areoid-referenced digital terrain models from the High Resolution Stereo Camera (HRSC; Neukum and Jaumann, 2004) on Mars Express (data product IDs: H1916_0000_DA4, H1927_0000_DA4, and H1938_0000_DA4) to generate a topographic map of the entire crater at 75 m/pixel (Figure 2a). This topographic data provides valuable context for the other data sets.

We augmented the regional HRSC topography with a digital elevation model of the proposed landing site, traverse path, and part of the western mound derived from CTX stereo pair images P16_007356_1749_XI_05S222W and P18_008147_1749_XN_05S222W. The procedure for generating topographic models based on CTX stereo imaging is described by Broxton and Edwards (2008) and Edwards and Broxton (2006). Briefly, the image pair is re-projected and aligned, then pre-processed to enhance edges and ensure insensitivity to biases in brightness and contrast in the stereo correlation step. For "pushbroom" cameras like CTX, the process uses a camera model to account for the changing position of the camera during image acquisition. The stereo correlation step identifies corresponding points in the pair of images, and a 3D model is created by finding the intersection between the lines of sight for each pair of corresponding pixels, thus localizing the point in three-dimensional space. A final step interpolates missing values in the elevation model.

Gale Crater context

Overview

Gale is a 155 km diameter crater at the boundary between the southern highlands and Elysium Planitia (Figure 1). The rim of the crater is degraded but still clearly identifiable (Figure 2), and the surrounding terrain has a knobby and mantled appearance, visible in the CTX mosaic in Figure 3. This basemap provides context for the figures discussed in this and later sections.

The large mound of layered material is shaped like a wide crescent, with the "horns" of the crescent pointing to the southwest and southeast. The peak of the mound (838 m elevation) is higher than the degraded northern rim and somewhat lower than the highest point on the southern rim (1448 m). Gale Crater is superimposed on the boundary between the southern highlands and northern lowlands, and this regional slope likely contributes to the difference in elevation between the northern and southern rim. However, the southern rim is approximately 3 to 4 km higher than the nearby floor, whereas the northern rim is ~2 km higher than the northern floor, suggesting that there is significant degradation of the northern rim and/or more material filling the northern crater floor relative to the southern portion of the crater. The lowest point in Gale Crater (-4674 m; marked with an arrow in Figure 2a) is in the northwest portion of the floor, near the location of the proposed MSL landing ellipse, which is at an elevation of approximately -4400 m.

The east and west portions of the mound have a lower elevation and are characterized by numerous yardangs (Figures 4e, 4f), thin (<20 m) layers of varying tone, and a thermal inertia varying from ~300-700 J m^{-2} K^{-1} $s^{-1/2}$. The peak of the mound and material in the 20 km to the east and west of the peak resemble the knobby terrain of the

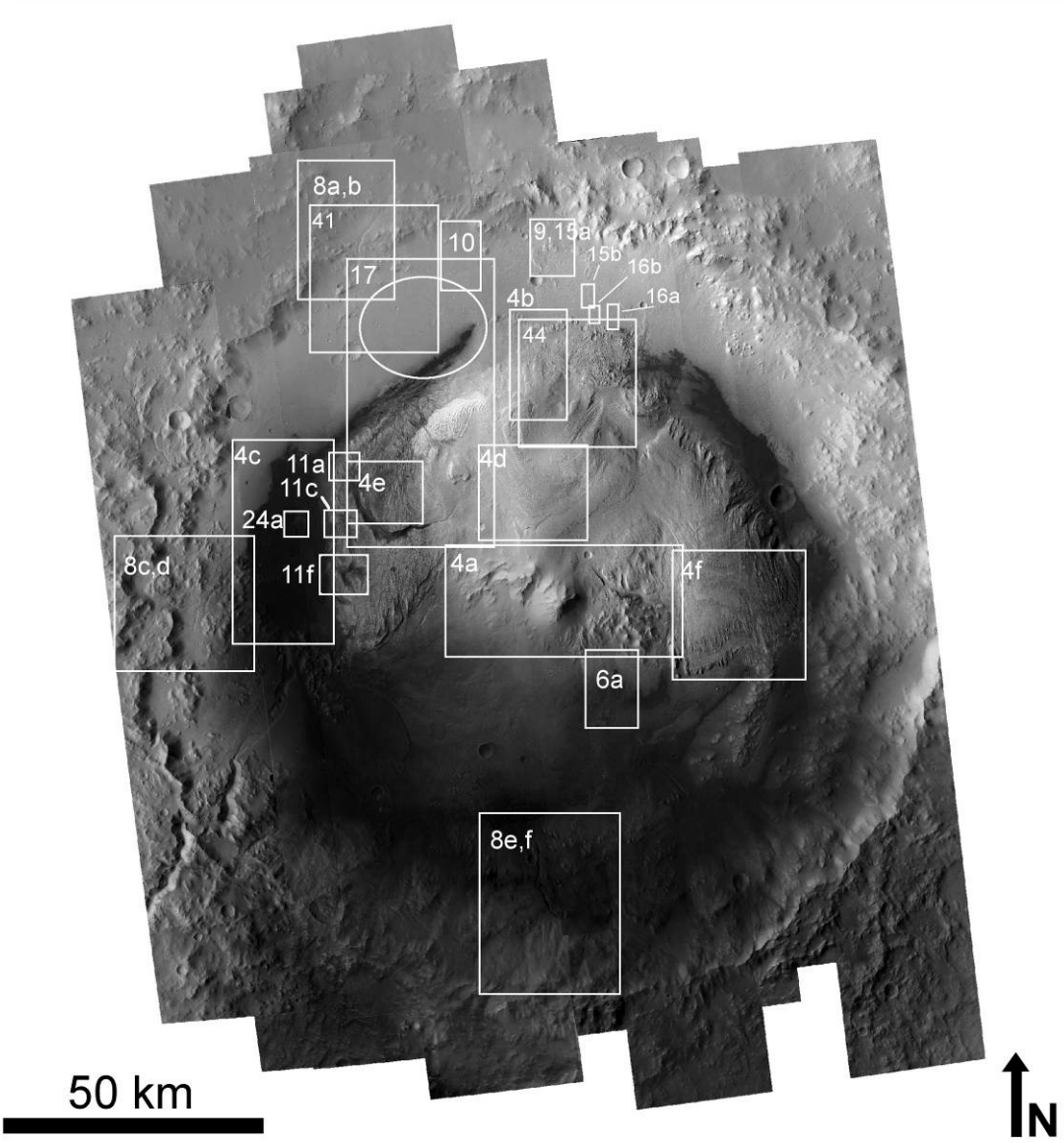

Figure 3. CTX mosaic of Gale crater. Boxes and labels indicate the locations of other Figures. The proposed MSL landing site is indicated by the white ellipse. Refer to Table 1 for a list of CTX images used in the mosaic. (figure3.jpg)

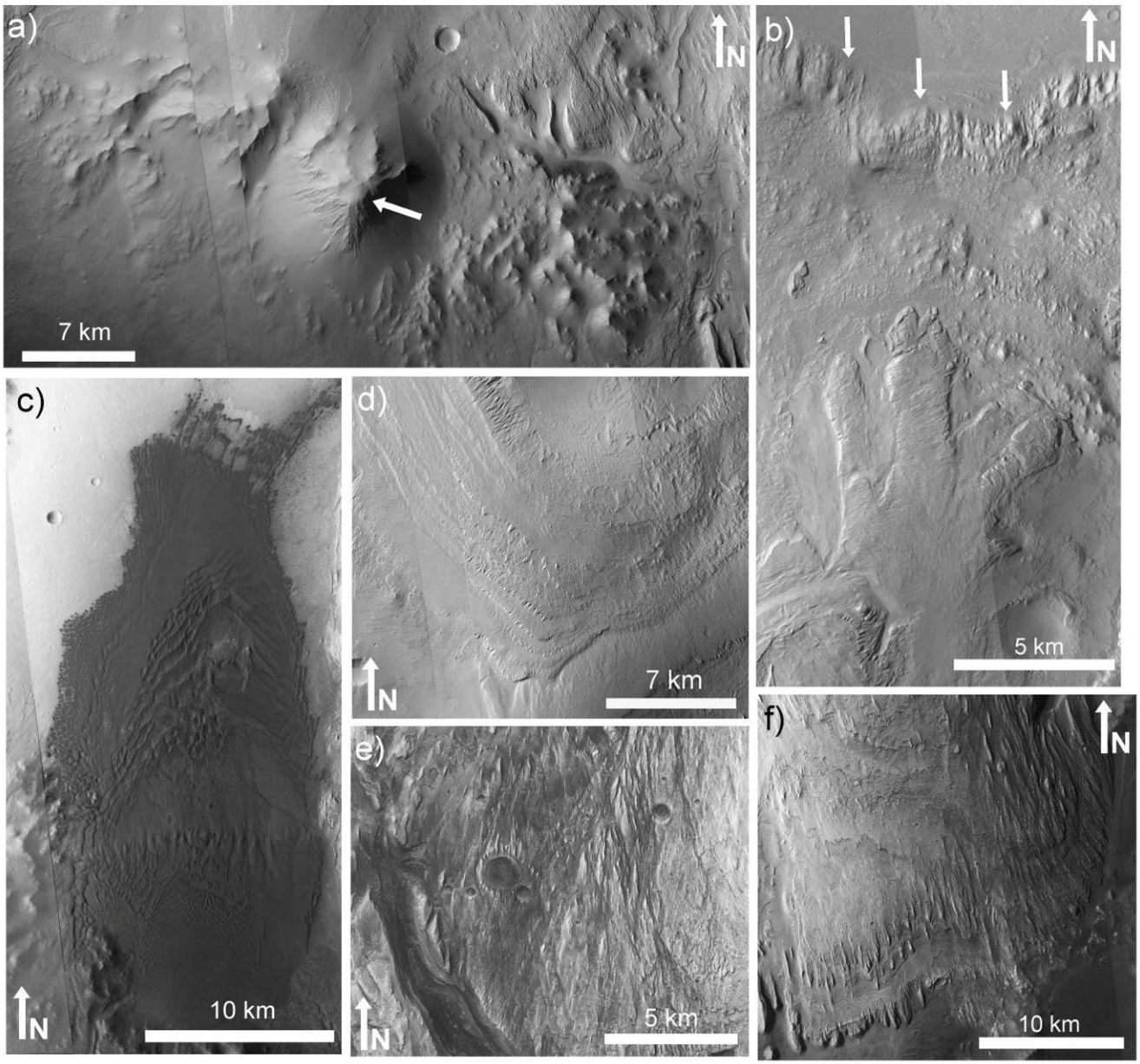

Figure 4. (a) The peak of the central mound (marked by an arrow) and its surroundings. **(b)** A row of small elongated hills (marked by arrows) outline the northern edge of the mound, and lobate features extend part of the way down to the floor. **(c)** A large sand sheet in the western crater floor. **(d)** The terraced layers of the upper mound. The western mound **(e)** and eastern mound **(f)** are layered and eroded into a yardang-like texture. Refer to Figure 3 for context. Refer to Table 1 for CTX Image IDs. Illumination is from the left. (figure4.jpg)

crater wall and surrounding plains (Figure 4a). The northern portion of the mound (Figure 4b) is fringed by rounded and somewhat elongated hills, and lobate features are present on the northern slopes of the mound itself.

Dark-toned aeolian material occurs on the crater floor and exhibits a variety of forms, including isolated barchan and dome dunes <100 m in diameter, transverse ridges, and an extensive (~372 km^2) sand sheet to the west of the mound (Figure 4c). The thermal inertia of the dark dunes is ~350-400 J m^{-2} K^{-1} $s^{-1/2}$ which is consistent with loose sand-sized material (Edgett and Christensen 1994).

The southern floor and rim have a lower albedo than the northern floor and rim and most of the mound. This corresponds to an increase in the low- and high-Ca pyroxene parameters in OMEGA maps (Figure 5). We interpret this as a region that is less mantled by ferric dust, exposing more mafic underlying material. The high-Ca pyroxene signal is highest within the crater but the low-Ca pyroxene signal extends south of the rim and correlates with the dark-toned wind streak in that area.

We used empirical equations by Garvin et al. (2003) to estimate Gale Crater's pristine depth and rim height. Garvin et al. (2003) do not list a depth to diameter equation for craters larger than 100 km, so we applied their equation for complex craters ($d = 0.36D^{0.49}$; 7 km < D < 100 km) to estimate a pristine depth of 4.3 km for Gale Crater (diameter D = 155 km). In general, larger impact basins have a smaller depth to diameter ratio (Pike *et al.* 1980), so we would expect the equation for complex crater depth to provide an upper limit on the depth of the pristine Gale Crater. We used the equation for rim height of craters of diameter D > 100 km ($h = 0.12D^{0.35}$) to calculate an initial rim height of 0.7 km. Therefore, by adding the pristine depth and rim height, we calculate an original floor-to-rim elevation difference of approximately 5 km.

The actual maximum floor-to-rim difference for Gale is 6.1 km, implying that if the limit imposed by the equation is correct, a substantial amount of additional erosion has occurred in the northern crater, removing any crater-filling material and possibly portions of the original crater floor. We should, however, note that the 6.1 km value is the elevation difference between the highest point on the southern rim and the lowest point in the northern crater floor, so it likely is influenced by the regional slope of the dichotomy boundary. The southern part of the floor is only 3-4 km below the southern rim suggesting that parts of the crater floor have experienced partial infilling.

Survey of inferred fluvial features

Using the 6 m/pixel CTX basemap, we searched Gale Crater for valleys and sinuous ridges that may represent fluvial channels and inverted channels, respectively.

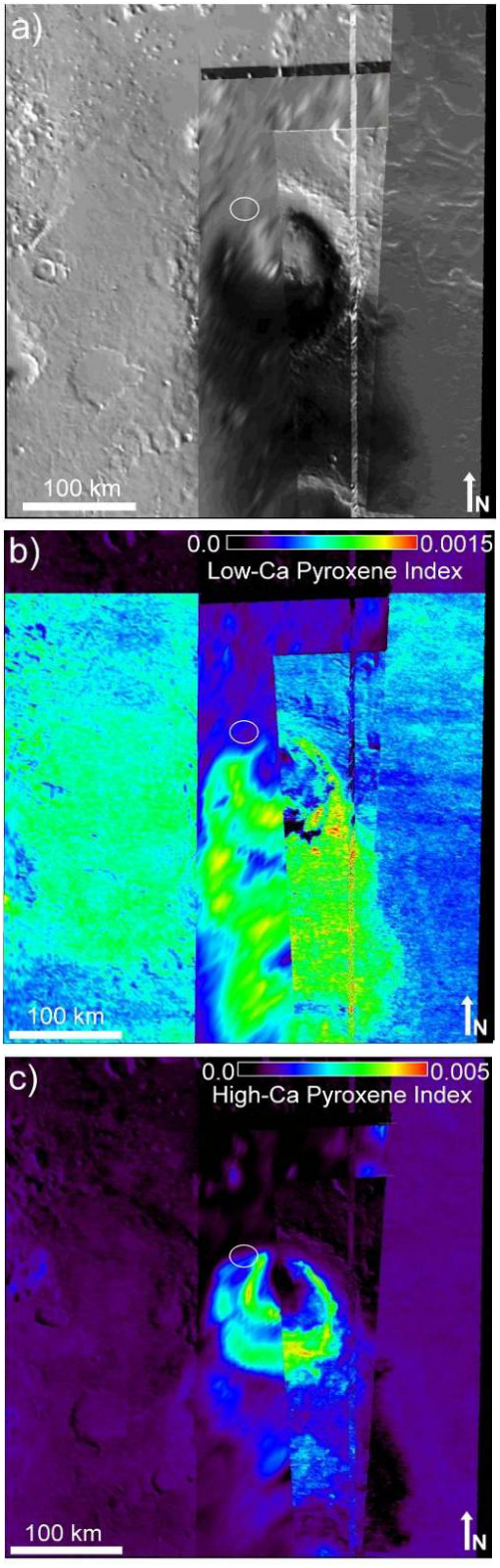

Figure 5. (a) OMEGA mosaic of Gale crater. Images in the mosaic vary greatly in resolution (see Table 4) **(b)** Map of the Low-Ca pyroxene index, adapted from Pelkey et al. (2007). **(c)** Map of the high-Ca pyroxene index, also adapted from Pelkey et al. (2007). (figure5.jpg)

Inversion of relief occurs when topographic lows, such as fluvial channels become more erosion resistant than the surrounding terrain due to processes such as filling by lava flows, cementation, and/or "armoring" by relatively coarse-grained material (Pain et al. 2007; Williams et al. 2009). When erosion and weathering strip away the less-resistant surrounding material, the channel remains as a raised ridge or series of hills or mesas. This phenomenon is observed in arid environments on Earth such as Oman (Maizels 1990) and the Colorado Plateau (Williams et al. 2009), and has been suggested as the origin of the sinuous ridges that are common on Mars (Edgett 2005).

An alternate explanation for sinuous ridges is that they could be eskers. Eskers have been invoked to explain sinuous ridges elsewhere on Mars (Kargel and Strom, 1992). However, dueto the lack of clear evidence for glacial activity at Gale Crater and the presence of multiple negative-relief channels which transition to sinuous ridges in more-eroded areas (Figure 6), it seems most likely that the sinuous ridges in Gale Crater are inverted channels formed by subaerial water flow.

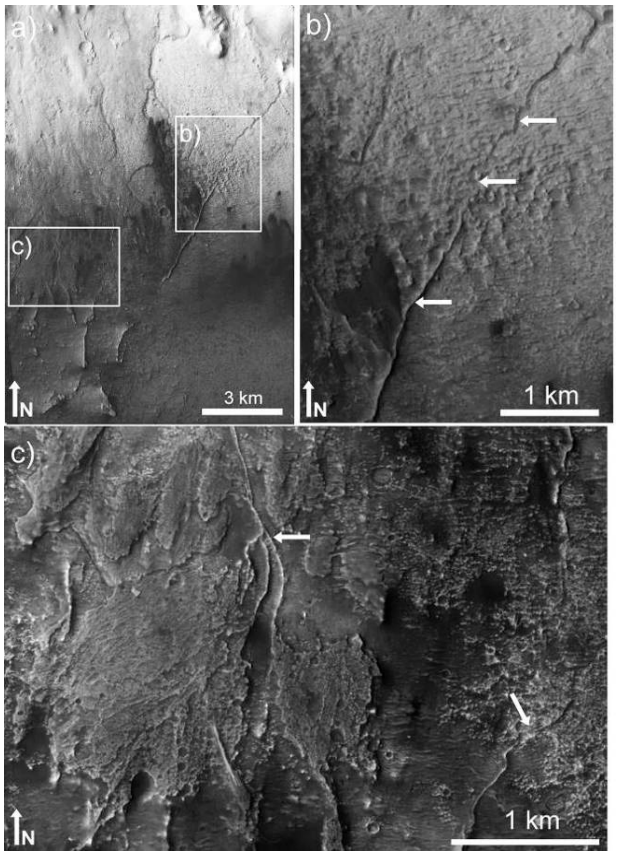

Figure 6. (a) CTX inset of the terrain to the southeast of the central mound peak. Multiple channels extend from the base of the mound onto the crater floor. White boxes indicate the insets shown in (b) and (c). **(b)** A close-up of one channel (marked by arrows) in the pitted mound-skirting unit. Where the unit is eroded away, the channel remains in inverted relief. **(c)** This HiRISE inset shows a branching inverted channel (arrow, middle) that feeds into a positive-relief fan-shaped feature. Another example of a channel transitioning from negative to positive relief is marked by an arrow on the right, above the scalebar. Illumination is from the left in all parts of this figure. Refer to Tables 1 and 2 for CTX image IDs and HiRISE image IDs, respectively. Location: 5.653°S 138.035°E. (figure6.jpg)

Features in Gale Crater that we interpret as fluvial in origin are shown in red (negative relief) and yellow (positive relief) in Figure 7. The crater walls are dissected by valleys, suggesting that flowing water has played a role in eroding the crater. All of the observed valleys on the crater rim appear to lead into the crater with no obvious surface outlet. Several of the valleys form third or fourth-order branching networks (Figure 8). One of these dendritic valleys in the northwestern crater rim ends at the apex of the fan-shaped feature in the proposed MSL landing site (Figures 8a & 41). Many other valleys and ridges, particularly on the northern rim, lead to fan-shaped mesas on the crater floor, as shown in Figures 9 and 10.

The largest valley (marked with an arrow in Figure 3) enters the crater through the southwestern rim and continues for ~40 km across the crater floor before disappearing beneath the western dune field. Several other canyons (also marked with arrows in Figure 3) are apparent on the western mound. The largest of these transitions headward to a shallower, narrower channel that appears to be partially exhumed from beneath the terraced layers of the upper mound. Several of the canyons on the western mound end in fan-shaped extensions of the mound that appear to overlap the underlying mound-skirting unit (Figure 11). These features are discussed in subsequent sections.

Inverted channels, typically less than 100 m in width, and in some cases >10 km long, are common on the crater floor, as shown in Figure 7 and in more detail in Figure 12. South of the mound, several channels transition to inverted channels as the unit in which they are carved becomes more extensively eroded (Figure 6). This unit is ridged and appears to be related to the mound-skirting unit discussed in a later section. The transition from negative to positive relief channels occurs at the edge of this unit, where it breaks up into a rough surface of many small outcrops (*e.g.*, Figure 6b). This boundary is not apparent in the THEMIS thermal inertia map. Several examples of sinuous ridges (sinuosity index of ~2) and finely branching ridges are exposed within the proposed landing ellipse (Figures 13 & 14). These are discussed in the sections concerning the mound-skirting and hummocky plains units.

Also common (as shown in Figures 7 and 12) on the northern crater floor are chains of mesas that appear to be associated with the fan-shaped mesas at the base of the northern crater wall (*e.g.*, Figure 10). They have a similar surface texture (Figure 15) and in some cases the fan-shaped mesas are connected to the chains of mesas on the crater floor by channels or inverted channels. Figure 16 shows an example of the chains of mesas branching in a manner similar to fluvial channels. The chains of mesas

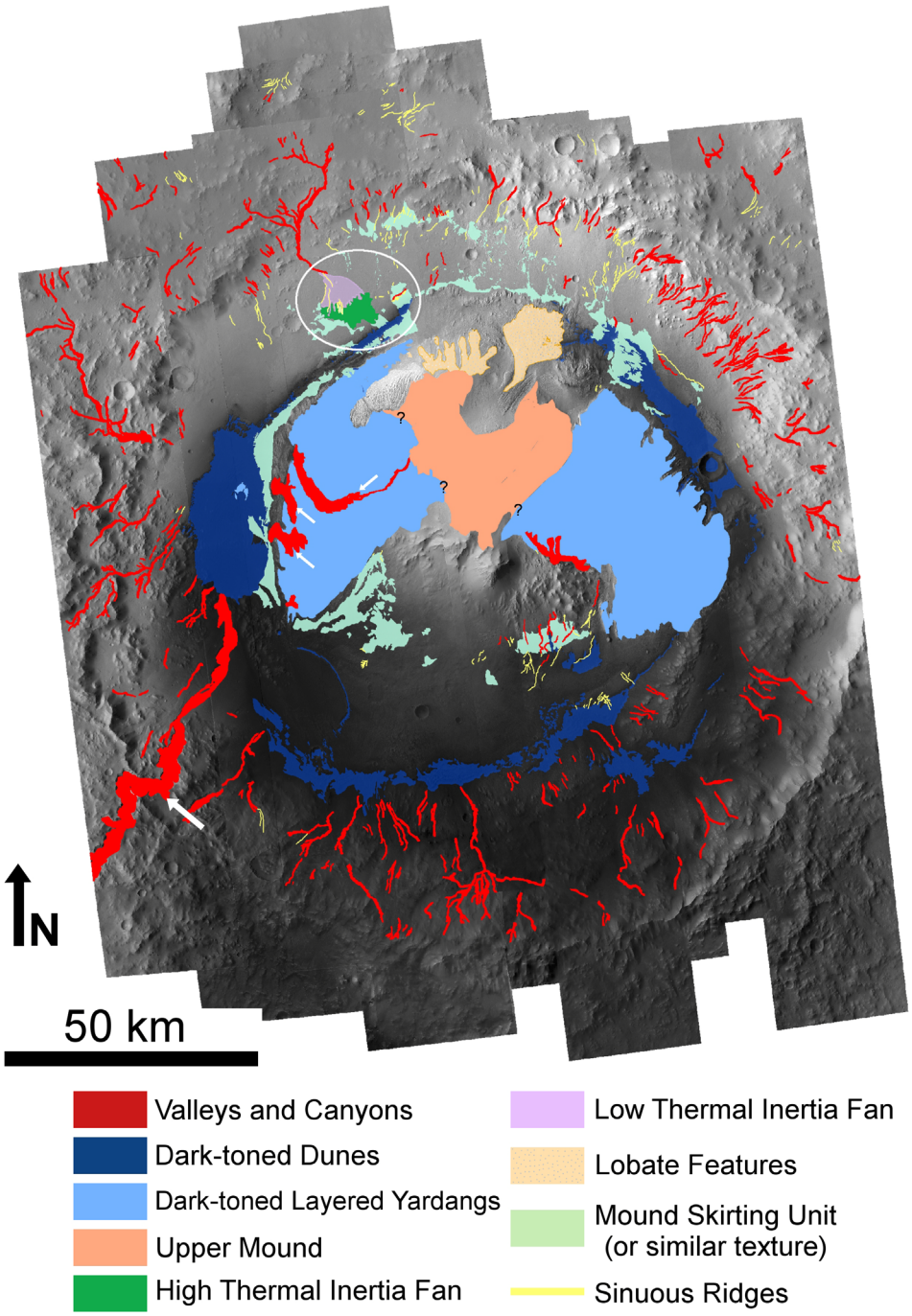

Figure 7. Unit map of Gale Crater. Refer to Figure 17 for a more detailed unit map of the proposed MSL landing site. The proposed landing site is indicated by the white ellipse. Arrows mark the large channel in the southwestern crater rim and the three large canyons on the western flank of the mound. Question marks indicate locations where aeolian material obscures the contact between the upper mound and the dark-toned layered yardangs. Uncolored areas are "undivided" or ambiguous material. Some units were mapped locally near the landing site (Figure 17) but are not shown here. Refer to Table 1 for a list of CTX images used in the mosaic. (figure7.jpg)

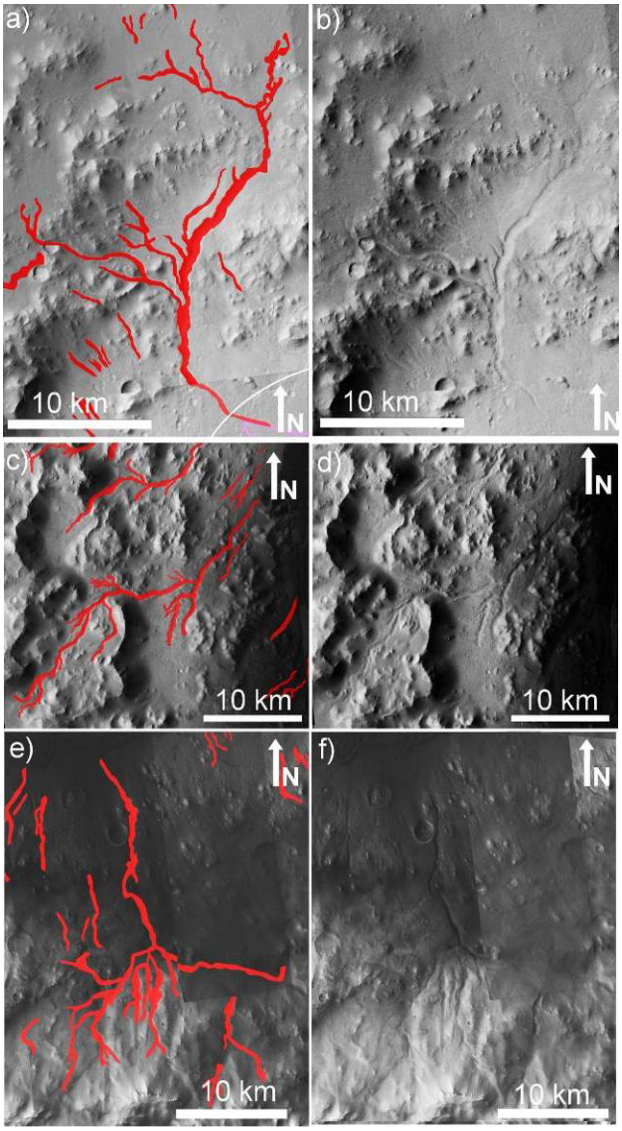

Figure 8. (a,b) The branching valley on the northern crater rim that ends in the fan-shaped feature in the proposed landing ellipse. The edge of the ellipse is visible in the lower right corner. **(c,d)** Another example of a branching valley on the western rim of Gale crater **(e,f)** A third example of a branching valley on the southern rim and floor. Refer to Figure 3 for context and Table 1 for CTX image IDs. Illumination is from the left. Locations: **(a,b)** 4.237°S 137.247°E **(c,d)** 5.389°S 136.699°E **(e,f)** 6.334°S 137.782°E (figure8.jpg)

can extend from the crater wall to the base of the mound, where they merge with the similar-textured mound-skirting unit (Figure 16).

Gale Crater units

In this section, the units of the northwestern crater floor and mound are discussed in detail. Units were distinguished primarily by their geomorphologic characteristics, although thermal inertia and composition also were used in some cases. Figure 3 and Figure 7

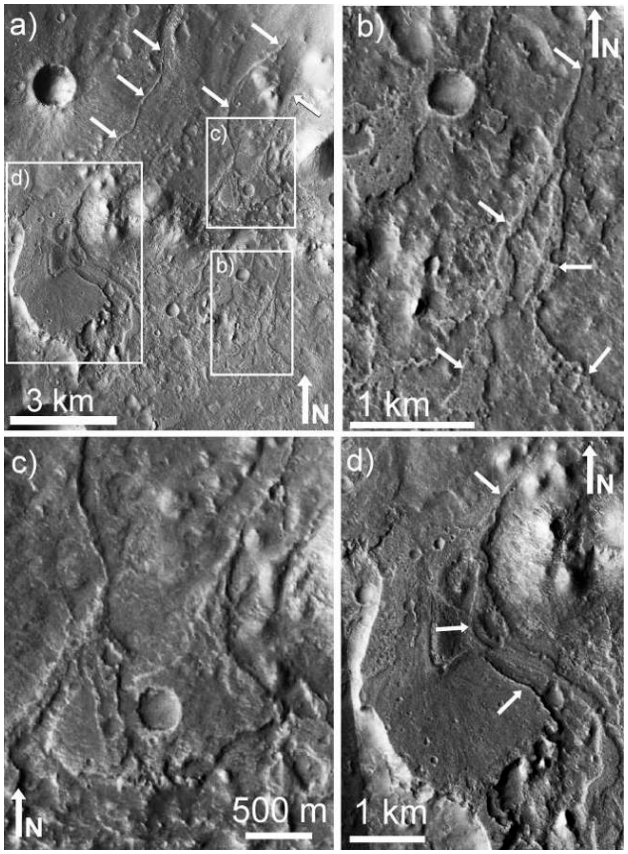

Figure 9. (a) Ridges interpreted to be inverted channels (marked by arrows) leading down from the northern rim transition to raised fan-shaped mesas. **(b)** This fan-shaped mesa maintains two distinct narrow branches. **(c)** Two inverted channels form adjacent fan-shaped mesas. **(d)** A more complex fan-shaped mesa that preserves an inverted channel along its eastern edge (marked by arrows). Refer to Table 1 for CTX image IDs. Illumination is from the left. Location: 4.252°S 137.848°E (figure9.jpg)

provide context for the figures in this section. Figure 17 shows a detailed map of the landing site and northwestern mound units discussed, and Figure 7 shows units and features that were mapped over the entire crater. Regions of the maps that are not colored can be considered "undivided" material. These locations often had an ambiguous appearance, or represented terrains with less relevance to our primary focus on the proposed MSL landing ellipse and surroundings. Table 5 summarizes the unit properties. Some simplifications and uncertainties are necessarily involved in arriving at our unit map and hypothesized stratigraphy in Gale Crater. For example, in some cases units have sharp boundaries, such as the light-toned yardangs, but in other cases, the transition between units can be ambiguous, such as some contacts between the mound-skirting unit and the hummocky plains or the transition between the dark-toned layered yardangs and the upper mound.

Dark-toned layered yardang-forming unit

Observations. Much of the surface of the lower mound is

Table 5. Summary of unit properties.

Unit	Min Elevation (m)	Max Elevation (m)	CTX Albedo	Thermal Inertia ($J\ m^{-2}\ K^{-1}\ s^{-1/2}$)	Morphology	Key Figures
Dark-Toned Layered Yardangs	-4460	-1800	0.18-0.22	300-700	Thin layers of varying properties forming large yardangs.	19, 20, 21 22, 23
Light-Toned Yardangs	-3390	-1674	0.26	390	Fine layering and joints, scalloped texture.	17, 47, 25
Thin Mantle Unit	-4070	-1140	0.20-0.23	400	Small patches that drape topography, characteristic "feathery" erosion.	21, 27, 28
Upper Mound	-2140	490	0.24	300	Cliff-bench layers, scalloped texture. potential cross-beds.	29, 30, 31
Mound-Skirting Unit	-4390	-2940	0.16-0.21	430-780	Pitted, mesa-forming, parallel ridges in some locations.	6, 7, 12, 15, 16, 18, 33
Light-Toned Ridge	-4320	-4170	0.19-0.21	600	Breaks into poorly defined layers downhill, ends abruptly uphill.	18, 37, 36
Phyllosilicate-Bearing Unit	-4210	-4090	0.16	550	Rippled surface but fractures and dunes on top suggest lithification.	38
Light-Toned Basal Unit	-4490	-4212	0.18-0.20	500-540	Fractured light-toned rock, possible faint layers.	34, 39
Dark-Toned Basal Unit	-4513	-4415	0.15-0.16	760	Darker-toned fractured rock.	39
Hummocky Plains	-4670	-4150	0.21	480	Hummocky, ranging from smooth to rocky.	13, 41
Low Thermal Inertia Landing Site Fan	-4500	-4190	0.21	460	Primarily smooth, possibly mantled.	40, 41, 42
High Thermal Inertia Landing Site Fan	-4520	-4440	0.21	620	Rugged fractured rock.	40, 41, 42, 43
Lobate Features	-4350	-1200	0.24	460-670	Some show erosion-resistant upper layer. Fan-shaped unit is rugged with potential pressure ridges and streamlined texture.	44, 45, 46

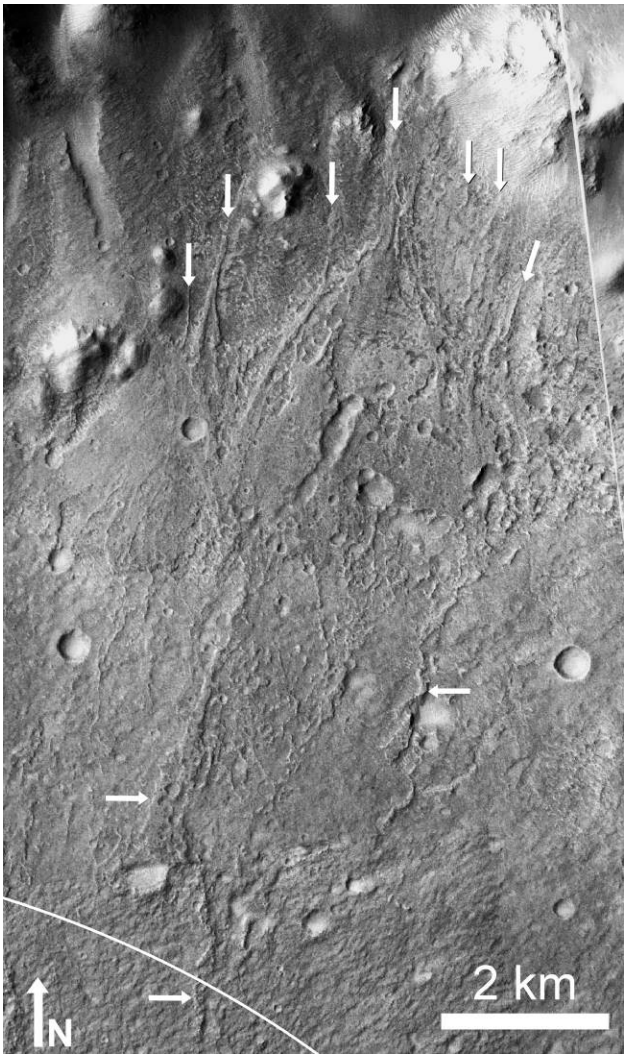

Figure 10. Ridges interpreted to be inverted channels (marked by vertical arrows) become raised fan-shaped mesas near the northern rim. Chains of mesas (marked by horizontal arrows) extend from the fan-shaped mesas across the crater floor. The northeast portion of the landing ellipse is visible in the lower left. Refer to Table 1 for CTX Image IDs. Illumination is from the left. Location: 4.270°S 137.523°E (figure10.jpg)

characterized by a layered, moderate to dark-toned yardang-forming material (*e.g.*, Figures 3, 7 and 17). We have chosen to focus our discussion in this section on the western mound, but the eastern mound shows a similar layered and yardang-forming morphology and has therefore been mapped as dark-toned layered yardang-forming material in Figure 7. The upper extent of the dark-toned layered yardang forming material is often uncertain due to aeolian material obscuring the contact with the upper mound.

The thermal inertia of the surface of the western mound varies from approximately 300 to 700 J m^{-2} K^{-1} $s^{-1/2}$. The dark-toned layered yardang-forming material is cut by several large canyons on the western side of the mound, as well as a small filled channel on the northwestern flank of the mound, near the proposed MSL landing site (mapped in Figure 17, shown in Figure 18c). The channel was first noted by Malin and Edgett (2000) and extends from beneath aeolian bedforms at the base of the light-toned yardang-forming unit and ends in a raised ridge on top of a mesa-forming outcrop of mound-skirting unit.

At CTX and MOC scales, some portions of the dark-toned layered yardang-forming unit have clear layers of varying CTX albedo (~0.18-0.22) that are relatively easy to trace. Milliken et al. (2010) have identified a "marker bed" (Figure 19) in the layers of the mound near the proposed MSL landing site that is also present in the stratigraphic section exposed by the large canyons in the western mound, and possibly in the layered outcrops in the southeastern mound.

In other locations higher on the mound the surface becomes rougher and is eroded into more densely spaced yardangs. In these locations, individual beds become difficult to trace. Figure 20 shows a typical DTY surface on the western mound. CRISM observations (Milliken et al. 2009, Milliken et al. 2010) indicate that this dark-toned layered yardang-forming unit contains hydrated sulfate minerals, indicative of aqueous alteration. The beds of this portion of the mound are typically less than ~20 m thick, and have been shown to be parallel, with a dip of 2-4° to the northwest. (Milliken et al. 2010) The erosional expression of the layered rocks that make up the dark-toned layered yardang-forming unit varies from cliff-bench, boulder shedding layers (Figure 21a) to more-erodible layers which form smooth slopes (generally <10°). The beds in these smooth locations appear "blurry" (Figure 21b).

The surface of the dark-toned layered yardang-forming material is often covered with polygonal ridges. (Figure 22) In some cases, a dark line marks the ridge centers (Figure 22d). The topographic lows between the ridges are darker toned than the ridges themselves. On the western mound, larger ridges and clusters of ridges cut across the yardang texture of the mound (Figure 20).

Near the head of the largest canyon on the western mound the surface of the dark-toned layered yardang-forming material is characterized by parallel east-west-oriented lineations at an interval of 30 to 50 m (Figure 23).

Approximately 4.5 km to the west of the mound, in the large dark-toned dune field, there is an outcrop of layered yardang-forming material that borders a circular depression. (Figure 24)

Interpretations. We interpret the "yardang-like" texture of the dark-toned layered yardang-forming unit to be due primarily to aeolian erosion. However, the large canyons and smaller filled channels in the dark-toned layered yardang-forming material provide evidence for fluvial erosion of the unit. This provides an important temporal constraint, implying that the unit was deposited and significantly eroded at a time when fluvial processes could still occur at the surface of Mars.

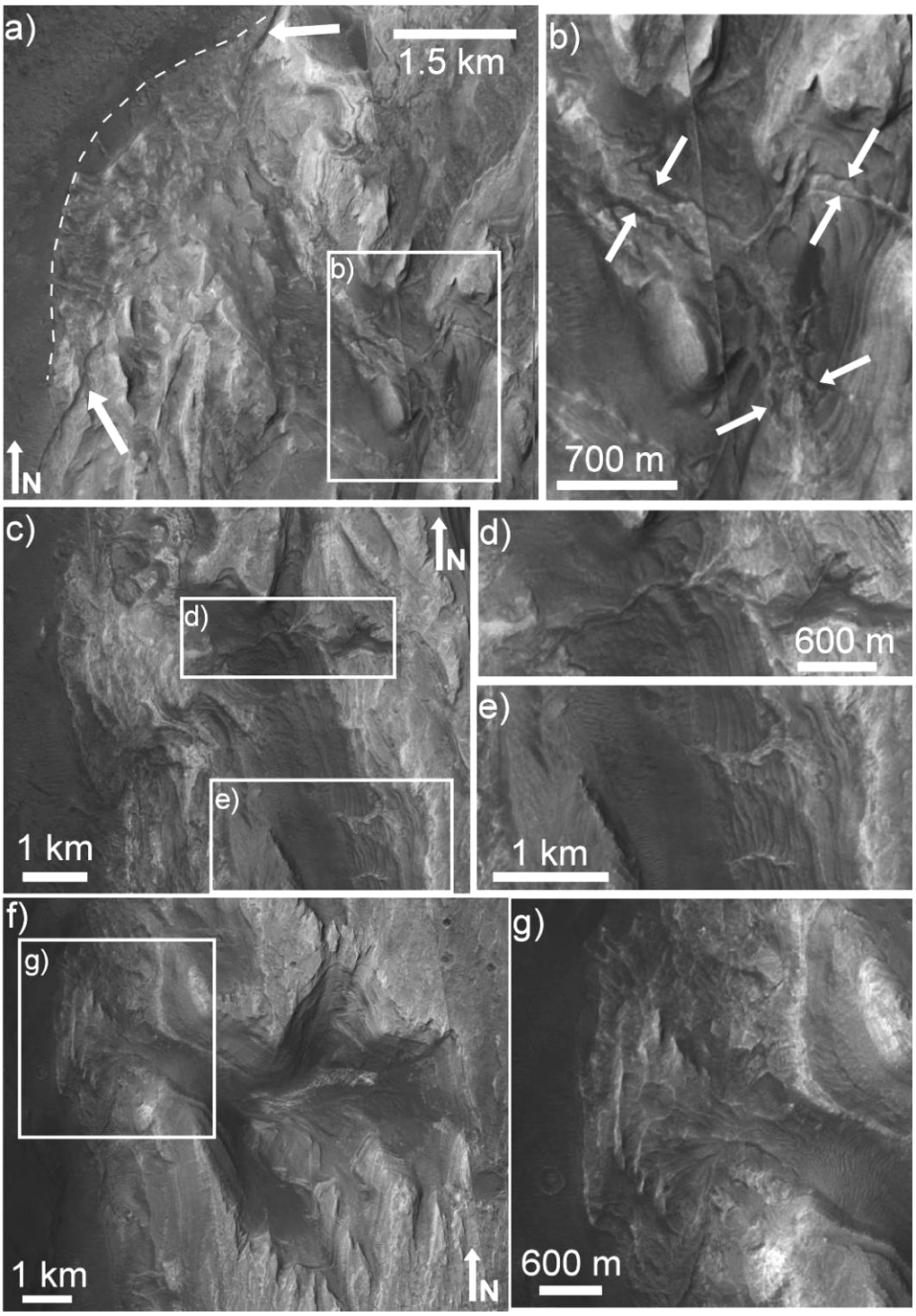

Figure 11. a) A wide fan-shaped deposit of mound material (boundary marked by the dashed line) overlaps the mound-skirting unit in this location, but is thin enough that the edge of the mound skirting unit is still apparent (marked by arrows). The material emerges from a large canyon which preserves a filled channel in its floor and walls, shown in **b)**. **c)** a second fan-shaped deposit of material overlapping the mound-skirting unit. **d)** and **e)** show the location of ridges in the wall of the canyon that leads to the fan-shaped deposit in c). **f)** a stubby branched canyon leads to a third fan-shaped deposit that overlaps the mound-skirting unit, shown in **g)**. Refer to Figure 3 for context and Table 1 for CTX image IDs. Illumination is from the left. Locations: **a)** 4.951°S 137.180°E **c)** 5.126°S 137.153°E **f)** 5.277°S 137.126°E (figure11.jpg)

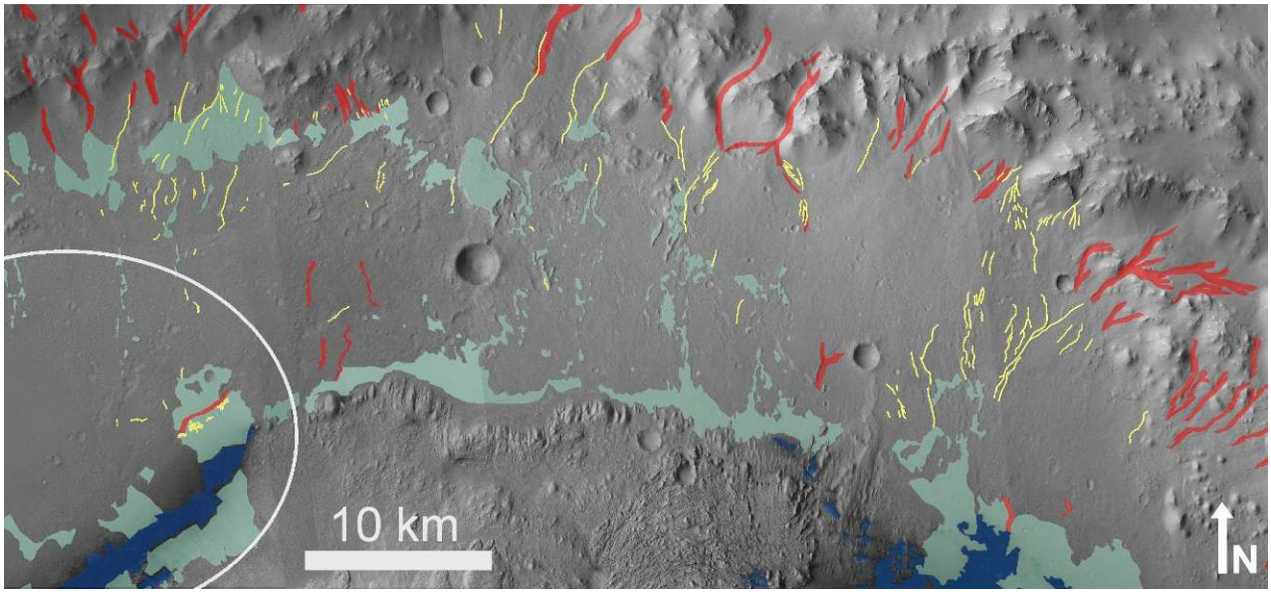

Figure 12. A closer view of the northern crater floor. Valleys interpreted as fluvial channels are marked in red and ridges interpreted as inverted channels are marked in yellow. Blue marks the location of dark-toned dunes. Light green indicates surfaces with a texture characteristic of the 'mound-skirting' unit. Note the numerous mesas of mound skirting unit and the numerous inverted channels. The landing ellipse is visible at left. Illumination is from the left. Refer to Table 1 for CTX Image IDs. (figure12.jpg)

We interpret the erosion-resistant polygonal ridges on the surface of the dark-toned layered yardang-forming material to be the result of differential erosion of filled or cemented fractures, similar to the much smaller-scale "boxwork" observed in some caves on Earth (Bakalowicz et al. 1987). Thomson and Bridges (2008) first suggested this explanation for the Gale Crater ridges and similar erosion-resistant ridges on Mars have previously been interpreted as evidence of alteration and fluid flow through fractured rocks (Okubo and McEwen 2007).

The darker line observed in the center of some ridges could be the fracture itself, while the lighter-toned ridge is formed by the surrounding erosion-resistant cemented or altered rock. Alternatively, the darker central line could represent a variation in the albedo of the material filling the fracture.

It is also possible that the erosion-resistant ridges are dikes formed by the intrusion of igneous rock along fractures. However, dike swarms tend to be parallel, en echelon, or radially oriented, rather than polygonal (Neuendorf et al. 2005). Given the geomorphic evidence that water has played a role in Gale Crater, and the presence of hydrated sulfates in the dark-toned layered yardang-forming material, we favor an aqueous alteration interpretation.

The observed “blurring" between thin beds with similar erosional characteristics (Figure 21b) could be due to a gradual change in the depositional setting, or due to the debris from the eroding layers obscuring an otherwise sharp contact. The continuity of bedding planes such as the marker bed shown in Figure 19 over many kilometers suggests that the depositional process that formed the layers of the lower mound was widespread and uniform.

The parallel lineations near the head of the large western canyon (Figure 23) have been interpreted as lithified subaerial or subaqueous bedforms (Edgett and Malin 2005). The lineations do not appear to be due to the exposure of bedding planes in cross-section. If the lineations were due to the exposure of bedding planes, their orientation in plan view would correspond to the depth of erosion into the local topography, eventually becoming parallel with the beds in the wall of the canyon, similar to contours on a topographic map. This is not observed. An alternative hypothesis is that the features observed are due to preferential erosion along parallel zones of weakness. The surface does appear to be fractured, but there are no obvious larger joints running parallel to the features.

We interpret the outcrop of layered material to the west of the mound (Figure 24) as an outlying portion of the lower mound, possibly related to the dark-toned layered yardang-forming material. The outcrop appears to be an eroded pedestal crater with a morphology similar to those observed in the MFF (Kerber and Head 2010). The presence of this outcrop supports the hypothesis that the layered mound material was once more extensive and may have filled the crater.

Light-toned yardang-forming material

Observations. The light-toned yardang-forming material is a distinctive, high CTX albedo (~0.26), uncratered feature on the northwest flank of the Gale Crater mound (Figure 17). The surface of the light-toned yardang

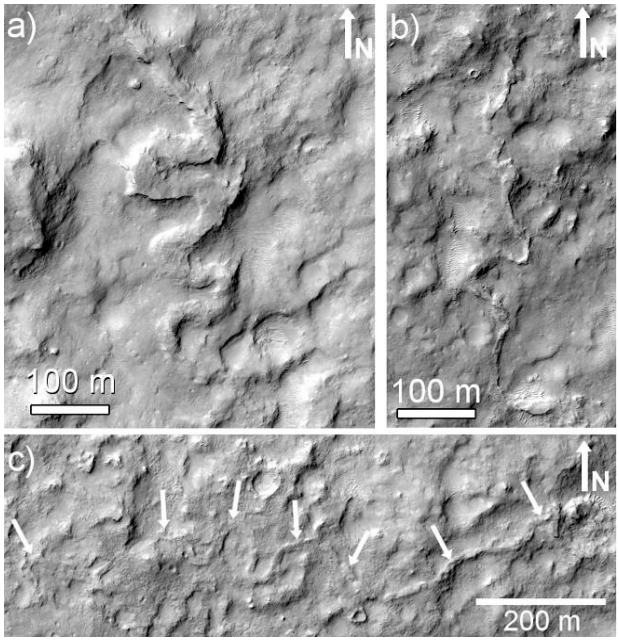

Figure 13. (a), (b) and **(c)** are three examples of sinuous ridges, interpreted to be inverted channels, in the hummocky plains unit within the landing ellipse. **(a)** has a sinuosity index of ~2, and **(b)** and **(c)** have sinuosity indices of ~1.35. All three are shown at the same scale, and are from HiRISE observation PSP_009751_1755. The inverted channels appear to have a vertical relief of several meters. Illumination is from the left. Locations: **a)** 4.404°S 137.535°E; **b)** 4.461°S 137.523°E **c)** 4.501°S 137.484°E (figure13.jpg)

material has a low-to-moderate thermal inertia (~390 J m^{-2} K^{-1} $s^{-1/2}$) and does not appear to be covered by the dust that mantles the upper mound unit and portions of other nearby units. In CTX and MOC images, the fine details of the surface texture are not visible, and the material appears to be a massive light-toned deposit, with a surface that has been eroded into yardangs. HiRISE images reveal that this material is actually very finely layered (Figure 25a), and in places parallel joints and boulders are visible. None of the joints in the light-toned yardangs show the erosional resistance observed in the lower mound.

Much of the surface of the light-toned yardang-forming material is covered with a texture of smooth, contiguous, shallow depressions (Figure 25b). Similar textures on Tharsis Montes and at White Rock in Pollack Crater have been referred to as "scalloped" (Bridges et al. 2010) and we adopt that term here. This texture occurs both on flat surfaces and slopes and high points within the light-toned yardang-forming unit. Boulders are not common on the light-toned yardang-forming unit and are typically found near outcrops with joints.

This unit has previously been noted (Malin and Edgett 2000) to lie unconformably on the darker-toned layered yardang surface, most clearly demonstrated by a crater that is partially exhumed from beneath the light-toned yardang-forming unit (Figure 26). In addition, the filled channel in the dark-toned layered yardang surface (Figure 18) may emerge from beneath the light toned yardangs (Malin and Edgett 2000).

Thomson and Bridges (2008) used MOLA tracks to fit a plane to the contact between the light-toned yardang unit and the underlying mound. They found that the best-fit plane is non-horizontal. We used a CTX stereo DEM to conduct the same exercise and found that the best fit plane has a slope of roughly 12°, similar to the slope of the mound. We calculated an approximate maximum thickness of the deposit by assuming that the best fit plane represents the surface of the underlying mound. The greatest vertical distance between that plane and the surface of the light-toned yardang unit gives a maximum thickness of ~200 m.

Interpretations. The scalloped texture of the light-toned yardang-forming material suggests that it is soft enough for aeolian erosion to scour shallow pits into the surface. However, the presence of joints and boulders in the material indicates that it is rigid enough to fracture and for fragments to retain their shape. The presence of joints also suggests that the material is old enough to have been subjected to stresses that would cause widespread fracturing, but the observed unconformity (Figure 26) shows that the light-toned yardangs are young enough that the underlying dark-toned layered yardangs had time to erode and accumulate craters before the lighter unit was deposited.

The lack of craters on the surface of the light-toned yardang-forming material itself suggests that it is either quite young, eroding rapidly, or both. The lack of dust on the surface of the light-toned yardang-forming material may also be evidence of ongoing erosion.

Although the scalloped texture sometimes appears similar to fields of small aeolian bedforms, the presence of the texture on slopes and high points is more consistent with it being the erosional expression of the rock. Bridges et al. (2010) have suggested that a similar texture may be due to the formation of bedforms by saltating dust aggregates and the erosion of a uniquely martian "duststone".

The light-toned layered yardang-forming material shows some similarities to "White Rock" in Pollack crater (-8S, 335W). White Rock is a ~12 km by ~15 km outcrop of relatively light-toned yardang-forming material first observed in Mariner 9 images (McCauley 1974) and has been studied extensively (*e.g.*, Ruff et al. 2001 and references therein). White Rock exhibits a texture similar to the "scalloped" texture discussed above (Figure 25), but does not appear to have the fine-scale layering, parallel jointing, and occasional boulder-shedding outcrops observed on the light-toned layered yardang unit, suggesting that the light-toned yardang-forming material is stronger. This is consistent with thermal inertia measurements: White Rock has a TES-derived thermal inertia of 232 ±14 J m^{-2} K^{-1} $s^{-1/2}$ (Ruff et al. 2001) which is somewhat lower than the estimated THEMIS thermal

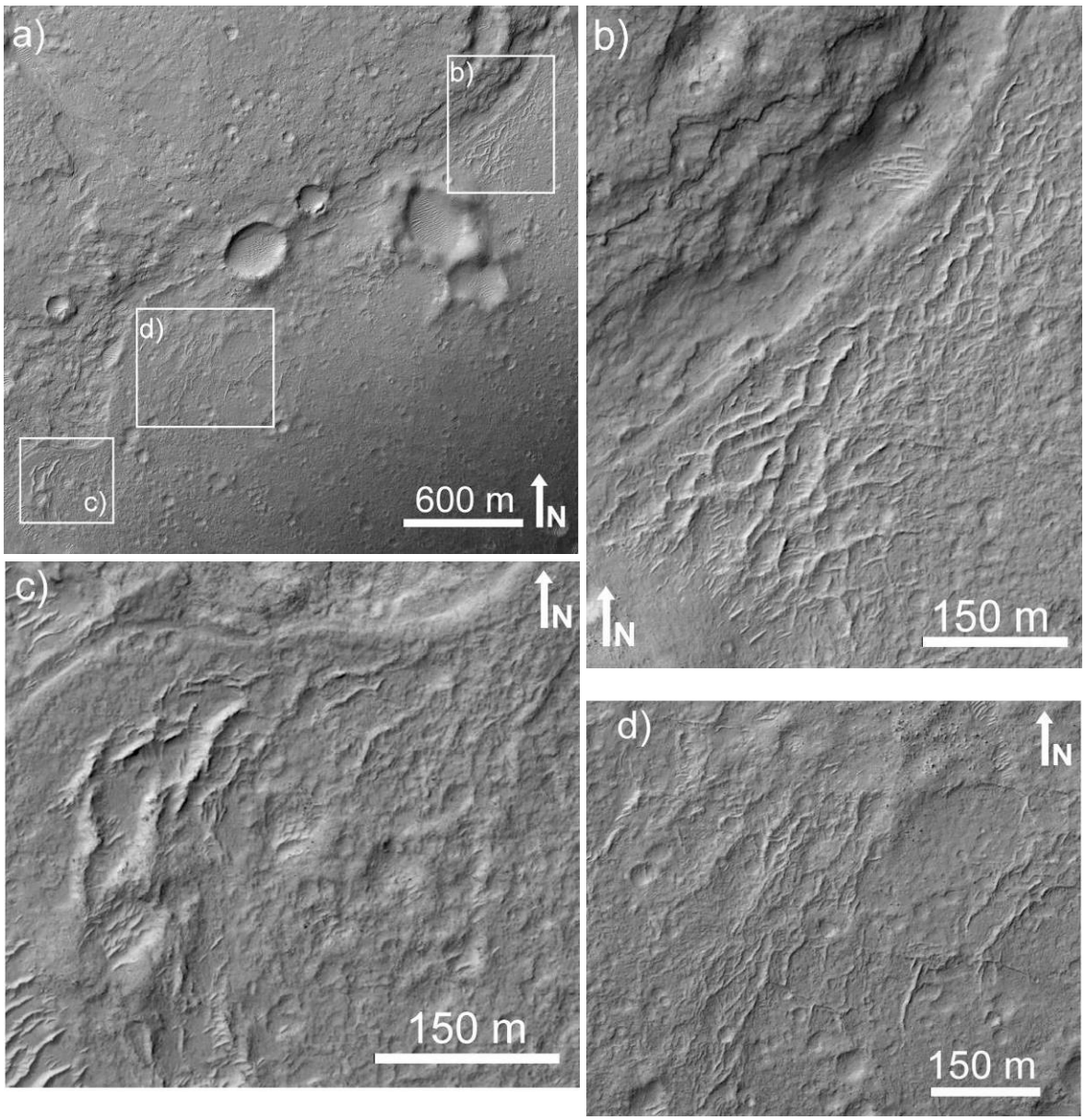

Figure 14. (a) Subframe of HiRISE observation PSP_009571_1755 showing the Gale crater floor in the eastern portion of the landing ellipse. A channel-like feature in the mound-skirting unit is flanked on its southern side by branching ridges, shown in insets **(b)**, **(c)** and **(d),** which may be inverted fluvial channels. Illumination is from the left. Location: 4.497°S 137.548°E (figure14.jpg)

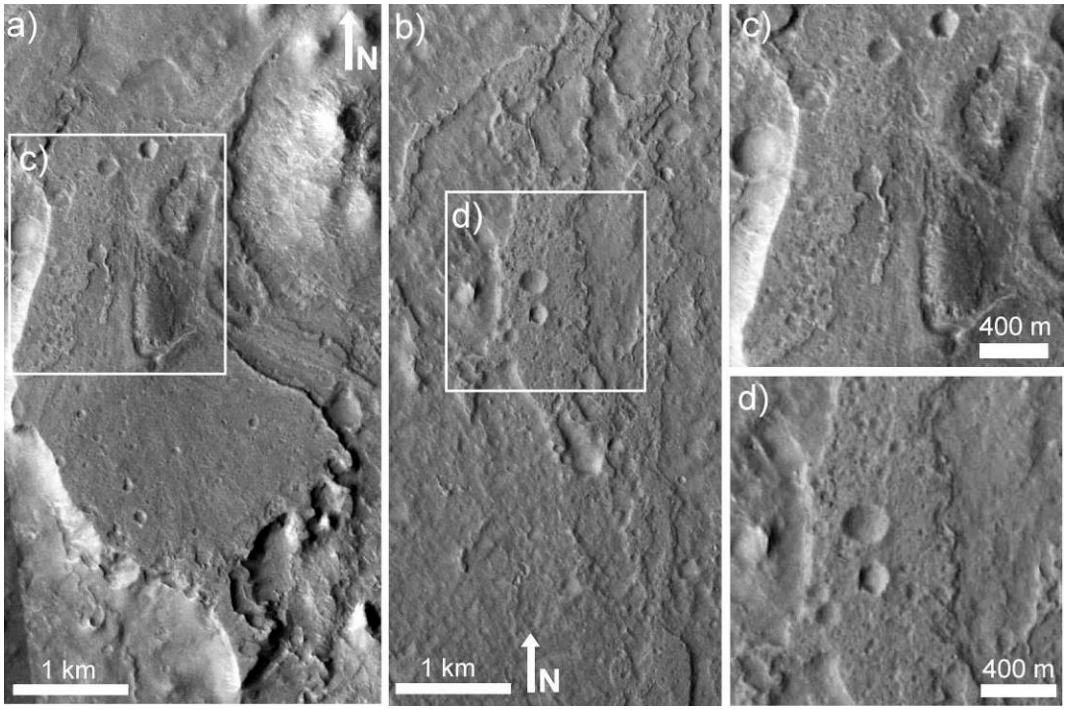

Figure 15. (a) A fan-shaped mesa (previously shown in Figure 9). **(b)** Mesas on the crater floor (see Figure 3 for context). **(c,d)** close-ups showing the texture of the mesas in **(a)** and **(b)**, respectively. Refer to Table 1 for CTX image IDs. Illumination is from the left. Locations: **a)** 4.267°S 137.835°E **b)** 4.394°S 137.948°E (figure15.jpg)

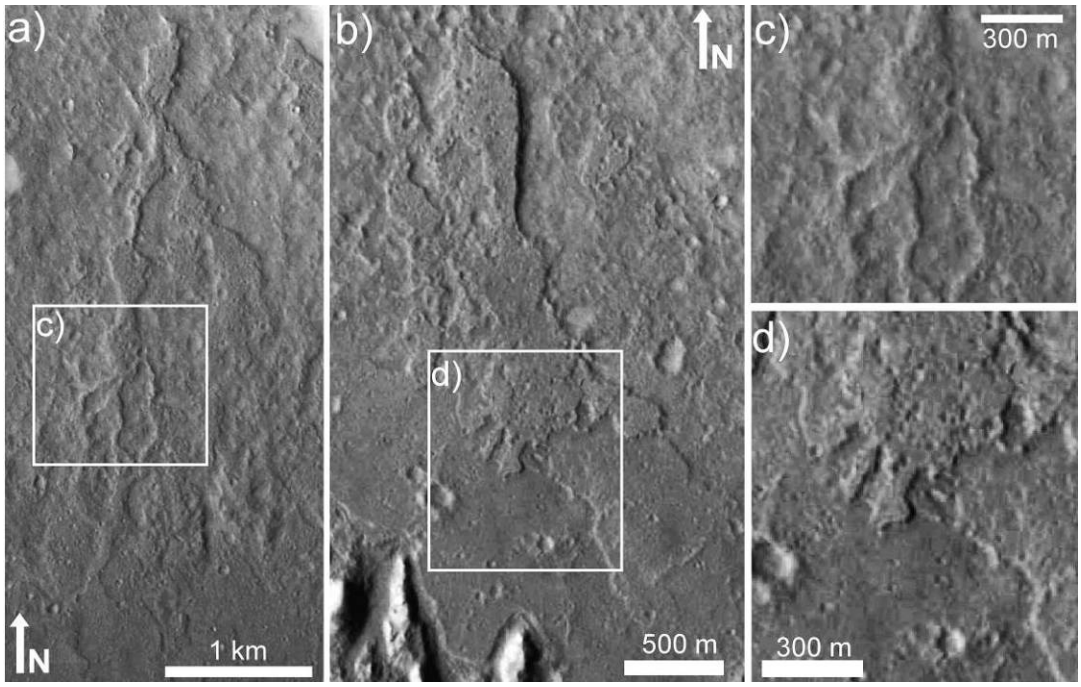

Figure 16. The mesas on the crater floor branch in a manner similar to fluvial channels, as shown in **(a)** and **(c)**. **(b)** shows a location where the mesas overlap the mound-skirting unit, which has a similar texture. Refer to Figure 3 for context. Refer to Table 1 for CTX image IDs. Illumination is from the left. Locations: **a)** 4.461°S 138.032°E **b)** 4.454°S 137.967°E (figure16.jpg)

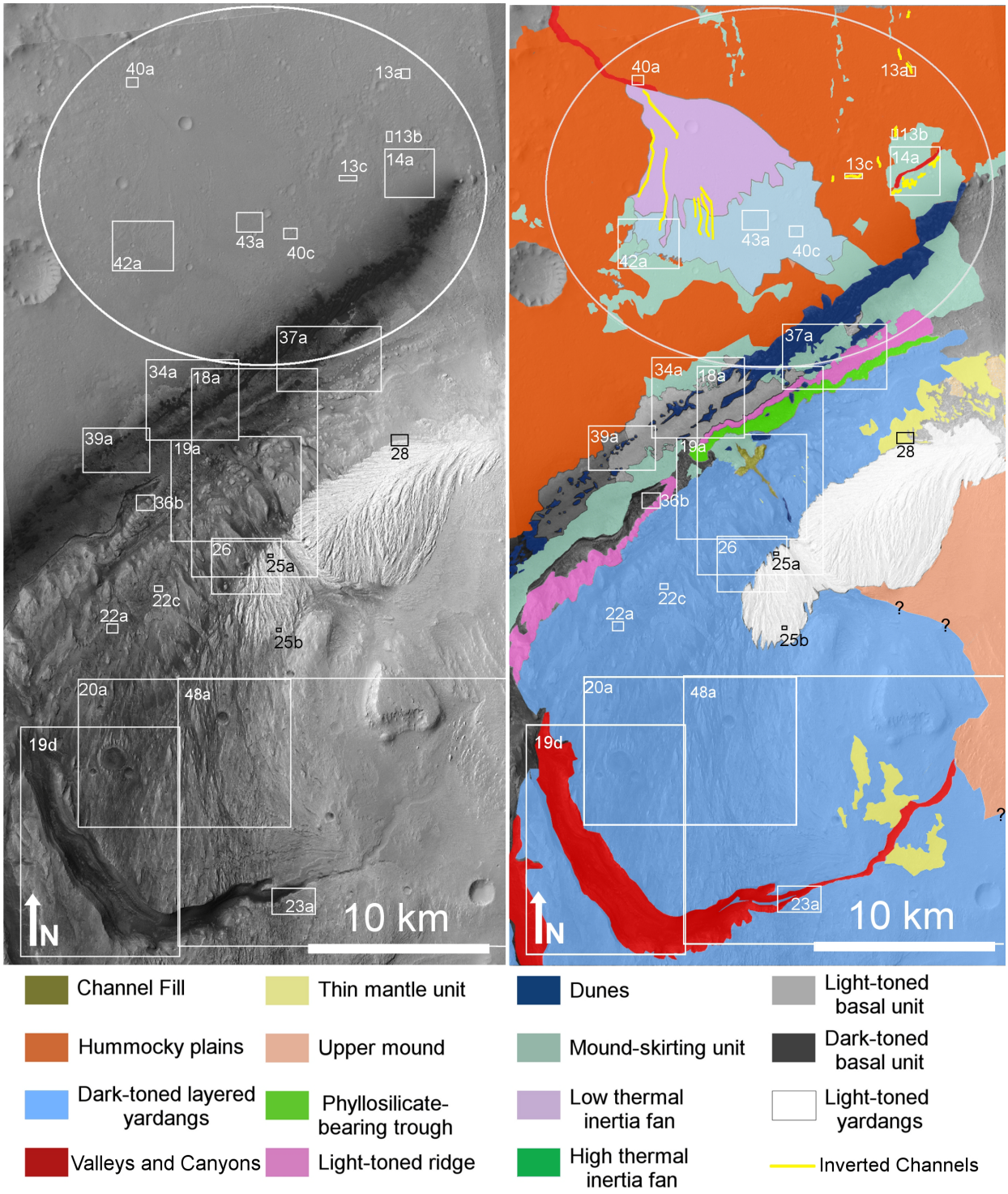

Figure 17. a) CTX mosaic of the proposed MSL landing site and northwestern mound in Gale Crater. Boxes show the location of other figures. **b)** A unit map of the same area shown in **a)**, with units identified in the key above. Elevation increases to the lower right in this map. Question marks indicate uncertainty in the boundary between the upper mound and the dark-toned layered yardangs due to aeolian bedforms obscuring the contact. Uncolored areas are "undivided" or ambiguous material. Refer to Table 1 for CTX image IDs.(figure17.jpg)

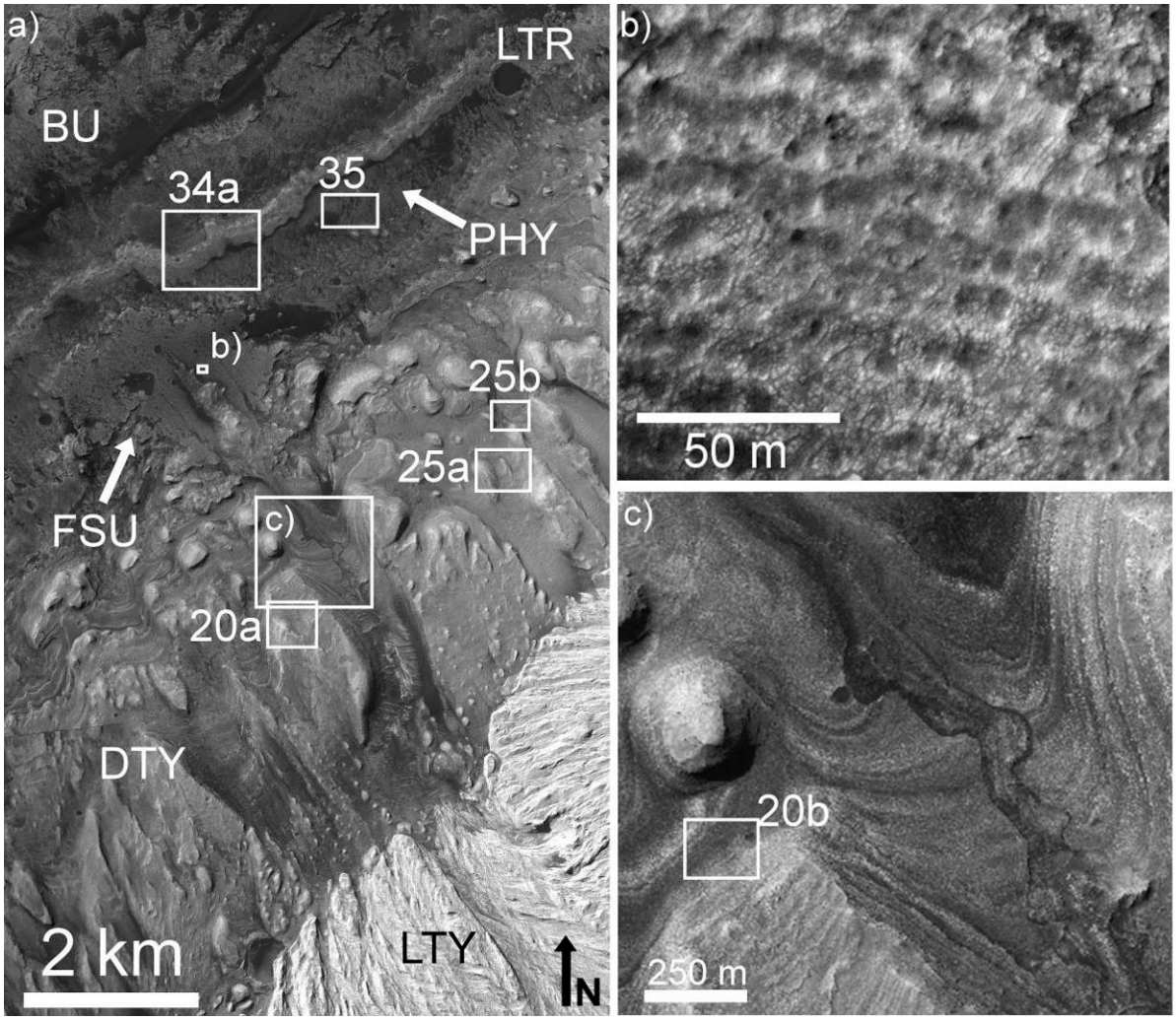

Figure 18. a) CTX and HiRISE mosaic of the area near the filled channel and outcrop of mound-skirting unit, with illumination from the left. The light-toned basal unit (BU) is in the upper left of the frame and elevation increases from -4760 to a maximum of -2800 at the lower right. The light-toned ridge (LTR), phyllosilicate-bearing trough (PHY), dark-toned layered yardang-forming material (DTY) and light-toned yardang-forming material (LTY) are all visible in this frame. **b)** A close-up of the surface of the outcrop of mound-skirting unit, showing a texture that may be due to lithified and fractured bedforms. The outcrop is associated with a filled channel, shown in **c)**, which carves the dark-toned layered yardangs. This channel was first noted by Malin and Edgett (2000). Refer to Tables 1 and 2 for CTX and HiRISE image IDs. Location: 4.770°S 137.398°E (figure18.jpg)

inertia for the light-toned yardang unit (~390 J m^{-2} K^{-1} $s^{-1/2}$). We calculate an average CTX albedo of ~0.20 for White Rock and an average albedo for the light-toned yardang unit of ~0.26. Although the two units differ somewhat in detail, the similarities in morphology between White Rock and the light-toned yardang unit may indicate a similar origin.

Thin mesa-forming material

Observations. In some locations on the mound, the underlying terrain is obscured by a thin unit that occurs primarily in isolated patches or mesas (Figure 27). This thin mesa-forming material appears to conform to pre-existing topography and occurs on both the dark-toned layered yardang-forming material of the lower mound and the upper mound unit. The thin mesa-forming material shows no obvious layering in full-resolution HiRISE images.

North of the light-toned yardang-forming material, the thin mesa-forming material is more extensive and obscures the layered nature of the mound. The thin mesas are partially overlain by aeolian deposits of the same tone, giving the surface a distinctive "feathery" appearance (Figure 28).

Interpretations. We interpret the patches of thin mesa-forming material on the mound as outcrops of a formerly more extensive unit. The material appears to lie unconformably on top of the dark-toned layered yardang-forming material and the upper mound unit. The fact that it conforms to the underlying topography leads us to speculate that it originated as an airfall deposit. Lithified

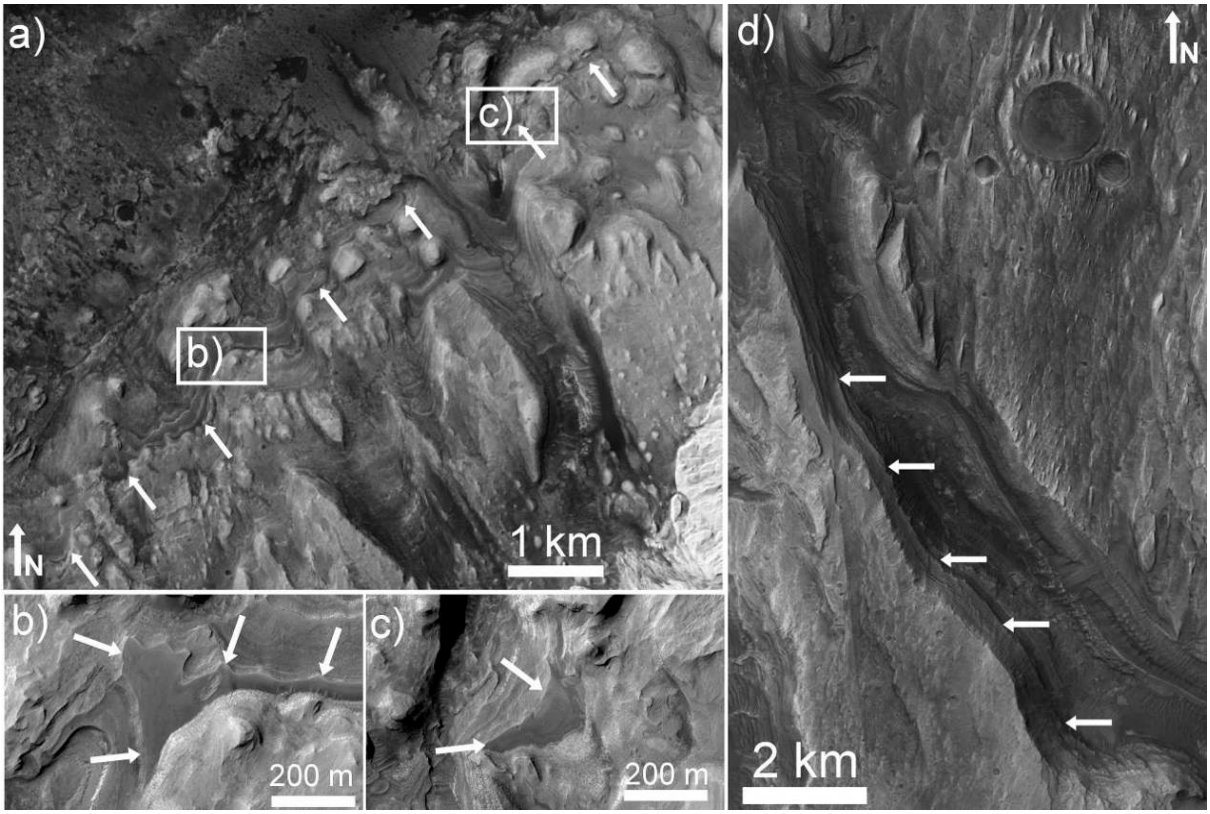

Figure 19. a) Milliken at al. (2010) identified a distinctive smooth, dark-toned "marker bed" (indicated by arrows) within the dark-toned layered yardang unit that is traceable for many km. This bed is also observed in the canyon on the western mound and in the layered outcrops of the southeastern mound. The bed is erosion resistant and preserves small craters on its surface. **b)** and **c)** show two exposures of the marker bed, several km apart. **d)** The large canyon on the western mound exposes many layers that are traceable over >10 km. Refer to Tables 1 and 2 for CTX and HiRISE Image IDs. Locations: **a)** 4.788°S 137.392°E **d)** 5.105°S 137.303°E (figure19.jpg)

aeolian materials such as pyroclastic or impact-generated dust and ash are both possible origins for the material in the thin mesa-forming deposit. The lack of layering within the thin mesa-forming material implies that it either represents a single discrete event, or is very finely layered below the limit of available imaging resolution.

Upper mound

Observations. The upper Gale mound is characterized by large, terraced packages of finely bedded layers. The edges of the packages are highly eroded (Figure 29, 30), and the upper mound generally has a uniform, relatively high CTX albedo (~0.24) and a surface with a very low thermal inertia (~300 J m^{-2} K^{-1} $s^{-1/2}$). Aeolian ripple-like bedforms with a similar albedo to the upper mound material are common, and often obscure the contact between the upper mound and the underlying units. No obviously fluvial features have been identified in HiRISE images of the upper mound unit.

Much of the upper mound has a similar "scalloped" texture to that seen on the light-toned yardangs. The texture does not appear to be controlled by topography: it occurs on smooth areas as well as rugged slopes, whereas bedforms tend to collect in depressions. Figure 31 shows an example of bedforms in a depression on the upper mound and the scalloped texture on nearby rugged terrain.

The bench portion of some of the large packages of upper mound layers exhibits a pattern of light and dark lines (Figure 30). In some locations the lines appear in concentric rings or as a sinuous pattern but in other locations, the lines in the pattern truncate others or form sharp angles. The surface of the bench where this occurs appears to be quite planar.

Interpretations. The albedo and thermal inertia of the upper mound surface have been interpreted as indicating the presence of a dust mantle (*e.g.*, Pelkey et al. 2004). Pelkey et al. (2004) have suggested that this dust mantle is due to control of local winds by the topography of the mound, but they acknowledge that detailed mesoscale modeling of wind patterns in Gale Crater is required to evaluate this hypothesis.

The scalloped texture on the upper mound, like that observed on the light-toned yardang-forming material, is similar in appearance to aeolian bedforms, but its presence on rugged slopes and outcrops implies that the texture may be due to the erosional characteristics of the upper mound material. We interpret the jagged edges of

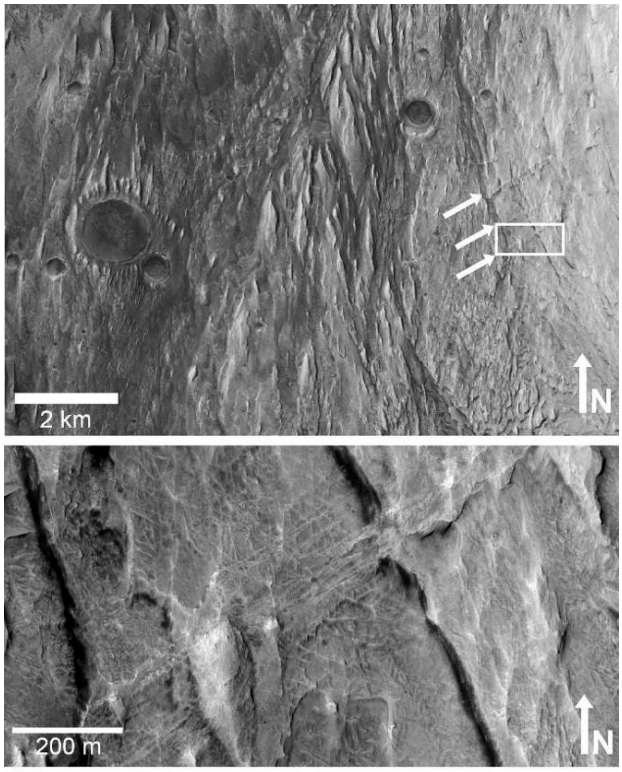

Figure 20. a) A CTX view of the dark-toned layered yardang unit. Numerous yardangs make individual layers difficult to follow. The surface shows craters many of which are eroded and may have been exhumed. On the right, several erosion-resistant fractures are marked by arrows. **b)** A HiRISE close-up of one of the large erosion-resistant fractures, revealing numerous smaller raised fractures. The larger fracture appears to be up to tens of meters high. Illumination is from the left. Refer to Tables 1 and 2 for CTX and HiRISE image IDs. Location: 5.072°S 137.303°E (figure20.jpg)

the large packages of layers in the upper mound as the result of aeolian erosion into yardang-like outcrops.

The pattern on the surface of the upper mound benches initially appears to be due to finely layered rock eroding to different depths, revealing contours by exposing the edges of layers of varying tone. However, the truncating sets of lineations and sinuous nature of many of the lines is more similar to large-scale (hundreds of meters) aeolian cross-beds than to patterns produced by the erosion of parallel layers. In addition, the generally planar nature of the surface is inconsistent with the varying depths of erosion necessary to explain the pattern if it were due to the exposure of parallel layers.

Although crossbeds are more familiar on cliff faces, they can be expressed on any plane through a cross-bedded rock, and can form very complex patterns depending on the geometry of the exposure and the original bedforms (*e.g.*, Rubin and Carter 2006). Figure 32 shows an example of a horizontal cross-section of large dunes preserved in a playa at White Sands National Monument. The exposed cross-beds and sinuous beds are smaller than those observed in the upper Gale mound, but are similar in appearance. The similarity between the observed pattern in the upper Gale Crater mound and the cross-beds exposed at White Sands leads us to speculate that the upper mound unit may have been formed by the lithification of a large aeolian dune field.

An alternative to the cross-bedding hypothesis is the deformation and erosion of previously parallel layers. This combination of processes could generate complex patterns in the upper mound material, but it would have to have deformed the small-scale beds while leaving the larger beds that form the cliff-bench layers of the upper mound intact and parallel. We therefore favor the aeolian cross-bed hypothesis.

Despite the similar "scalloped" texture, the upper mound unit appears to be distinct from the light-toned yardang-forming material. The upper mound has more prominent layering, and although the upper mound unit does form yardang-like outcrops at the edges of the largest layers, the large-scale texture formed by the yardangs is distinct from that observed on the light-toned yardang unit.

Mound-skirting unit

Observations. The mound-skirting unit is an erosion-resistant, mesa-forming material characterized by a texture that is generally smooth over hundreds of meters, but which at smaller scales is marked by numerous small (~10-60 m) pits and/or parallel ridges (Figure 33). The ridges are several meters high and occur at regular intervals of 30-50 m. Figure 7 shows a map of the occurrence of the mound-skirting unit and other units with a similar pitted or ridged texture. As with all unit maps, this grouping is a simplification: in some cases two distinct units with this texture overlap with a sharp boundary.

The mound-skirting unit generally has high thermal inertia (~720-780 J m^{-2} K^{-1} $s^{-1/2}$). However, in some locations along the base of the northern mound and on the mesas on the crater floor and near the northern rim, the thermal inertia is lower (~450 J m^{-2} K^{-1} $s^{-1/2}$) despite the unit having a similar erosional expression.

The mound-skirting unit is present on the crater floor and extends up onto the lower slopes of the mound in some locations. It typically truncates in a scarp, dropping down to the lowest units of the mound (Figure 34). On the northern crater floor (Figure 12) the groups of mesas that extend from the crater wall down to the base of the mound have a texture similar to the mound-skirting unit, as do the raised fan-shaped mesas at the base of the northern wall (Figure 15).

South of the mound, channels in the mound skirting unit transition into sinuous ridges at the unit's edge (Figure 6), and within the landing ellipse, a finely branching network of ridges occurs in the mound-skirting unit (Figure 14).

In several locations (Figure 11) material from the northwestern mound appears to extend out onto the top of

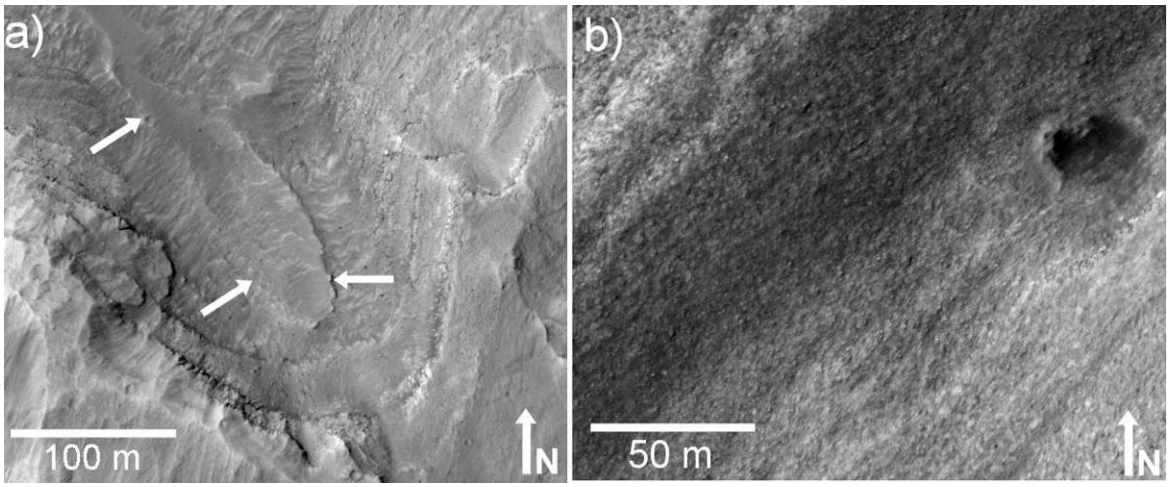

Figure 21. a) Cliff-forming, boulder-shedding layers in the dark-toned layered yardang unit. Also note the oblong patch of thin mantle unit, marked by arrows. **b)** Smooth "blurred" layers in the dark-toned layered yardang unit. In the upper right is a partially exhumed and/or heavily eroded crater. HiRISE image ID: PSP_009294_1750. Illumination is from the left. Locations: **a)** 4.796°S 137.398°E **b)** 4.787°S 137.395°E. See Figure 18 for context. (figure21.jpg)

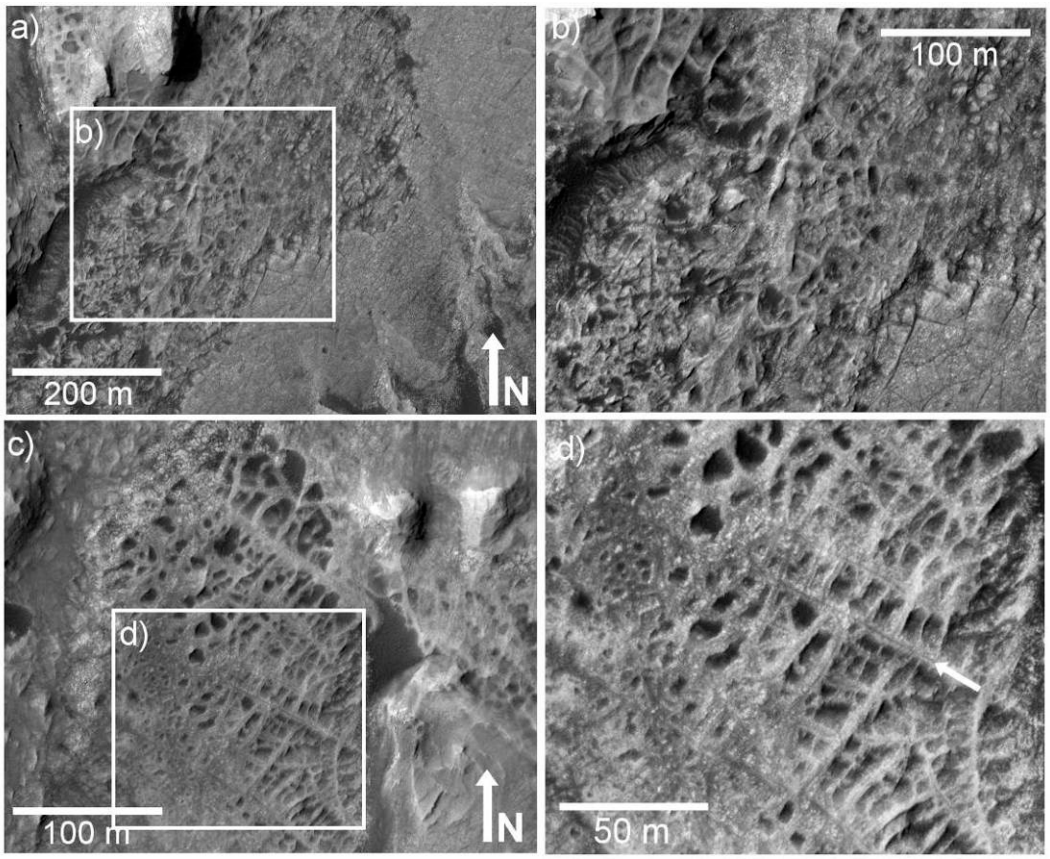

Figure 22. a) Here, a smooth but fractured surface has partially eroded away, leaving a rough surface with ridges in some places where fractures used to be, shown in a close-up in **b)**. **c)** Better-defined erosion-resistant ridges interpreted to be filled or altered fractures. **d)** is an inset of **c)**, and dark lines are visible along the center of the larger ridges (one example is marked with an arrow). HiRISE image ID: PSP_001752_1750. Illumination is from the left. Locations: **a)** 4.914°S 137.271°E **c)** 4.878°S 137.313°E (figure22.jpg)

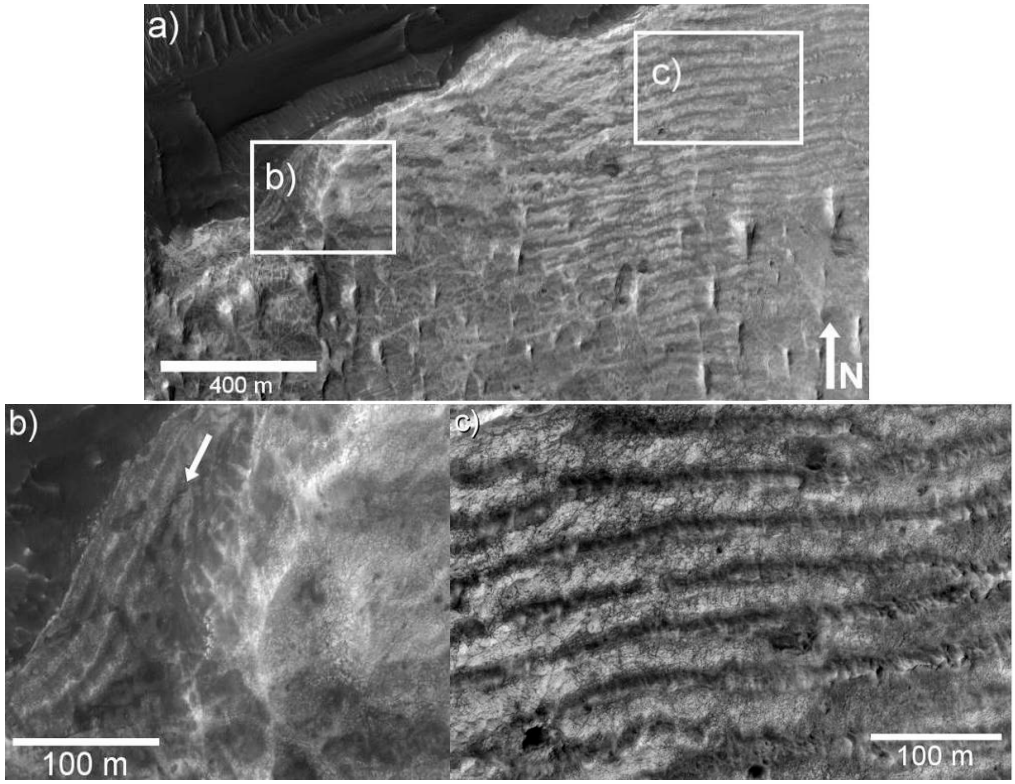

Figure 23. a) Near the end of the channel (seen at top of image) that forms the large canyon in the western mound, a lineated surface is being exposed beneath small yardangs, as first noted by Edgett and Malin (2005). **b)** Close-up, showing beds in the canyon wall. If the parallel features in **a)** and **c)** were bedding planes, their orientation in plan view would correspond to the depth of erosion, following the wall of the canyon, similar to contours on a topographic map. That they do not suggests that they are not exposed bedding planes. **c)** Close-up of the corrugated surface shows that it is extensively fractured. This figure is a subframe of HiRISE image PSP_008147_1750 with illumination from the left. Location: 5.165° S 137.430° E (figure23.jpg)

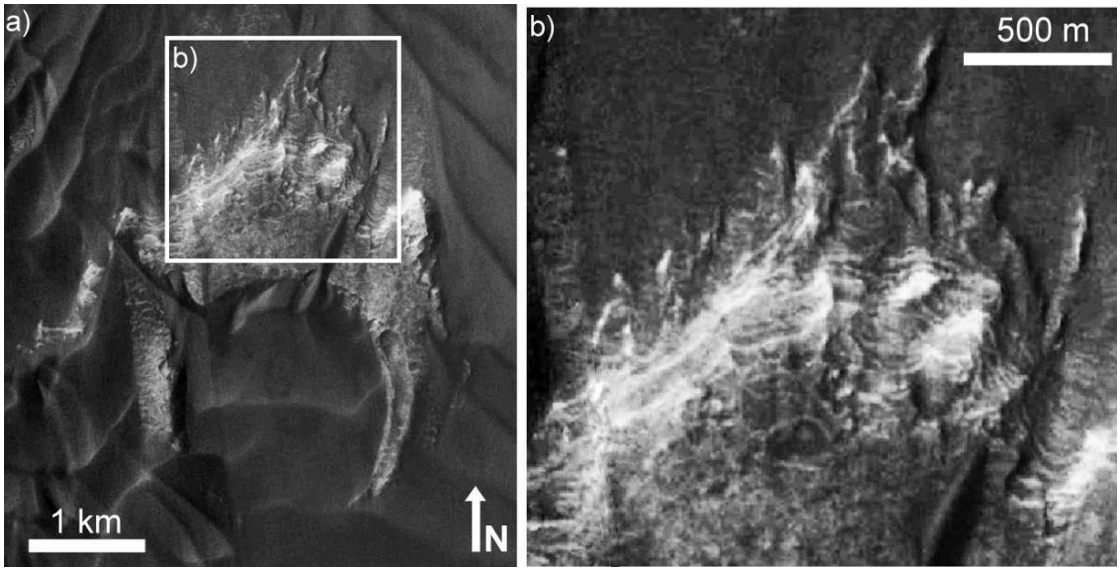

Figure 24. (a) A light-toned layered outcrop within the large dune field west of the mound supports the hypothesis that the layered mound was once much more extensive. A ~2 km crater in the outcrop is partially buried by dunes. **(b)** A close-up of the outcrop. Refer to Table 1 for CTX image IDs. Illumination is from the left. Location: 5.133°S 137.213°E (figure24.jpg)

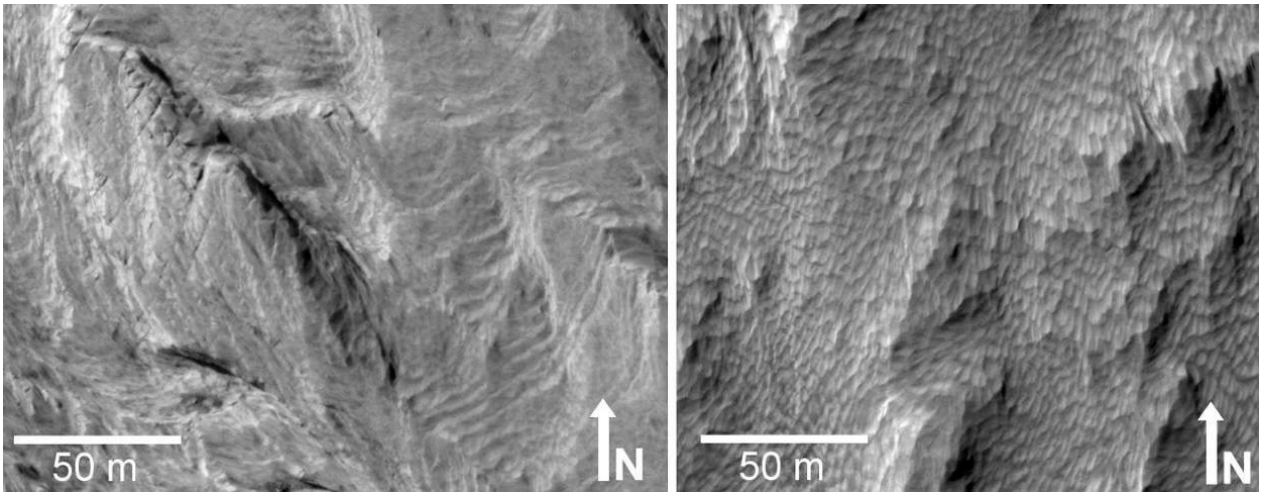

Figure 25. a) The light toned yardang unit shows very fine layering (bottom right) and numerous parallel joints in the rock (upper left). **b)** Much of the surface of the light toned yardang unit is covered with shallow hollows. Refer to Table 2 for HiRISE image IDs. Locations: a) 4.854°S 137.414°E b) 4.916°S 137.419° E (figure25.jpg)

the mound-skirting unit. These are also locations of canyons in the mound, several of which have channel- or fracture-like features in their floors or walls, cutting across the bedding of the mound.

The filled channel on the northwest flank of the mound (Figure 18) ends in a distinctive 3.5 km^2 outcrop of material with a pitted texture very similar to the mound-skirting unit. Figure 18b shows a close-up view of the surface of the outcrop, which exhibits a reticulate pattern. Milliken et al. (2008) have also noted the similarity in texture and spectral signature between this outcrop and the mound-skirting unit (Figure 33).

Interpretations. The characteristic texture of pits or ridges in an otherwise smooth surface may be due to a resistant layer developing defects which are then exploited by erosion. Erosion-resistant units tend to preserve impact craters (Edgett 2009), which may explain the numerous pits in the mound-skirting unit surface. The typically high thermal inertia suggests a coherent material, consistent with the mound-skirting unit's apparent erosion resistance. The parallel ridges that occur in the mound-skirting unit (Figure 30) may be eroded lithified bedforms, or preferential erosion along parallel joints.

The presence in some locations of multiple overlapping units with the mound-skirting unit texture (Figure 16) suggests that in some cases multiple layers with the necessary erosional characteristics are present.

The transition between channel and sinuous ridge that occurs at the edge of the mound-skirting unit south of the mound leaves little uncertainty that the sinuous ridges are inverted channels (Figure 6). We likewise interpret the finely branching ridges (Figure 14) in the landing site as inverted channel deposits.

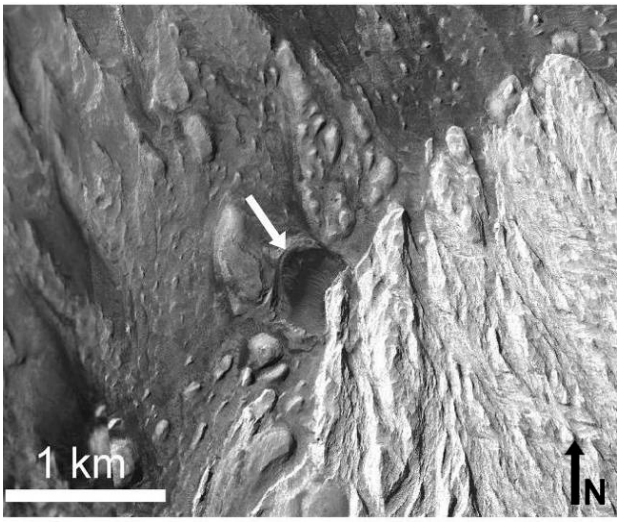

Figure 26. A crater in the dark-toned layered yardang unit is partially buried beneath the light-toned yardang unit marking an erosional unconformity previously identified by Malin and Edgett (2000). Refer to Table 1 for CTX Image IDs. Illumination is from the left. Location: 4.860°S 137.420°E (figure26.jpg)

Alternatively, it is also possible that the finely-branching raised features are erosion-resistant fractures, similar to those observed on the dark-toned layered yardang-forming unit. However, the features branch and anastomose in a manner that is more consistent with fluvial channels than with fractures.

Another possibility is that the finely-branching features are lithified aeolian bedforms, and there do appear to be small modern bedforms between some of the features. However, the features themselves appear to follow the curvature of the southern edge of a channel-like feature in the mound-skirting unit and lack the periodicity common to aeolian bedforms. In addition, thin sinuous ridges occur

that are isolated from the other ridges in the network, which would be unusual for aeolian bedforms.

The fan-shaped nature of the deposits at the base of the western mound (Figure 11) which overlap the mound-skirting unit, and their correlation with large canyons, suggests that they are debris from erosion of the mound. This provides a constraint on the time of deposition for the mound skirting unit, suggesting that the mound was still eroding after the mound-skirting unit was emplaced. The non-bedded features in the walls of the canyons may be filled channels or fractures associated with the erosion of the mound and the formation of the canyons and fans of debris.

Due to its association with the filled channel, Thomson et al. (2008) have suggested that the outcrop of material shown in Figure 18a is a depositional fan. However, this does not explain the similarity between this outcrop and the rest of the mound-skirting unit.

We suggest that the fan-shaped outcrop that is visible today is a portion of the more-extensive mound-skirting unit, and that the outcrop was buried by fan-shaped debris deposits similar to those shown in Figure 11. The debris may have protected the underlying mound-skirting unit surface from erosion but now has mostly eroded away, leaving a fan-shaped "footprint" on the preserved surface. A cartoon of this scenario is shown in Figure 35. This scenario reconciles the similarity of the outcrop to the rest of the mound-skirting unit with its location at the end of the filled channel. The reticulate pattern on the surface of this outcrop may be the result of lithified aeolian bedforms.

Light-toned ridge

Observations. The light-toned ridge is a prominent feature of the lower mound near the proposed MSL landing site (Figures 17, 18). The feature has a CTX albedo of ~0.19 with some locations as high as 0.21, and stands out against the surrounding low-albedo (~0.16) units. The surface of the unit has a relatively high thermal inertia (~600 J m^{-2} K^{-1} $s^{-1/2}$). Close inspection with the CTX DEM and HiRISE images reveals that this light-toned unit is a ridge, not simply the edge of a layer.

On its northwest side, the ridge breaks down into a >10° slope of layered, fractured light-toned rock (Figure 36) that shallows and merges with the light-toned basal unit, which is discussed in a later section. On the southeast side, the light-toned ridge ends abruptly with a short (<10 m) drop down to a trough between the ridge and the mound.

Following the light-toned ridge from its narrowest portion to the northeast, it becomes less well defined and spreads out into a broader band of light-toned layers (Figure 37a). Where it begins to spread, the ridge has a similar texture to adjacent exposures of the mound-skirting unit (Figure 37c). However, farther to the northeast, mesas of the

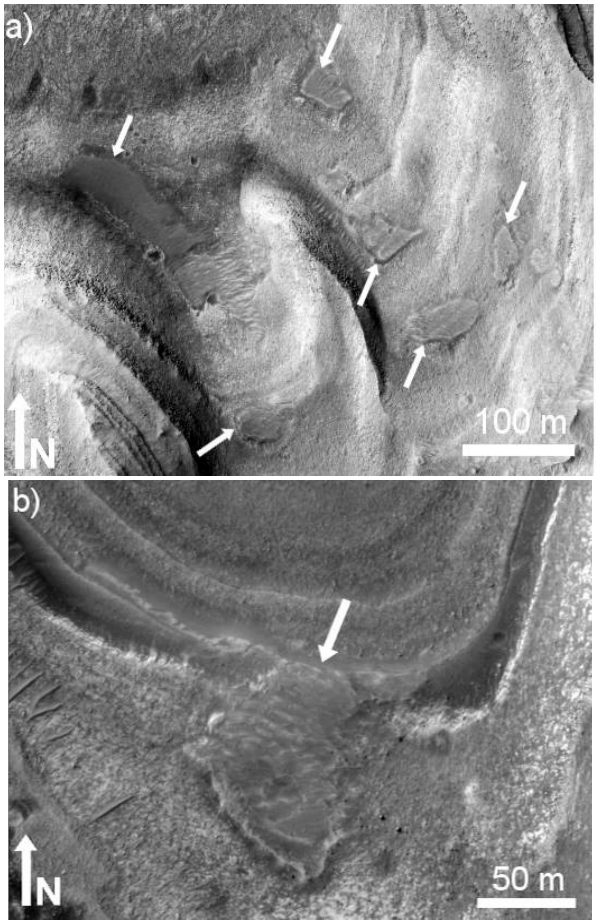

Figure 27. a) Patches of the thin mantle unit (marked by arrows) on the smooth slope of the dark-toned layered yardang unit. b) A patch of thin mantle unit obscures a layer in the dark-toned layered yardang unit. Both a) and b) are subframes of HiRISE observation PSP_009149_1750 with illumination from the left. Refer to Figure 18 for context. Locations: **a)** 4.767°S 137.436°E **b)** 4.755°S 137.441°E (figure27.jpg)

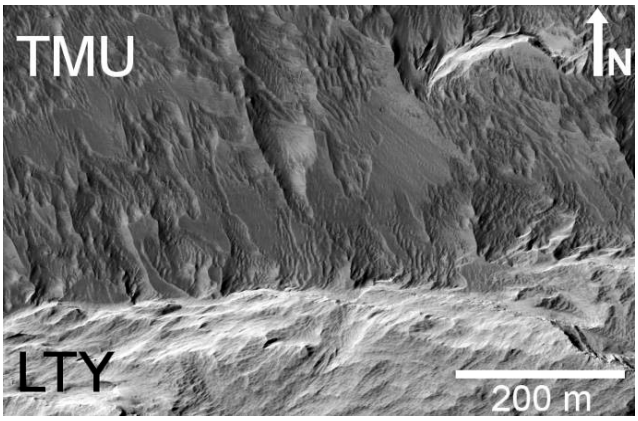

Figure 28. The thin mantle unit (TMU) has a characteristic "feathery" erosional expression, seen in the upper portion of this image. It is not clear whether the thin mantle unit is emerging from beneath or simply abuts the light-toned yardangs (LTY) in this location. This is a subframe of HiRISE observation PSP_009861_1755. Illumination is from the left. Location: 4.744°S 137.529°E (figure28.jpg)

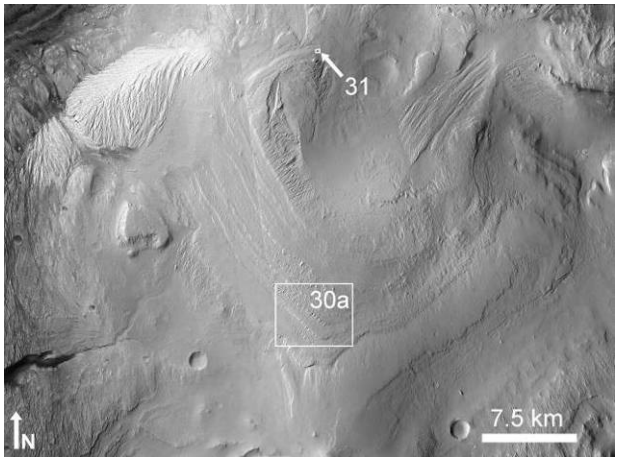

Figure 29. An overview of the layered upper mound unit. The boxes show the locations of Figures 30 and 31. Refer to Table 1 for CTX image IDs. Illumination is from the left. (figure29.jpg)

mound-skirting unit appear to overlie the light-toned layers of the broadened ridge (Figure 37b).

To the southwest of the fan-shaped outcrop of mound-skirting unit there is a gap between the edge of the mound-skirting unit and the layers of the mound. In this location, the lowest mound layers are light-toned, fractured material similar in morphology to the northwest side of the light-toned ridge (Figure 36b). The rock on the southeast side of the trough, across from the light-toned ridge is similarly light-toned and fractured.

Interpretations. The light-toned ridge appears to be part of a more extensive layer in the lower mound. We interpret the fractured light-toned outcrops on the southeast side of the trough and the light-toned outcrops to the southwest (Figure 36) as expressions of the same layer as the light-toned ridge. There is no obvious explanation for why the light-toned material eroded to form a ridge while other outcrops of the material are simply exposed as layers in the mound.

We interpret the light-toned ridge as stratigraphically lower than the mound skirting unit. Near the mesas of mound-skirting unit (Figure 37b) the ridge appears to be more extensively eroded than it is in the location where it appears similar in appearance to the mound-skirting unit (Figure 37c).

Phyllosilicate-bearing Trough

Observations. The phyllosilicate-bearing trough (mapped in Figure 17) is a depression that parallels the south-east side of the light-toned ridge, and shows a clear nontronite signature in CRISM observations (Milliken et al. 2010). The same phyllosilicate signature is not clearly visible on the opposite (northwest) side of the light-toned ridge, but a thin bed with a similar signature has been detected in the large canyon in the western mound (Milliken et al. 2010).

The trough has a slightly lower thermal inertia (~550-590 J m^{-2} K^{-1} $s^{-1/2}$) than the light-toned ridge. The surface of the material in the trough is characterized by undulating ridges (Figure 38). In some cases, the ridges share the light-toned, fractured texture typical of nearby bedrock, and dark material on the surface of the trough floor forms small aeolian bedforms with sharp boundaries.

Interpretations. The surface of the phyllosilicate-bearing trough is suggestive of aeolian bedforms (Figure 38) but we infer it to be a hard surface based on the sharp boundaries of the small dunes of dark-toned aeolian material that occur in parts of the trough floor. It is possible that the phyllosilicate-bearing unit is composed of lithified aeolian bedforms but it may also be a soft sedimentary rock that erodes in an undulating pattern. Either possibility could be consistent with the observed moderately high thermal inertia.

The lack of a matching phyllosilicate signature on the northwest side of the light-toned ridge suggests that the phyllosilicates are present only in a thin layer which is not visible on the northwest side of the ridge due to the limited resolution of CRISM. If the observed phyllosilicates do represent the exposed surface of a very thin bedding plane, dip measurements (Milliken et al. 2010) indicate that it would emerge near the base of the ridge on the northwest side.

Alternatively, the phyllosilicate-bearing material may be altered material confined to the trough. However, the presence of a thin bed with a similar phyllosilicate signature in the walls of the large western canyon (Milliken et al. 2010) leads us to favor the "thin bed" hypothesis.

Light-toned basal unit

The light-toned basal unit is distinguished from the crater floor units by a sharp drop of ~10 m (Figure 34a). The light-toned basal unit has a CTX albedo of up to 0.20, and is primarily composed of fractured rock that in some locations has a subtle texture suggestive of layering (Figure 39b). It has a moderate thermal inertia ranging from roughly 500-540 J m^{-2} K^{-1} $s^{-1/2}$. Mesas of mound-skirting unit are common on top of the light-toned basal unit (Figure 34b), and much of the basal unit is covered by dark-toned mafic dunes. The light-toned basal unit slopes upward in a series of poorly-defined fractured, light-toned layers to form the northwestern side of the light-toned ridge unit (Figure 36a).

Dark-toned basal unit

The dark-toned basal unit (Figure 39) has a higher thermal inertia (~780 J m^{-2} K^{-1} $s^{-1/2}$) than the light-toned basal unit. It has an albedo of 0.15-0.16 and occurs to the southwest of the landing ellipse and the light-toned basal unit. The transition between the light and dark-toned basal units (Figure 40) is sharp and the dark-toned basal unit appears to be topographically lower than the light-toned

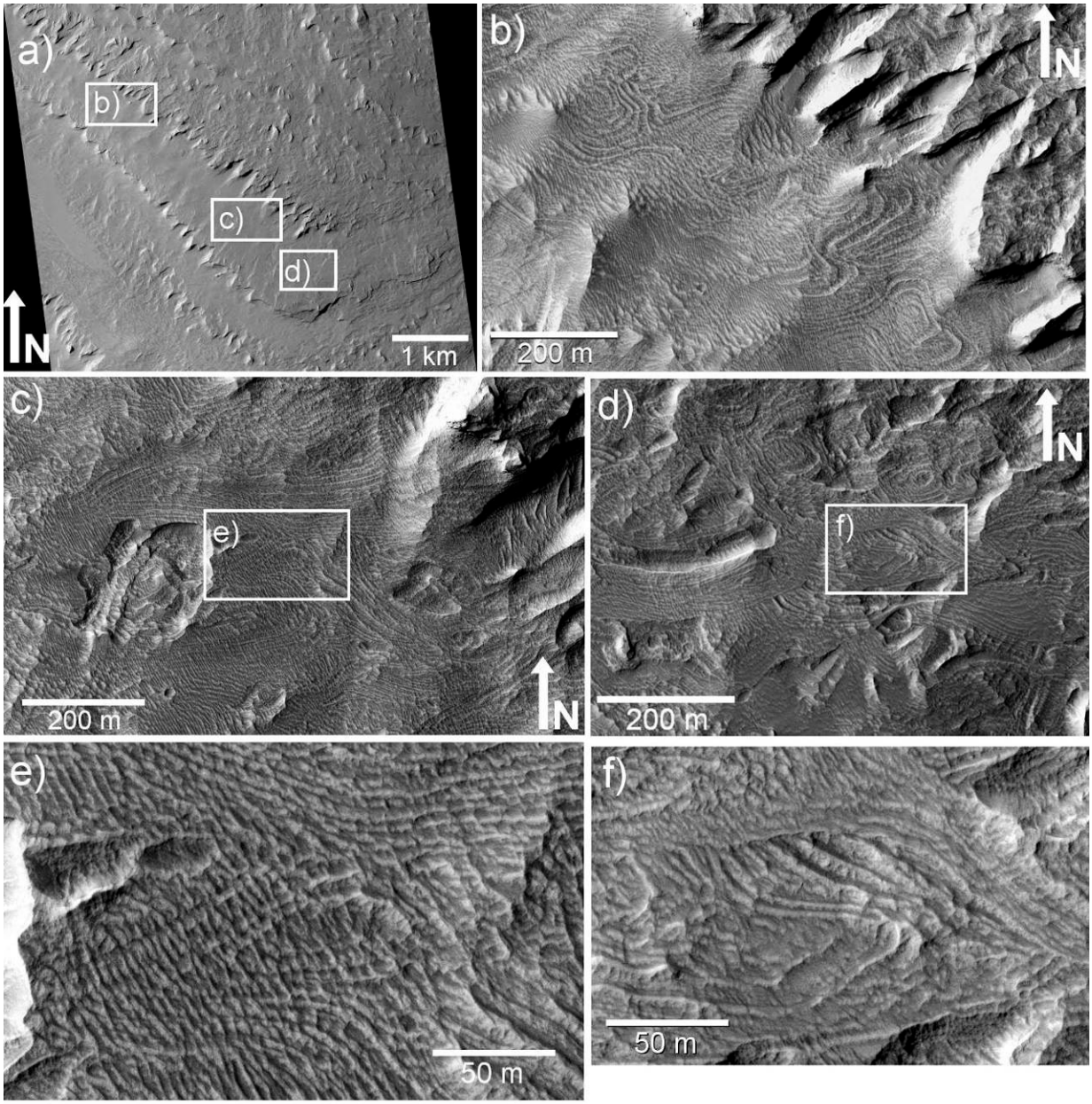

Figure 30. a) A view of the large, cliff-bench packages of layers of the upper mound (see figure 29 for context). The cliffs have been eroded by the wind into yardangs. The white rectangles indicate the locations of **b)**,**c)** and **d)**. **b)** The surface texture of the "bench" portion of the upper mound. Here it forms concentric rings, separated by bands that "pinch" together. **c)** Another location on the bench of an upper mound layer, exhibiting bands that appear to "zig-zag", as shown in **e)**. **d)** A third location, with curved groups of bands that truncate each other, similar to aeolian crossbeds. **f)** is a close-up of the potential crossbeds in **d)**. All frames in this figure are from HiRISE image PSP_001620_1750. Illumination is from the left. Locations: **b)** 5.063°S 137.726°E **c,e)** 5.087°S 137.753°E **d,f)** 5.098°S 137.767°E (figure30.jpg)

basal unit. This suggests that it is either stratigraphically lower or that the dark-toned unit is younger and fills a depression that had been eroded into the light-toned basal unit.

Hummocky plains unit

Observations. Much of the crater floor near the proposed landing site is a hummocky terrain of smoothly-varying thermal inertia (~480 J m^{-2} K^{-1} $s^{-1/2}$). It has a uniform CTX albedo (~0.21) similar to other units in the northern crater floor. In locations in which the surface has a lower thermal inertia, this unit has a subdued appearance (Figure 13). In locations with higher thermal inertia, the unit appears more rugged and in some cases is marked by light-toned polygons (Figure 40).

Sinuous ridges are visible in several locations on the hummocky plains unit (Figure 13). They occur on a very

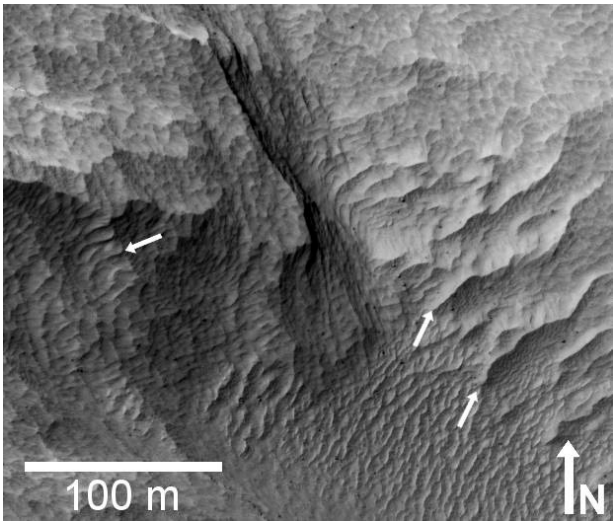

Figure 31. The upper mound unit has a "scalloped" texture similar to that observed on the light-toned yardang unit (Figure 25). The texture does not appear to be controlled by topography and occurs even on rugged slopes (for example, the location marked by the leftmost arrow), as shown in the left portion of this image. On the right, aeolian bedforms (marked by arrows) are collected in a depression. This image is a subframe of HiRISE observation PSP_009927_1750. Location: 4.732°S 137.756°E (figure31.jpg)

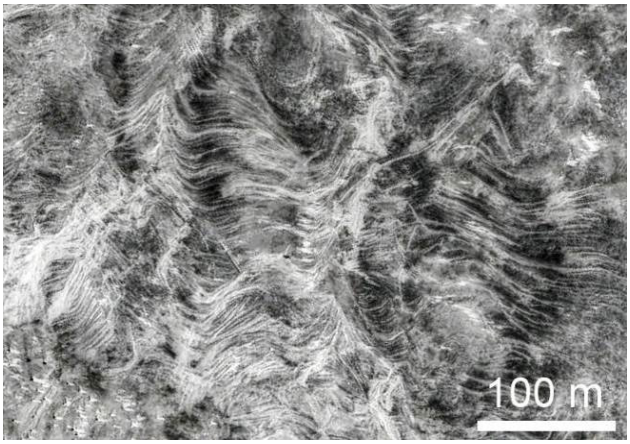

Figure 32. A contrast-enhanced example of crossbeds and sinuous patterns exposed in a playa at White Sands National Monument (32.818°N 253.679°E). The dry upper portion of the dunes has been removed by wind, revealing a horizontal cross-section through the lower moisture-immobilized portion of the dunes. The exposed beds are similar in appearance to the patterns shown in Figure 30. Image credit: USFWS/DigitalGlobe/Google (figure31.jpg)

shallow (~1°) slope and have a vertical relief of several meters.

Interpretations. The variable thermal inertia of the hummocky plains unit is likely due to varying degrees of mantling with unconsolidated material. The polygonal markings in high thermal inertia locations may be fractures, similar to the erosion-resistant fractures observed on the dark-toned layered yardang-forming unit, although less pronounced.

We interpret the sinuous ridges on the hummocky plains as inverted channels. Their sinuous nature and low slope are consistent with formation by slow-flowing water. These inverted channels also imply that the crater floor was once buried and has been eroded by at least their current height, but they do not constrain the maximum burial depth.

Northwestern fan-shaped feature

Observations. The proposed MSL landing site in Gale Crater is centered on a large (80.4 km^2) fan-shaped feature, the apex of which coincides with the end of a dendritic valley network on the northern crater wall (Figures 8a, 41). The fan-shaped feature can be divided into two units: a smooth, lower thermal inertia (~460 J m^{-2} K^{-1} $s^{-1/2}$) unit that extends from the apex of the fan down to about two thirds of the way to the distal margin, and a rockier, high thermal inertia (~620 J m^{-2} K^{-1} $s^{-1/2}$) unit that forms the distal end of the feature (Figure 41). Mesas similar to the outcrops of mound-skirting unit seen elsewhere on the crater floor partially trace the borders of the fan and occur in the middle of the smooth low thermal inertia unit, The western distal end of the fan is marked by many ridges that are roughly aligned north-to-south (Figure 42). These ridges make the boundary of the western edge of the fan difficult to define precisely.

The smooth, low thermal inertia fan unit, seen in the bottom half of Figure 40a, has a subdued, mantled texture. It has many hollows which are typically filled with a smooth light-toned material.

The high thermal inertia portions of the fan-shaped unit are layered, fractured material. Evidence of layering can be seen in the walls of craters within the unit (*e.g.*, Figure 40d). Where the fan-shaped feature transitions from low to high thermal inertia, the surface becomes rockier and less mantled. Much of the high thermal inertia unit is a distinct lower stratigraphic layer, marked by a sharp ~10 m drop. However, in many locations the thermal inertia of the terrain increases even before the drop down to the stratigraphically lower unit. In patches of the smoother surface, particularly near the transition to higher thermal inertia, the smoother surface exhibits polygonal features similar in scale to the fractures in the high thermal inertia material (Figure 43).

Interpretations. We interpret the northwestern fan-shaped feature as a lithified alluvial fan, based on its shape and its position at the end of a branching valley on the northwestern crater wall. The roughly flow-aligned ridges in the western portion of the fan may be inverted channels or remnants of debris flow lobes.

The pits in the smooth low thermal inertia fan unit may be impact craters, filled by dust or other unconsolidated, sediment. The polygonal features in the low thermal inertia fan suggest that it is either rigid enough to fracture,

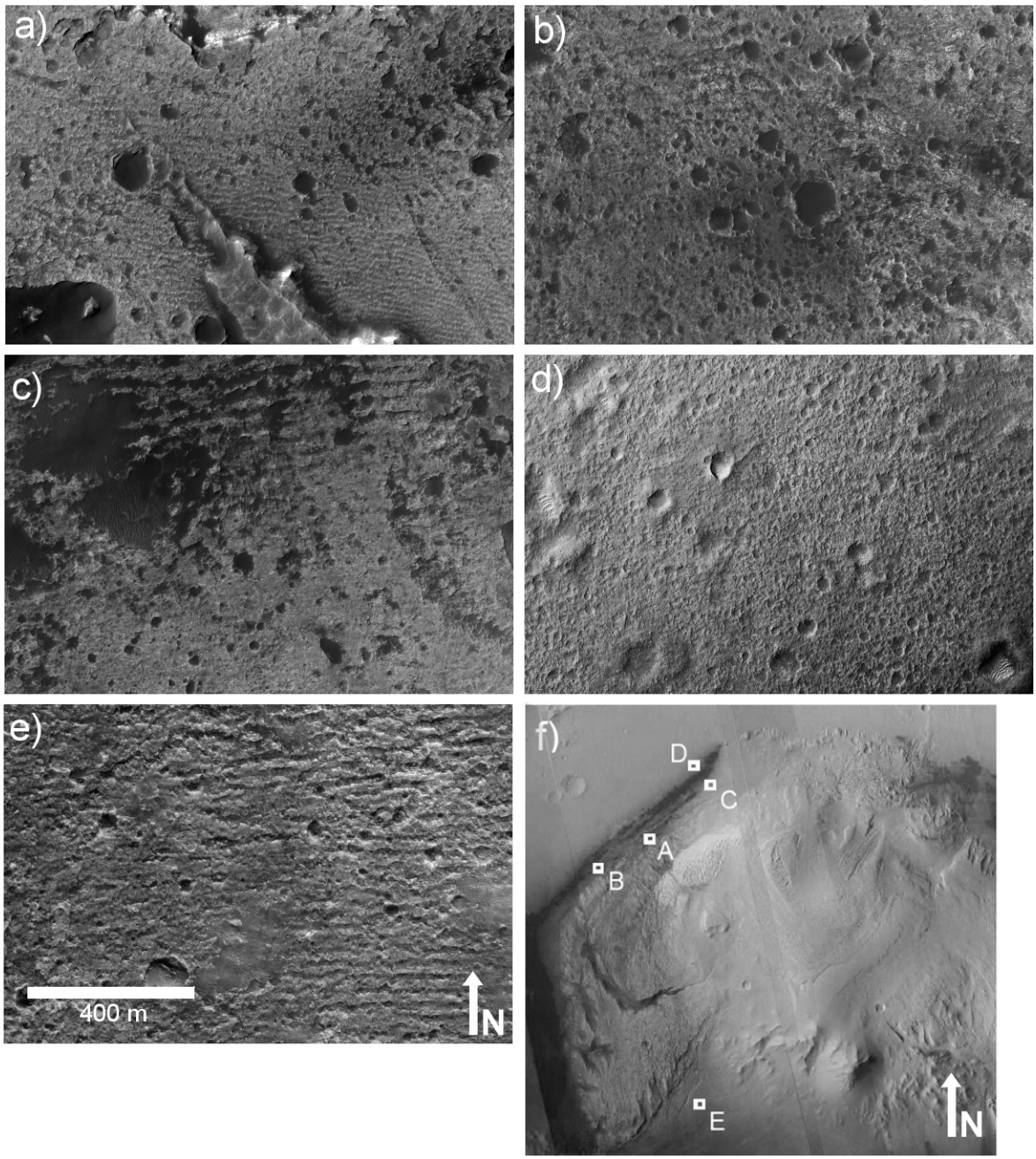

Figure 33. HiRISE images of the mound-skirting unit, all shown at the same scale, with illumination from the left. **a)** The fan-shaped outcrop of mound-skirting unit (see text for discussion). **b)** Several kilometers southwest of **a). c)** A similar texture to the northeast of **a)** transitions into a "washboard" texture of long parallel ridges. **d)** The same pitted texture appears farther out on the crater floor. It is less obvious because these pits are not filled with dark material. **e)** The "washboard" and pitted texture also appears to the south of the mound. **f)** A CTX mosaic showing the locations of **a-e).** Refer to Table 1 for CTX image IDs and Table 2 for HiRISE image IDs. Locations: **a)** 4.749°S 137.381°E **b)** 4.794°S 137.266°E **c)** 4.617°S 137.510°E **d)** 4.580°S 137.490°E **e)** 5.490°S 137.497°E (figure33.jpg)

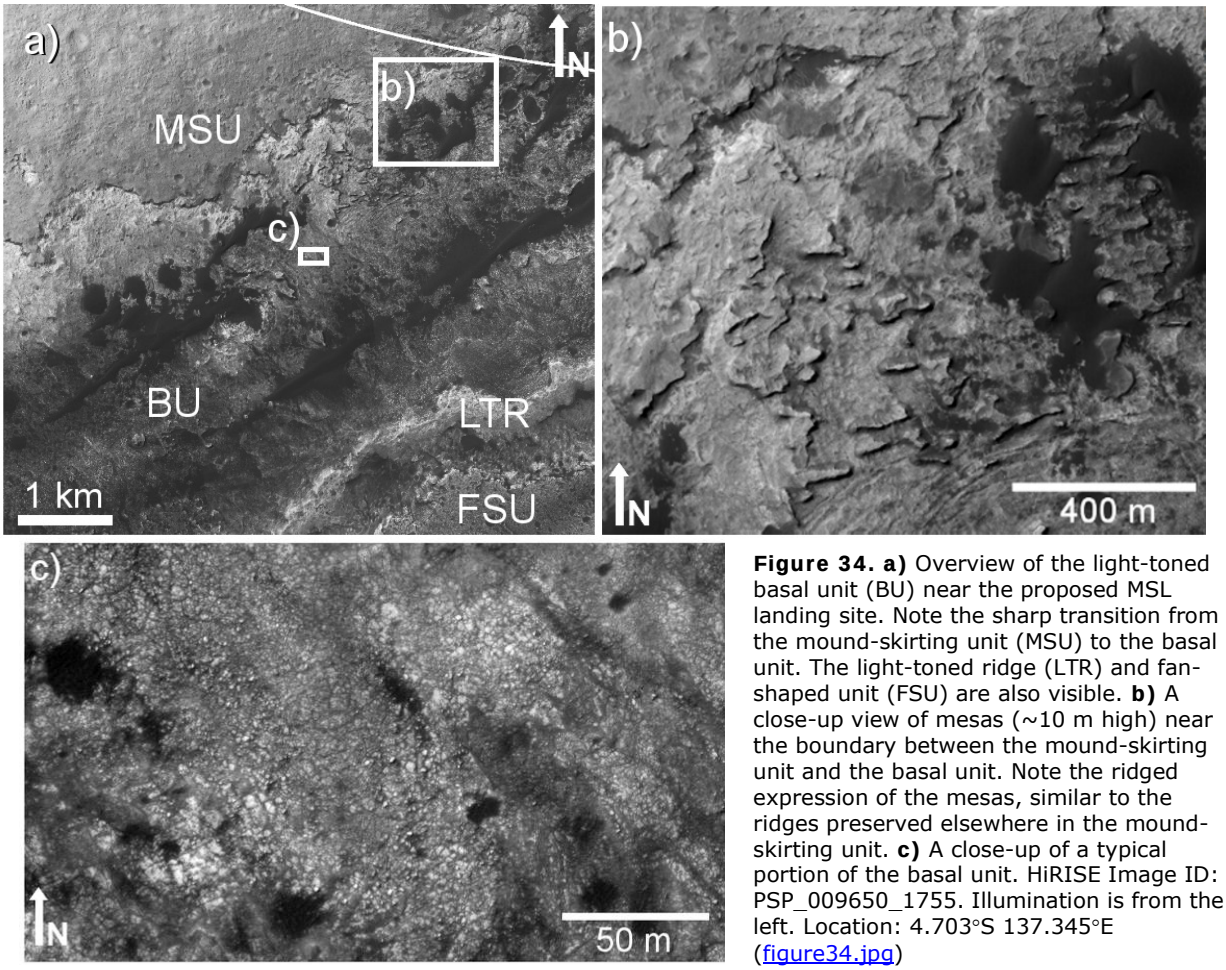

Figure 34. a) Overview of the light-toned basal unit (BU) near the proposed MSL landing site. Note the sharp transition from the mound-skirting unit (MSU) to the basal unit. The light-toned ridge (LTR) and fan-shaped unit (FSU) are also visible. **b)** A close-up view of mesas (~10 m high) near the boundary between the mound-skirting unit and the basal unit. Note the ridged expression of the mesas, similar to the ridges preserved elsewhere in the mound-skirting unit. **c)** A close-up of a typical portion of the basal unit. HiRISE Image ID: PSP_009650_1755. Illumination is from the left. Location: 4.703°S 137.345°E (figure34.jpg)

or that it is a thin (less than a few meters) unconsolidated material settling and filling cracks in the underlying high-thermal inertia material (Figure 43). Alternatively, the observed cracks could be due to volume changes in the "smooth fan" unit, such as those due to desiccation or periglacial activity. However the similarity in scale of the fractures in the smooth unit to those in the high thermal inertia fan (Figure 43) and the low thermal inertia of the smooth fan unit leads us to favor the interpretation of the low thermal inertia portion of the fan as a thin layer obscuring the high thermal inertia fan. We interpret the sharp drop that occurs near the transition in thermal inertia as the result of scarp retreat caused by the erosion of the smooth fan and an upper layer of high thermal inertia fan, exposing another underlying high thermal inertia layer.

Lobate features

Observations. Several large lobate features extend down the northern flanks of the Gale Crater mound (Figure 44). Closer inspection in MOC images reveals that these features are at least coarsely layered, with a continuous sharply defined layer apparent in Figure 45. Most of the lobate features have a relatively uniform width of 1-2 km for their entire length, an approximate thickness of hundreds of meters, and have a convex surface topography with well-defined edges. The uniform-width lobes do not extend all the way down the slope of the mound. The lobate features have slopes typical of the large-scale slope of the mound (~15°), and a moderate thermal inertia (~460 J m^{-2} K^{-1} $s^{-1/2}$).

The HRSC elevation data do not have a high enough resolution to determine the slope at the end of the lobate deposits, but MOC and CTX images show an abrupt drop at the end of the deposits that may be as steep as the angle of repose for dry, granular material. There are not obvious boulders on the surface of the lobate features in the available MOC images.

The largest, easternmost lobate feature is fan-shaped. It begins with a narrow concave "neck" with a width of ~1.8 km, sharply defined by a narrow ridge on the western side and a large (several hundred meters) cliff on the eastern side. The "neck" extends from a large alcove in the mound and is partly obscured by yardang-forming material and has a low thermal inertia (~360 J m^{-2} K^{-1} $s^{-1/2}$). The "neck" appears to truncate an outcrop of material on its western side. The fan-shaped lobate feature has a break in slope from ~15° to ~5° within its narrow portion, and begins to broaden ~1.5 km downhill from that point.

The fan-shaped portion has a rugged, chaotic texture, with roughly aligned ridges and depressions. The average

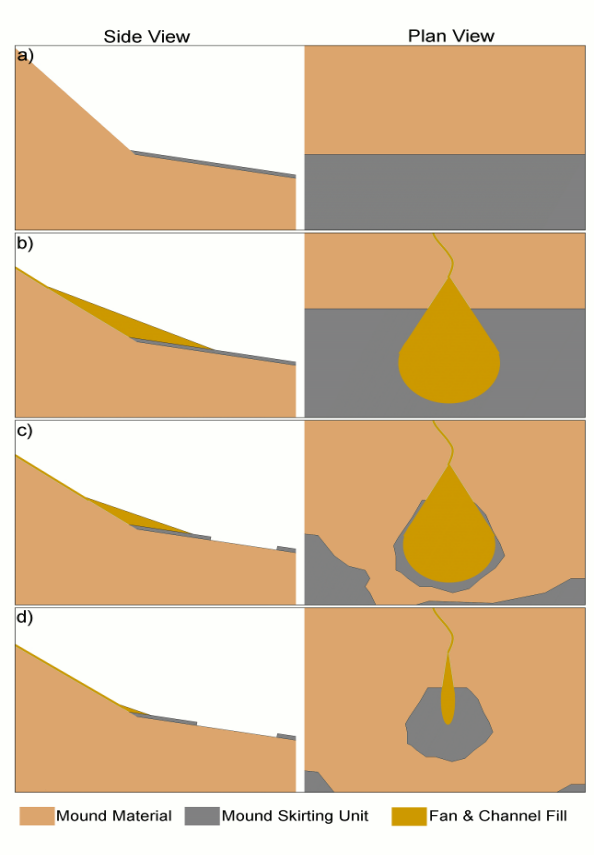

Figure 35. A cartoon showing our hypothesis for the origin of the fan-shaped unit discussed in Section 5.7. The left column shows a cross-sectional view and the right column shows a plan view. **a)** The mound-skirting unit extends part of the way up the layered mound material. **b)** The mound is eroded and a channel transports debris down slope and deposits it as a fan on top of the mound-skirting unit, similar to the fans observed elsewhere (Figure 11). **c)** Erosion causes the fan to shrink and the boundary of the mound-skirting unit to recede. **d)** Continued erosion removes most of the fan material, exposing a patch of the mound-skirting unit that has been protected by the fan. (figure35.gif)

thermal inertia of the fan-shaped portion of the easternmost lobate feature is ~470 J m^{-2} K^{-1} $s^{-1/2}$. At the edge of the feature, the thermal inertia increases to >670 J m^{-2} K^{-1} $s^{-1/2}$ and the texture becomes dominated by streamlined mesas and troughs. Closer inspection of the high thermal inertia surface reveals several apparent faults (Figure 46).

Interpretations. The lobate features may be the result of large landslides or debris flows, in which case the fact that the uniform-width features do not extend all the way to the crater floor could be attributed to limited debris supply. It is also possible that the features terminate at the former base of the slope, but the crater floor has been significantly eroded since their formation.

The erosion-resistant layer visible on the uniform-width lobate features (Figure 45) could be explained by multiple, superimposed flow events, but the vertical thickness of the lobes would make it unlikely for individual flows to follow the same path repeatedly. Alternatively, the landslide or debris flow deposits could form only the upper erosion-resistant layer, and the thickness of the lobes could be due to that layer preventing erosion of the underlying material. The erosion-resistance may be due to post-landslide cementation, possibly associated with burial if the landslide occurred prior to a period of net deposition in Gale Crater.

The apparent truncation of material by the neck of the fan-shaped lobate feature suggests that the process that deposited the feature was erosive, or that the truncated material was deposited against an obstacle that has since eroded away. The presence of yardang-forming material overlapping the neck of the fan-shaped lobate feature implies that the feature was once buried and has been exhumed.

The lobate features also are similar in morphology to terrestrial rock glaciers, although the evidence for burial beneath yardang-forming material implies that if the lobate features were glacial in origin, any ice would likely be gone. Figure 2 in Whalley and Azizi (2003) shows an illustration of rock glacier morphology. Rock glaciers are characterized by their "tongue-like" or lobate appearance, may have ridges and furrows on their surface, and terminate with a steep front at the angle of repose (Whalley and Azizi 2003). The uniform-width lobate features are most similar to the "tongue-shaped" rock glacier in the figure, although they do not originate in any obvious cirque.

The fan-shaped lobate feature does originate in an alcove on the mound, and most resembles the "piedmont or spatulate" rock glacier morphology in Figure 2 in Whalley and Azizi 2003. The texture within the fan-shaped feature is similar to pressure ridges, and is consistent with a viscous, glacier-like flow.

The lobate features appear to lack the boulders that would be expected if they were rock glaciers, though this may be due to the limited resolution of MOC and CTX. The lobate features could also be mantled with younger material that obscures the individual boulders. Another weakness in the rock-glacier hypothesis is the apparent erosion-resistant layer in the uniform-width lobate features. If these deposits were rock glaciers, and therefore composed of boulders, it would be difficult to form the sharp cliff observed.

If the lobate fan-shaped feature has a glacial or periglacial origin, the streamlined texture of the fan-shaped lobate feature may be related to melting of interstitial ice. Flow of meltwater from the deposit could have carved the observed streamlined features. Alternatively, if the fan-shaped feature was deposited during or prior to a period of fluvial activity at Gale Crater, the observed texture could be due to erosion during that period. The texture of the lobate fan-shaped feature could also be related to

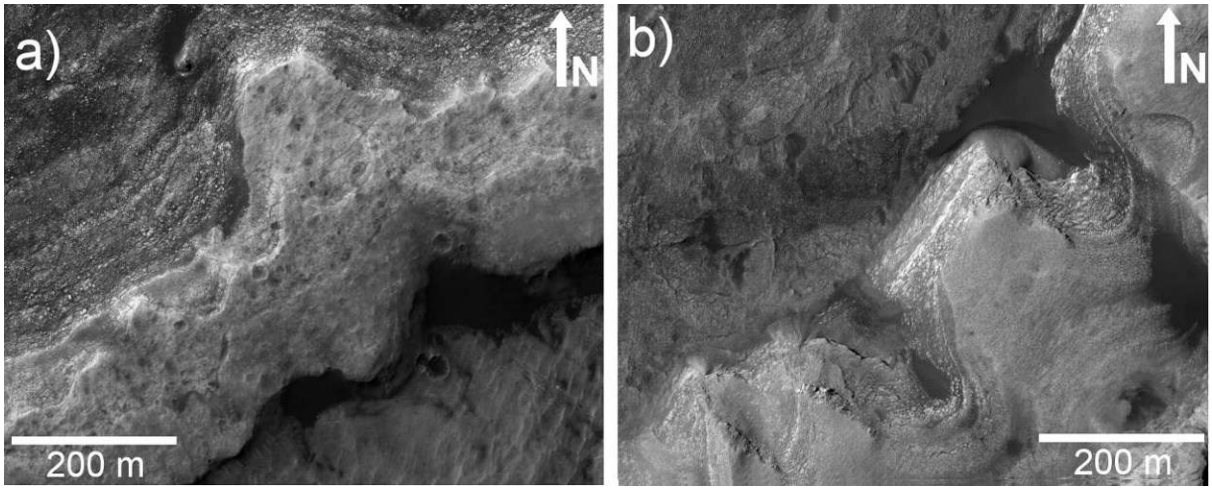

Figure 36. a) HiRISE close-up of the light-toned ridge unit. On the northwest side the ridge forms a rapidly shallowing slope comprised of fractured light-toned layers and their erosional debris. On the southeast side the ridge ends abruptly with a drop of 5 to 10 meters down to the phyllosilicate-bearing unit, detected by Milliken *et al.* (2009). **b)** Light toned layers to the southwest of **a)** exposed in a gap between the mound-skirting unit and the wall. It is possible that these are a continuation of the same material that forms the light-toned ridge. Refer to Table 2 for HiRISE image IDs. Illumination is from the left. Locations: **a)** 4.722°S 137.383°E **b)** 4.799°S 137.301°E (figure36.jpg)

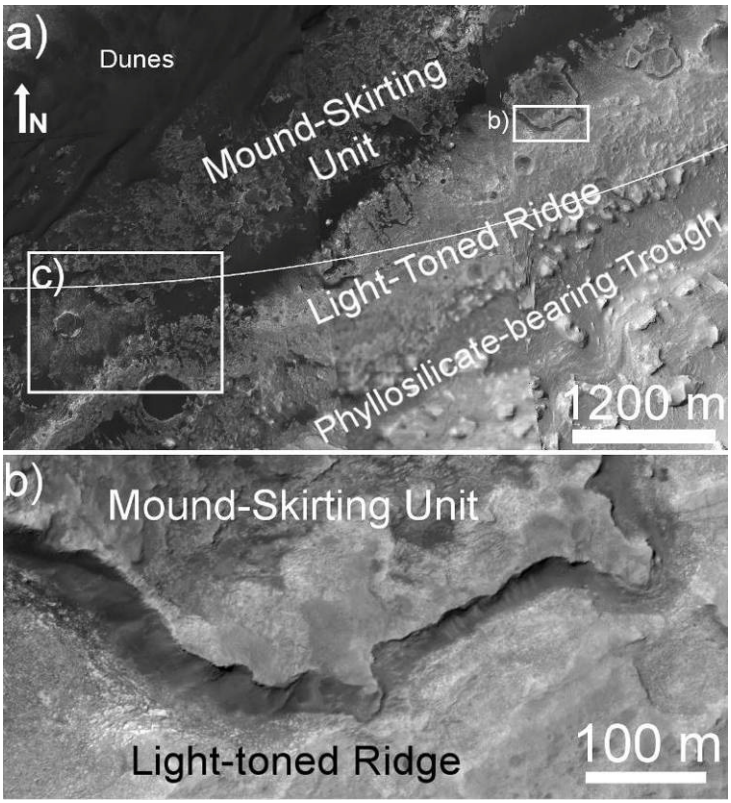

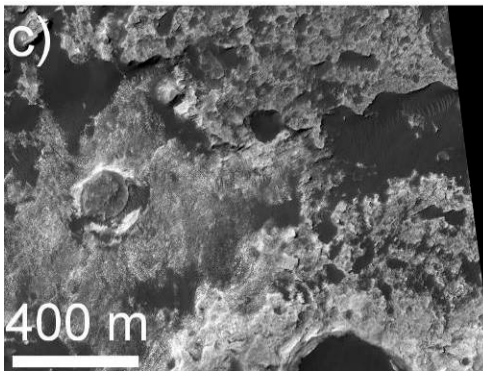

Figure 37. a) An overview of the light-toned ridge where it broadens. The curved line is the approximate edge of the MSL landing ellipse. **b)** Mesas of the mound-skirting unit appear to overlie the light-toned ridge unit in this location. **c)** However, in this location the mound-skirting unit and the light-toned ridge unit are less distinguishable. Refer to Tables 1 and 2 for CTX and HiRISE image IDs. Illumination is from the left. Location: 4.671° S 137.463°E (figure37.jpg)

compositional banding, which is seen in many flow features, including subaerial avalanches and debris flows, submarine debris flows, and glaciers (*e.g.*, Masson et al. 1993 and references therein). Compositional banding can be due to the initial stratigraphy of the source material or sorting during the slide event (Masson 1993). Although most subaerial debris flows and avalanches have simpler banding than the streamlined texture observed, pre-existing topography can induce more complex flow banding (Francis et al. 1985, Masson et al. 1993).

The faults observed in the streamline-textured surface are difficult to explain as part of the same mechanism that generated the texture. It is likely that they formed after the texture was emplaced, perhaps due to stresses exerted by burial of the lobate feature by the deposition of subsequent mound material.

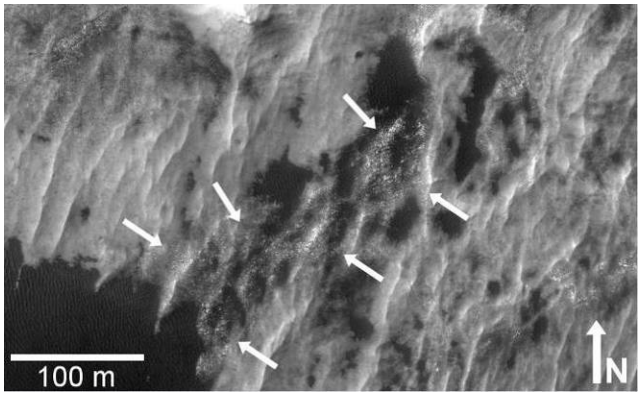

Figure 38. A typical portion of the phyllosilicate-bearing trough surface. The undulating ridges are similar to aeolian bedforms but in some locations, such as the area marked by arrows, they appear to be fractured. In addition, the dark material interacts with the ridges as if they are a hard surface, forming discrete small dunes. The phyllosilicate-bearing unit may be a soft rock that erodes to form this bedform-like morphology, or it may be lithified aeolian material. This figure is a subframe of HiRISE observation PSP_009294_1750. Illumination is from the left. Location: 4.716°S 137.411°E (figure38.jpg)

The lobate features are also morphologically consistent with volcanic lava or pyroclastic flows. However, there are no vents, cones, calderas, or other unambiguous evidence that the Gale Crater mound is a volcano. (Milliken et al. 2010) Therefore we do not favor a volcanic explanation for the lobate features.

There are three publicly released SHARAD radar profiles through the Gale Crater mound, one of which comes close to the lobate features. A full interpretation of the SHARAD data products, including a comparison with simulated off-nadir surface reflection ("clutter"; Cutigni et al. 2007) is beyond the scope of this paper. However, the available data products do not appear to show unambiguous evidence for sub-surface reflectors.

As mentioned above, the lobate features appear to have been buried, so it is unlikely that they would retain the banding due to ice-rich and ice-poor layers observed in radar profiles of terrestrial rock glaciers (Degenhardt and Giardino 2003). The evidence for burial also makes it unlikely that they are composed primarily of ice like the lobate debris aprons observed elsewhere on Mars (Holt et al. 2009).

Although both the landslide and rock glacier hypotheses have weaknesses, we interpret the lobate features to be related to a flow of some sort. HiRISE coverage of these features would be beneficial, and could test the compositional banding hypothesis by looking for a variation in texture and clast size in the streamline-textured feature.

Inferred stratigraphy of the Gale Crater mound and proposed MSL landing site

Based on the observations and interpretations described above, we have inferred the basic inter-unit relationships and stratigraphy of the Gale Crater landing site and the nearby mound, illustrated in the idealized cross-section in Figure 47.

The stratigraphically lowest mound units appear to be the basal units, although it is unclear whether the topographically lower dark-toned basal unit is a lower stratigraphic layer or has simply filled a depression in the light-toned basal unit. The thickness of the basal units is unknown. On the crater floor, a sharp cliff ~10 m high (Figure 39) marks the transition up from the basal units to the hummocky plains unit and the mound-skirting unit (Figure 34). The hummocky plains unit is an ancient eroded unit that varies from a mantled surface to bare, fractured rock. The high thermal inertia distal end of the fan-shaped deposit in the landing site overlies the hummocky plains and appears to be relatively thin (Figure 42). Above the high thermal inertia fan-shaped unit is the smoother, low thermal inertia surface of the fan. This thin, smooth upper layer, along with the upper layer of the high thermal inertia fan, appear to be eroding back to expose the surface of the high thermal inertia fan unit (Figure 43). Some outcrops of high thermal inertia fan material appear to be embayed by mound-skirting material (Figure 42), suggesting that although they are topographically higher than the mound skirting surface, they are part of the older fan units.

Mesas with a texture similar to the mound-skirting unit extend from the crater wall to the base of the mound (Figures 10, 12, 15, 16), overlying the fan and crater floor units. These mesas merge with the mound-skirting unit in some places, while in other places they form sharp boundaries despite a similar texture (Figure 16). In some cases the stratigraphic relationship between the mound-skirting unit and the hummocky plains unit is ambiguous, but generally the mound-skirting unit appears to overlie the hummocky plains.

At the foot of the mound, the basal unit merges in a series of poorly defined layers of fractured rock into the light toned ridge (Figure 36). Outcrops of the mound-skirting unit appear to overlie the lower layers of the light-toned ridge unit (Figure 37). On the southeast side, the ridge ends abruptly and drops down to a trough exposing a phyllosilicate-bearing surface which we interpret as the upper surface of a thin clay-bearing bedding plane. The dip of the bed and its thinness (Milliken et al. 2010) could explain why it is not seen on the northwest side of the light-toned ridge.

Above the phyllosilicate-bearing trough, the first mound layers appear to be similar to those that make up the light-toned ridge, based on their tone and fractured texture. The mound slopes up at an angle of ~12º onto the sulfate-bearing dark-toned layered yardang unit. The fan-shaped patch of the mound-skirting unit is stratigraphically above the light-toned ridge and a portion of the dark-toned layered yardang unit, suggesting that the mound-skirting

unit was deposited after these units. However, the fan appears to emerge from beneath a ridge of channel-filling material, constraining its time of deposition to before the channel in the dark-toned layered yardang unit was fully eroded and filled. Likewise, fan-shaped deposits of material emerging from canyons in the dark-toned layered yardang unit on the western mound extend onto the mound-skirting unit (Figure 11).

The layers of the upper mound unit were deposited unconformably on top of the dark-toned layered yardang-forming unit after it had been eroded, as indicated by the truncation of the large valley on the western mound by the upper mound layers (Figure 48). This unconformity represents an unknown amount of time, but could indicate that the upper mound unit is significantly younger than the lower mound and possibly Amazonian in age (Milliken et al. 2010).

In addition, the possibility that the upper mound material may be a lithified dune field is significant because a dune field would not be expected to form on top of a pre-existing mound. We therefore speculate that the early mound was buried after the initial erosion of the dark-toned layered yardang-forming material, allowing a dune field to form, become lithified, and erode back to the current mound.

The light-toned yardang unit also lies unconformably on top of the dark-toned layered yardangs, as indicated by a partially exhumed crater (Figure 26) (Malin and Edgett 2000). The mound surface immediately above the light-toned yardang-forming material is mostly obscured by aeolian bedforms but the light-toned yardang-forming

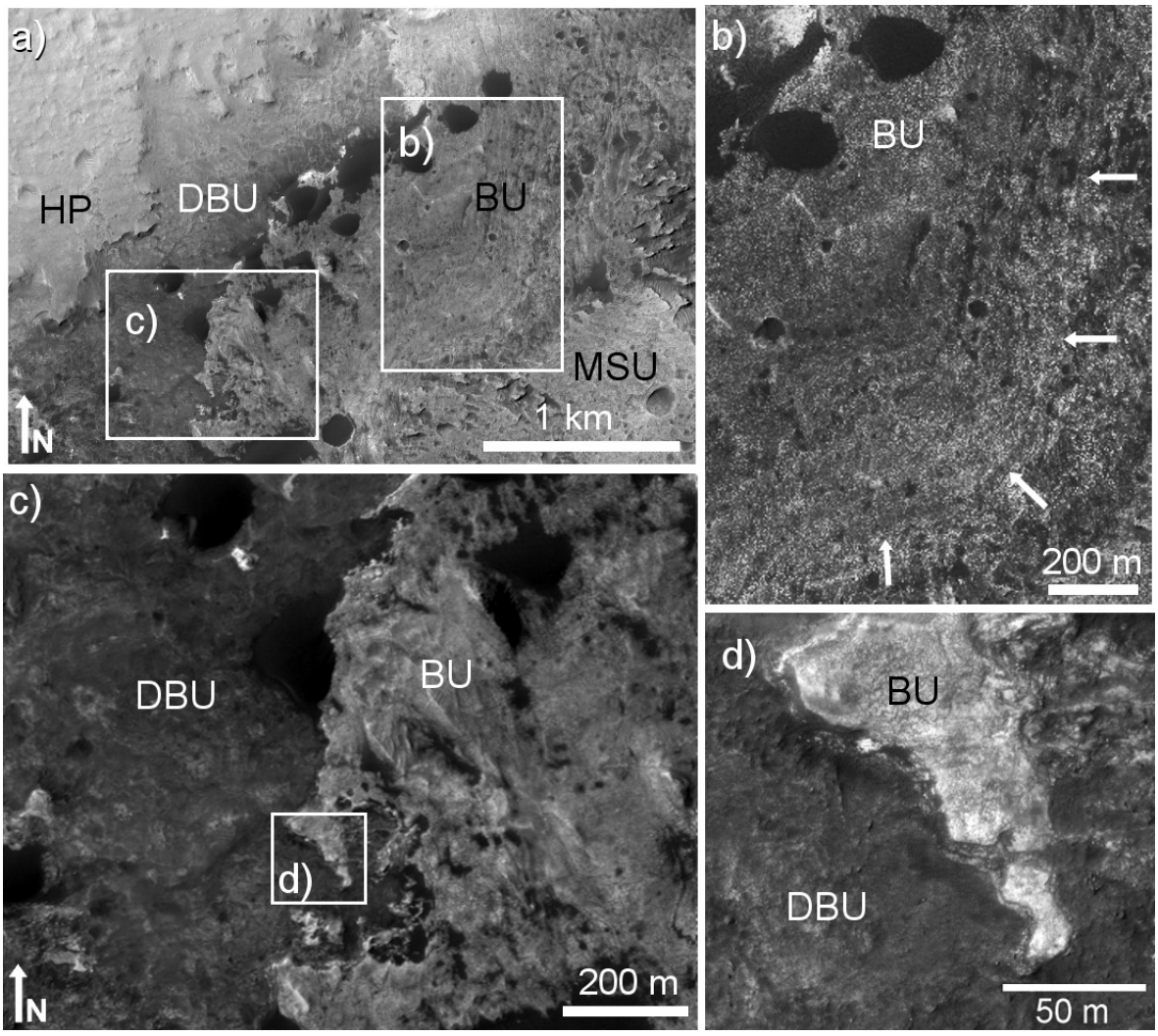

Figure 39. a) The dark-toned basal unit (DBU) is to the southwest of the light-toned basal unit (BU). Also visible is the mound-skirting unit (MSU) and the hummocky plains unit (HP). Very dark patches are small barchan dunes. **b)** The light-toned basal unit in this location exhibits a fabric that may be faint evidence of layering. The potential layers run perpendicular to the arrows. **c)** A closer view of the sharp transition between the light-toned and dark-toned basal units. d) A very close view of the transition. The light-toned basal unit appears to superpose the dark basal unit. HiRISE Image ID: PSP_001488_1750. Illumination is from the left. Location: 4.750°S 137.270°E (figure39.jpg)

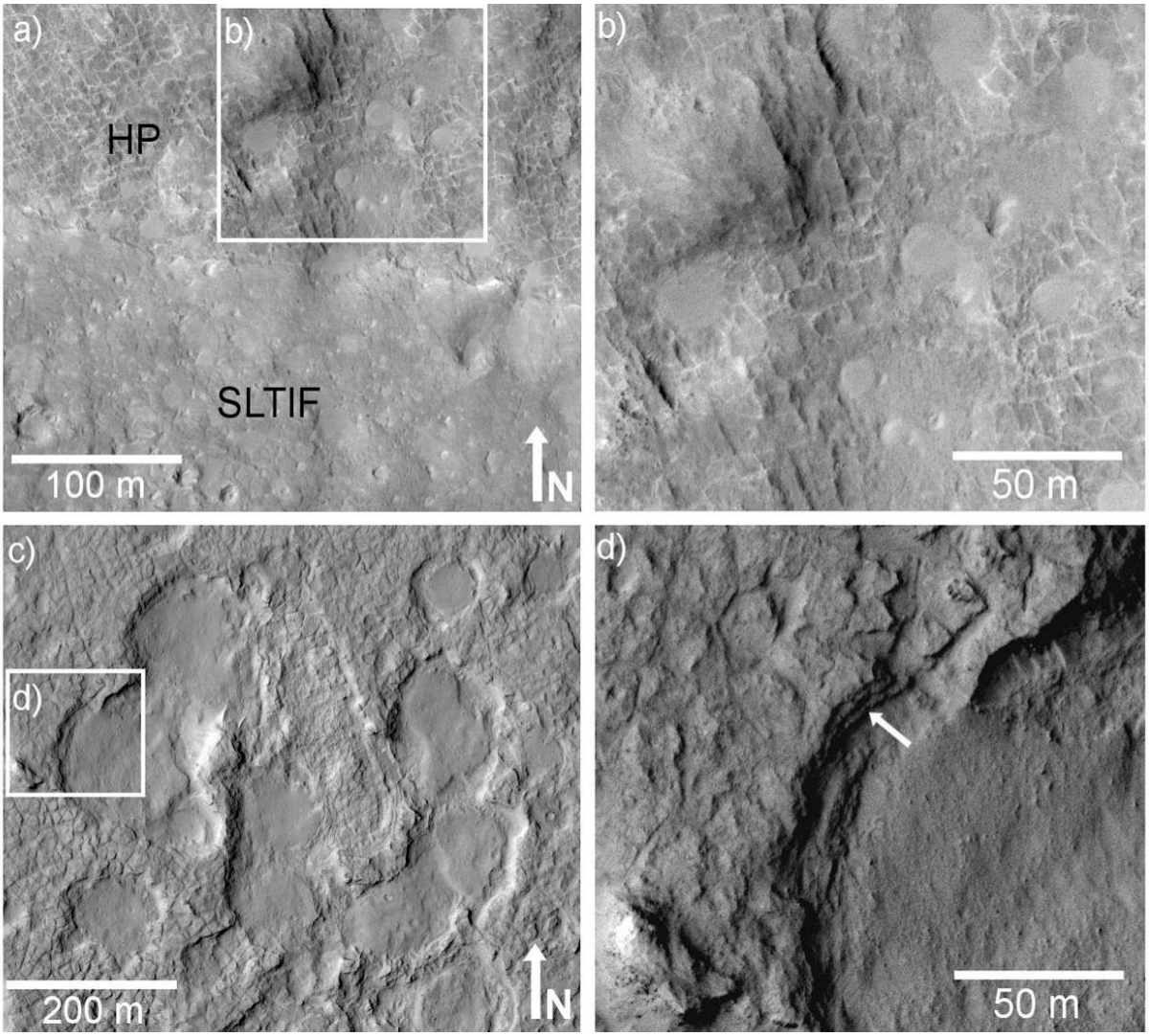

Figure 40. a) The northern boundary of the fan-shaped unit in the landing ellipse. The bottom half of this inset shows the "smooth low thermal inertia fan" (SLTIF) unit surface. This transitions sharply to hummocky plains (HP) showing light-toned polygonal features interpreted as fractures. **b)** A closer view of the hummocky plains unit, showing light-toned fractures similar to the erosion-resistant ridges on the mound. **c)** The distal end of the fan-shaped unit in the ellipse has a higher thermal inertia, consistent with its fractured, rocky appearance in this HiRISE image. Note the filled craters, some of which show layering in their walls, as indicated by the arrow in **d)**. **a)** and **b)** are subframes of HiRISE image PSP_009716_1755. **c)** and **d)** are subframes of HiRISE image PSP_010573_1755. Illumination is from the left. (figure40.jpg) Location: **a)** 4.417°S 137.296°E **c)** 4.535°S 137.438°E

material appears to be unconformable with and younger than the upper mound unit as well. The 12° tilt of the best-fit plane to the boundary of the light-toned yardang unit is similar to the average slope of the mound. This suggests that the light toned yardangs were deposited, presumably as part of a more extensive unit, after the rest of the mound, including the upper mound unit, had already been eroded to nearly its present state.

Patches of the thin mantle unit occur on the dark-toned layered yardang unit (Figure 27) and the upper mound layers, but not on the light-toned yardangs. In some locations (Figure 28) on the boundary of the light yardangs, it is unclear whether the thin mantle unit abuts the light yardang unit, or whether it emerges from beneath it. In other locations, the light-toned yardang unit is in direct contact with the surface of the dark layered yardang unit (Figure 26). This suggests that the thin mantle unit was already eroded away when the light-toned yardangs were deposited. Alternatively, the thin mantle unit may postdate the light-toned yardangs, but has been completely eroded off the soft light-toned yardang surface. The more erosion-resistant surface of the dark layered yardang unit might not undermine the thin mantle as rapidly, allowing it to persist.

Candidate rover traverses

In selecting a traverse for MSL at the Gale Crater landing site, an important consideration is what route to take to

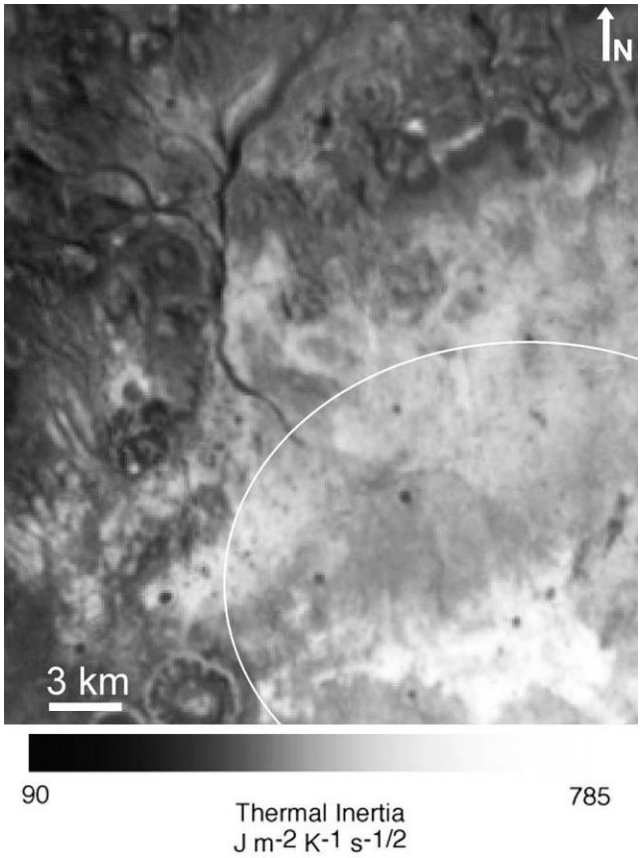

Figure 41. THEMIS thermal inertia map (Fergason *et al.* 2006) of the fan-shaped feature in the proposed MSL landing site. The branching valley that ends at the apex of the fan-shaped feature has a very low thermal inertia. The fan-shaped feature itself is divided into a proximal low thermal inertia portion and a distal high thermal inertia portion. (figure41.jpg)

the layered, hydrated-mineral-bearing mound, the primary target of a mission to Gale. The dark-toned dunes at the base of the mound might form a barrier to MSL, preventing a direct path to the mound from the center of the landing site. However, there are two locations near the landing ellipse that would allow MSL to access the mound without having to traverse the dunes, and we discuss a possible traverse for each of these (Figure 49, Table 6). We have chosen to end both traverses when they reach the light-toned yardang unit. If the rover reached that unit, it could continue climbing up similar slopes to the upper mound, or return to study other locations on the lower mound. We have also assumed that the rover would land precisely in the center of the ellipse. If MSL lands a significant distance from the center of the landing ellipse, that could factor heavily into which traverse it would follow to reach the mound.

The first possible traverse is similar to traverses previously proposed (Thomson et al. 2007). It would cover 29.4 km and begin (nominally) in the center of the landing ellipse on the fan-shaped unit and would bear toward the south-southwest. The initial portion of the traverse would allow investigation of the transition between the low- and high-thermal inertia portions of the fan-shaped deposit in the ellipse and the stratigraphy of the layers exposed in those units (Figure 49:A). The rover would then cross over onto patches of the mound-skirting unit and the hummocky plains unit (Figure 49:1B). Continuing to the southwest, the rover would leave the ellipse and reach the sharp transition between the mound-skirting unit and the basal unit near the location of numerous ridge-like mesas of the mound-skirting unit (Figures 34, 49:1C). MSL could test the hypothesis that these ridges are due to lithified bedforms or parallel joints by studying the texture, bedding, and composition of the rocks in these outcrops. The traverse would also pass near outliers of the dune field and MSL could observe the sand to determine its composition, physical properties, and activity, similar to the observations of the much smaller El Dorado ripple field by the Mars Exploration Rover Spirit. (Sullivan et al. 2008)

From this point, the rover would head south, across the surface of the basal unit and begin climbing the poorly defined layers leading up to the light-toned ridge unit. MSL would traverse through a gap between the southwest end of the light-toned ridge and the mound-skirting unit, and cross into the phyllosilicate-bearing trough (Figure 49:1D). Here the rover would be able to determine the precise mineralogy of the phyllosilicate unit, its phyllosilicate content, its depositional setting and weathering history, and its organic content.

After a full study of the phyllosilicate-bearing trough material, MSL could study the base of the fan-shaped outcrop, and then climb up its side to study the surface and determine whether it is indeed an outcrop of the mound-skirting unit. The rover would also analyze the ridge of channel-fill material on the fan (Figure 49:1E). This material might provide a sample from much higher on the mound, and therefore could be valuable in understanding units that the rover might never reach.

From the filled channel and outcrop, MSL would continue to climb, analyzing the layers of the mound as it drove (Figure 49:1F). At this point our proposed traverse differs slightly from previous traverses. The rover would turn to the southwest, away from the filled channel and climb up a set of layers of varying albedo to reach an expression of erosion-resistant ridges (Figure 49:1G). Here the rover could determine whether the ridges are indeed fractures made erosion-resistant by alteration or cementation, or whether they are due to igneous intrusion or other processes. Finally, the rover would turn to the southeast and continue to climb the mound, following the trough between two large yardangs and eventually reaching the light-toned yardang unit near the location (Figure 49:1C) of the partially exhumed crater shown in Figure 26.

Traverse 2 would cover 22.5 km and would begin by driving away from the center of the ellipse toward the southeast. In this direction, MSL would soon leave the fan-shaped unit and would cross onto the hummocky plains and mound-skirting units (Figure 49:2B). It would

Table 6. Summary of two potential traverses.

Traverse 1 = 29.4 km			Traverse 2 = 22.5 km		
Stop	Description	Rationale	Stop	Description	Rationale
1A	Transition between low- and high-thermal inertia fan-shaped unit	Search for conclusive evidence that this unit was an alluvial fan. Determine environmental conditions for deposition.	2A	Transition between low- and high- thermal inertia fan-shaped unit	Search for conclusive evidence that this unit was an alluvial fan. Determine environmental conditions for deposition.
1B	Edge of high-thermal inertia fan-shaped unit.	Investigate the transition to the hummocky plains and mound-skirting units. Determine nature of these units (composition, depositional setting, etc.).	2B	Edge of high-thermal inertia fan-shaped unit. Near inverted channels.	Investigate the transition to the hummocky plains and mound-skirting units. Determine nature of these units. *Optional: Traverse east to inverted channels. Search for biomarkers, evidence for duration of fluvial activity, etc.*
1C	Boundary between mound-skiting unit and basal unit. Near dark dunes.	Test lithified bedform and parallel joint hypotheses for mesas and ridges in skirting unit. Test mound origin hypotheses on basal unit (first mound unit encountered).	2C	Passage through sand dunes on mound-skirting unit.	Study dark dunes and mound skirting unit. Test lithified bedform and parallel joint hypotheses for the origin of ridges in the skirting unit.
1D	Phyllosilicate-bearing unit near fan-shaped unit.	Determine depositional setting for phyllosilicate-bearing and neighboring units. Begin assembling mound stratigraphy. Search for biomarkers in phyllosilicates.	2D	Edge of skirting unit, transition to basal unit.	Test mound-origin hypotheses on basal unit (first mound unit encountered).
1E	Channel fill atop fan-shaped unit.	Test hypothesis that fan-shaped unit is part of the mound-skirting unit. Analyze channel fill material and search for biomarkers.	2E	Mesas of mound-skirting unit on basal and light-toned ridge units	Test hypothesis that the light-toned ridge unit underlies the mesas in this location. Test origin of light-toned ridge.
1F	Fine layers and channel fill.	Continue to study mound stratigraphy. Test mound origin hypotheses. Search for biomarkers in sulfates.	2F	Phyllosilicate-bearing trough.	Determine depositional setting for phyllosilicates. Search for biomarkers in phyllosilicates. Begin to construct mound stratigraphy.
1G	Erosion-resistant ridges.	Test hypothesis that ridges are cemented fractures. Determine nature of putative cementing material and search for biomarkers.	2G	Dark-toned layered yardangs, partially mantled.	Continue to construct mound stratigraphy. Test mound origin hypotheses. Search for biomarkers in sulfates.
1H	Light-toned yardangs	Investigate contact between light-toned yardang unit and dark-toned layered yardangs. Determine nature of light-toned yardangs.	2H	Light-toned yardangs.	Investigate contact between light-toned yardang unit and dark-toned layered yardangs. Determine nature of light-toned yardangs.

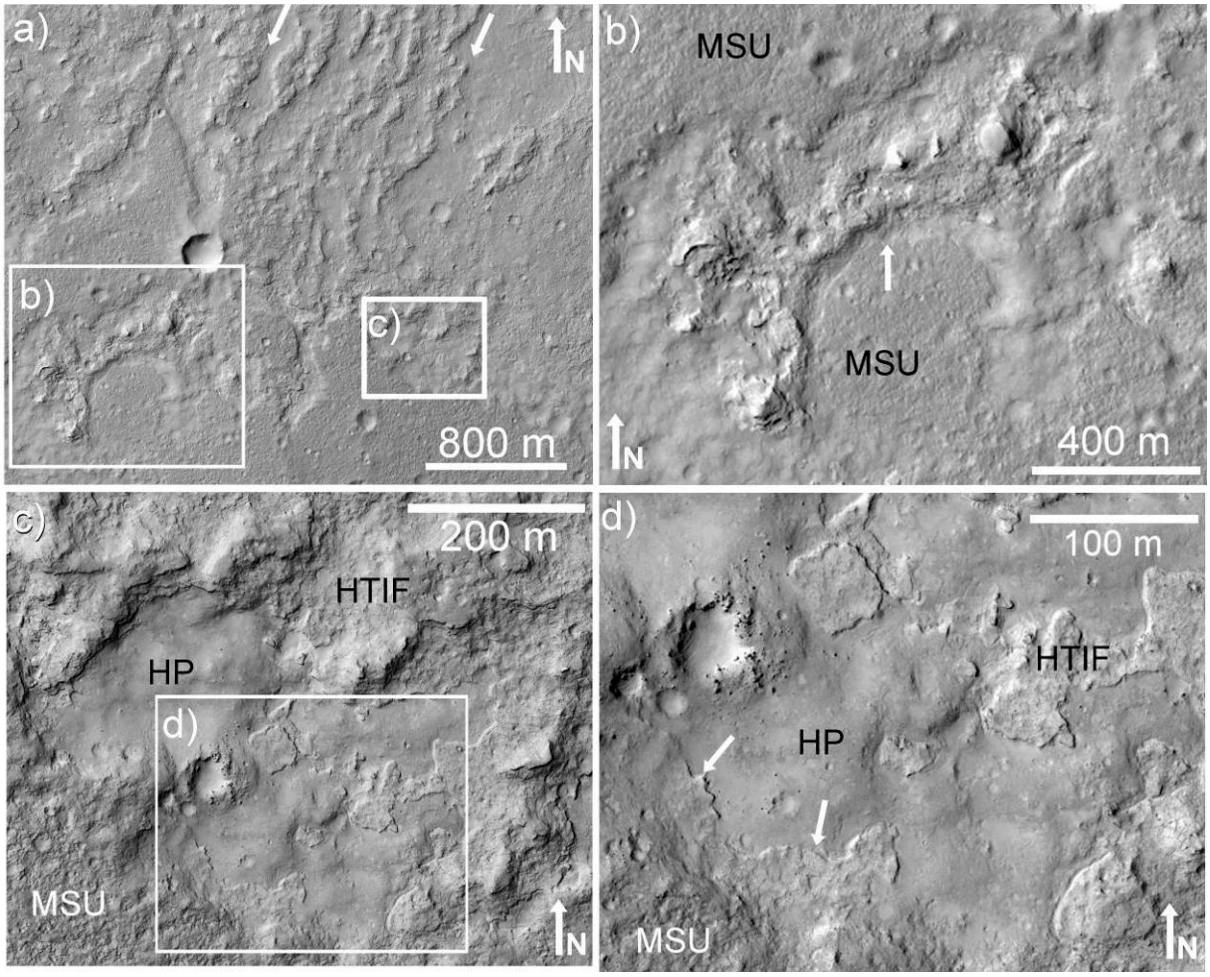

Figure 42. a) The western end of the landing site fan is characterized by numerous ridges of material roughly aligned with the direction of flow (indicated by arrows) on the fan. The mound-skirting unit (MSU) appears to embay outcrops of high thermal inertia fan and/or ridge material as shown by the arrow in **b)**. **c)** The boundary of the high thermal inertia fan (HTIF) is sometimes quite sharp. Here it drops down to a hummocky surface similar to the hummocky plains (HP; Figure 13). **d)** Arrows mark the edge of HTIF material emerging from beneath at the base of the MSU, implying that the MSU superposes the HTIF. This Figure shows subframes of HiRISE observation PSP_009716_1755 with illumination from the left. Location: 4.566° S 137.302°E (figure42.jpg)

then reach a more rugged, ridged portion of the mound-skirting unit and could continue toward the southeast while studying the unit and determining the origin of the ridges. There is a gap in the dune field on the ridged, mound-skirting unit (Figure 49:2C), and MSL would drive through this gap and then turn toward the southwest.

After crossing ~3.3 km of ridged, mound-skirting unit, MSL would arrive at the basal unit (Figure 49:2D). Continuing to the southwest, the rover could investigate one of the mesas of mound-skirting unit where it contacts the broadened light-toned ridge (Figure 49:2E), and then could proceed up the ridge itself. MSL would then descend onto the phyllosilicate-bearing trough and conduct a thorough analysis (Figure 49:2F). Continuing to the southwest, the traverse leads up onto the layers of the dark-toned layered yardang unit. In this area of the mound (Figure 49:2G), the thin mantle unit obscures many of the layers, but the numerous yardangs expose numerous outcrops for MSL to access so that it likely could still construct a stratigraphic column of the mound. The rover would work its way up the mound, eventually reaching the light-toned yardang unit (Figure 49:2H).

The initial leg of Traverse 2 comes close to some of the well-preserved inverted channel features in the ellipse (Figures 13, 14). Optionally, MSL could begin by traveling directly east, and studying one or several of these features before turning south to climb the layered mound. The proximity to these features is the primary advantage to Traverse 2. Disadvantages include the long traverse over the ridged mound-skirting unit and the mantled nature of the mound near the gap in the dunes. Traverse 2 is 22.5 km long and MSL would climb 1021 m during the traverse, crossing maximum slopes of about 10 degrees. In comparison, Traverse 1 is 29.4 km long and would climb 1155 m, crossing maximum slopes of about 15 degrees. The advantages of Traverse 1 are that it

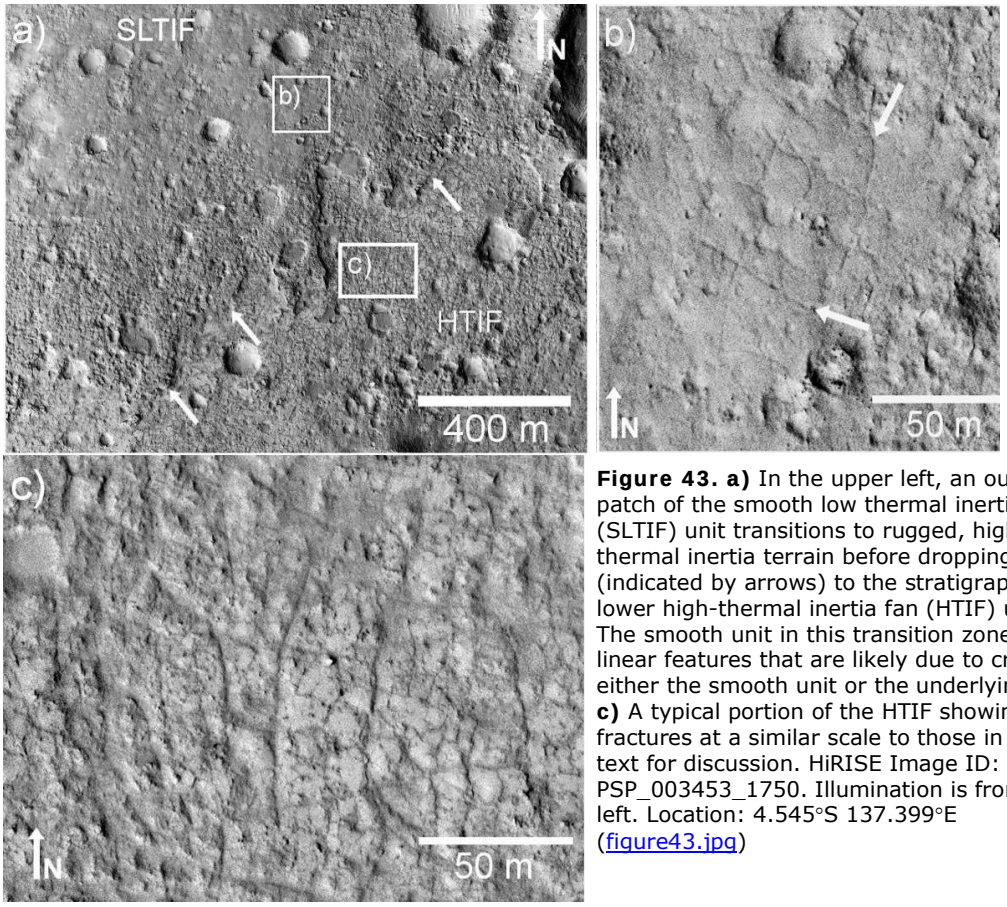

Figure 43. a) In the upper left, an outlying patch of the smooth low thermal inertia fan (SLTIF) unit transitions to rugged, high-thermal inertia terrain before dropping sharply (indicated by arrows) to the stratigraphically lower high-thermal inertia fan (HTIF) unit. **b)** The smooth unit in this transition zone shows linear features that are likely due to cracks in either the smooth unit or the underlying rock. **c)** A typical portion of the HTIF showing clear fractures at a similar scale to those in **b)**. See text for discussion. HiRISE Image ID: PSP_003453_1750. Illumination is from the left. Location: 4.545°S 137.399°E (figure43.jpg)

would climb a well-exposed, unmantled portion of the mound, and that therefore the stratigraphy and composition of the mound at that location have been well-studied (Figure 47; Edgett and Malin 2001; Milliken et al. 2009, Milliken et al. 2010).

Discussion and conclusions

Mound material origin hypotheses

There are several hypotheses for the origin of the layered material of the Gale Crater mound. The spring mound hypothesis advanced by Rossi et al. (2008) predicts rapid spatial facies variations in the mound's strata, evidence for draping or progradation, and structural control of deposition. The mound in Gale Crater does not show evidence of structural control or draping/progradation of the beds. The presence of uniform-thickness stratigraphic layers in the Gale Crater mound that are traceable for many kilometers (Figure 19) is inconsistent with the predicted rapid facies changes in a spring mound. Rossi et al. (2008) also claimed that craters with bulges lack evidence for a significant drainage basin associated with the crater. We have shown (Figure 7) that the rim of Gale Crater preserves numerous channels, inverted channels and fans that indicate that the crater was a drainage basin. Although the Gale crater mound does satisfy some of the other criteria listed by Rossi et al. (2008) for spring mounds (*e.g.*, sedimentary appearance, mound-like morphology, compositional variations correlated with stratigraphic variations) these criteria are not unique to spring mounds.

Scott et al. (1978), Greeley and Guest (1987), Scott and Chapman (1995), Malin and Edgett (2000) and Thomson et al. (2008) have suggested or discussed an aeolian origin for the material of the Gale mound. We observe textures on the upper mound unit that could be large-scale (hundreds of meters) crossbeds (Figure 30), similar to bedforms observed at White Sands National Monument on Earth (Figure 32). We interpret the observed textures as evidence that the upper mound has an aeolian origin. On Earth, crossbeds are often significantly smaller than those observed on the upper mound, so that the lack of crossbeds in HiRISE observations of the lower mound does not exclude an aeolian origin for these units. Although no crossbeds are observed in the lower mound units, the ridged morphology of portions of the mound-skirting unit and the dark-toned layered yardang unit may represent lithified aeolian bedforms.

A volcanic origin for the mound material has also been suggested (Scott et al. 1978; Greeley and Guest 1987; Scott and Chapman 1995). Lava flows produce strong, cliff-forming, boulder-shedding layers, but these properties do not uniquely identify a layer as a lava flow. Beds with this property are present in the Gale Crater mound (*e.g.*, Figure 21). The nearest obvious volcanic edifice to Gale Crater is Elysium Mons, ~1800 km north

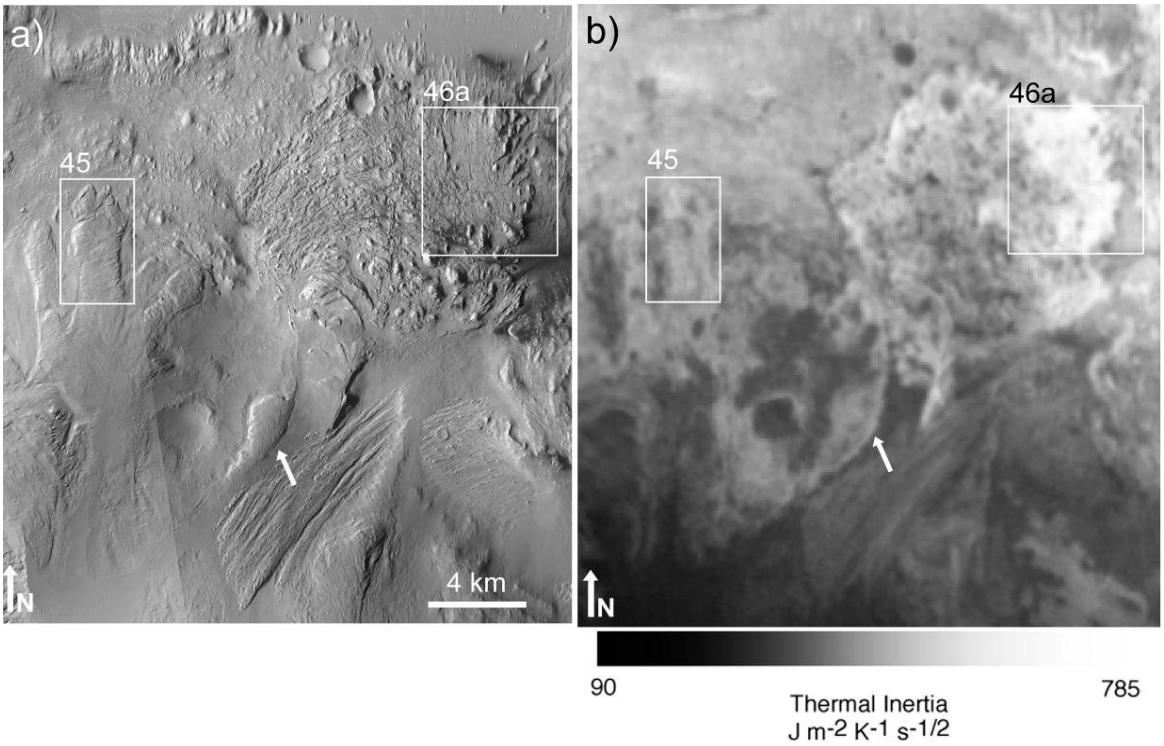

Figure 44. a) Overview of the northern flank of the Gale mound, showing the enigmatic lobate units. Illumination is from the left. Refer to Table 1 for CTX Image IDs. **b)** THEMIS thermal inertia map of the same area shown in **a)** (Fergason *et al.* 2006). Note the high thermal inertia of the northeastern portion of the fan-shaped lobate unit. Boxes provide context for Figures 45 & 46. The arrows mark the location where the "neck" of the unit appears to truncate a mesa of mound material. (figure44.jpg)

of Gale. Cratering counts of Elysium Planitia lavas have been used to infer a young age (<100 million years) (Hartmann and Neukum 2001) which would be incompatible with the likely Noachian/Early Hesperian age of the Gale Crater mound. We also find it unlikely that flows from an Elysium eruption could travel 1800 km south to Gale Crater. The presence of layers within the mound that do not form steep, boulder-shedding cliffs also implies that much of the mound is not composed of lava flows.

Pyroclastic deposits represent an alternative volcanic origin for the Gale Crater mound (Greeley and Guest 1987; Scott and Chapman 1995; Malin and Edgett 2000; Thomson et al. 2008). Hynek et al. (2003) have suggested that much of the light-toned layered material on Mars, including the MFF, is due to explosive volcanism, and Zimbelman et al. (2010) have mapped the Gale Crater mound as an outlying portion of the MFF. The yardang-forming morphology of the mound and the similarities between the pedestal crater outcrop west of the mound and those in the MFF, described by Kerber and Head (2010), suggest that the mound materials erode in a manner similar to the MFF. However, Malin and Edgett (2000) rule out a pyroclastic origin for much of the layered rock on Mars due to the rapid thinning of pyroclastic deposits with distance from the source and the lack of sources near observed layered sedimentary rock exposures. Wilson and Head (2007) have used models to show that explosive volcanism can produce "thick widespread deposits of ash and lapilli" on Mars and that small pyroclasts (~50 μm) can be transported ~10,000 km in the martian atmosphere. Wilson and Head (2007) also predict that fine-grained pyroclasts would "scavenge" water from eruption plumes and would therefore form fine-grained deposits containing ice and/or hydrated minerals and low-temperature alteration products. Wilson and Head (2009) calculate that on Mars a 1000 km^3 eruption would form ~1 m thick pyroclastic deposits at a distance of ~1000 km from the source. Multiple extremely large and/or nearby eruptions would therefore be required to create the Gale mound entirely from pyroclastic deposits. Due to the ~1800 km distance to the nearest obvious large volcano, it seems unlikely that pyroclastic deposits make up the bulk of the mound, though they are very likely to be present as thin beds.

Finally, Gale Crater has been suggested as the site of a former crater lake, and the mound has been suggested to comprise lacustrine or fluvial deposits (Greeley and Guest 1987; Scott and Chapman 1995; Cabrol et al. 1999; Malin and Edgett 2000). Lacustrine deposits are characterized by laterally continuous, finely-layered and highly variable bedding, confined to a closed basin (Malin and Edgett 2000; Grant et al. 2008). The layers of the Gale Crater mound fit this description. The presence of hydrated minerals on the Gale Crater mound (Milliken et al. 2009, Milliken et al. 2010) could indicate diagenesis of sedimentary material in an aqueous setting. However, it is not diagnostic of a lacustrine setting because the aqueous

minerals could also have formed elsewhere and been deposited in the crater. Thus, a lacustrine origin for the sedimentary rocks of Gale Crater cannot be ruled out based on our observations.

It would be naïve to suggest that a single process could adequately describe the entire stratigraphic column at Gale Crater. It is much more likely that the layers of the Gale Crater mound derive from a variety of sources and processes, preserving information about changing environments throughout the history of Mars.

MSL would be able to address the multiple remaining mound origin hypotheses, providing information that is unavailable from orbit. The detailed structure of the sedimentary rocks could be assessed by the cameras on the rover, revealing fine-scale layering, cross-bedding, and grain sizes. This information could immediately reveal the nature of the rocks of the Gale mound. More detailed study of the elemental, mineralogical and chemical composition would provide clues to the alteration history of Gale Crater, further constraining the depositional and post-depositional environments. The physical properties of the rocks and soils at the landing site could also be studied, as has been done with the Mars Exploration Rovers (Arvidson et al. 2004), based on the interaction between the rover and its surroundings (*e.g.*, tracks, trenching, drilling).

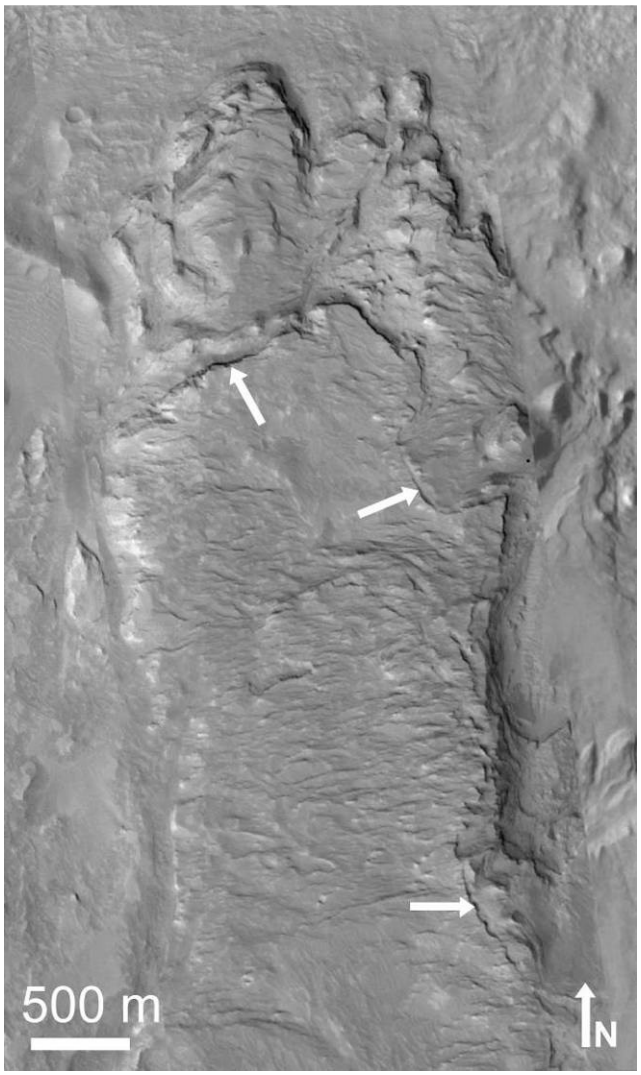

Figure 45. A closer MOC/CTX view of one of the uniform-width lobate units. Arrows mark the well-defined cliff-forming layer exposed at the edges of the unit. CTX Image ID: P01_001620_1749_XI_05S222W; MOC Image ID: M11/00989. Illumination is from the left. Location: 4.634°S 137.797°E (figure45.jpg)

Discussion of sediment transport

The height of the mound in Gale Crater, the laterally extensive nature of the exposed beds (Figure 19, Milliken et al. 2010), outcrops of layered material on the crater floor (Figure 24), and inverted channels (*e.g.*, Figure 13) all suggest that the Gale Crater mound material once filled the crater and has been significantly eroded. Furthermore, the canyons and channels carved into the surface of the mound suggest that the mound material had already been deposited and substantially eroded at a time when liquid water still flowed on the surface of Mars.

Malin and Edgett (2000) have argued that the burial and excavation of craters is common on Mars, citing other examples of large, partially exhumed craters. In the case of Gale Crater, the presence of apparent erosional unconformities in the mound suggests multiple episodes of erosion and deposition.

The excavation of Gale and other large craters requires the transport of tremendous quantities of material. As discussed by Malin and Edgett (2000), the transport pathways for this material are not fully known, but the lack of craters on many exposures of layered rock suggests some degree of ongoing erosion.

Valleys interpreted as fluvial channels are common on the crater walls. However, there do not appear to be any surface channels that lead out of the crater, therefore fluvial transport mechanisms are possible sources for the crater-filling material, but cannot directly explain the extensive exhumation. Likewise, mass wasting could partially explain the degradation of the crater rim and mound, but would result in debris collecting on the floor of the crater. Fluvial erosion and mass wasting could, however, have broken down crater-filling material until it was small enough for aeolian erosion and transport to occur.

Indeed, the only sediment transport process that appears plausible to explain the exhumation of Gale Crater is aeolian transport. This is consistent with numerous yardangs present on the mound, and ongoing or relatively recent aeolian erosion could explain the lack of numerous impact craters. To remove material from the crater entirely without breaching the crater rim, the material must be carried out of the crater in suspension. This implies that the material filling Gale and other similarly filled and exhumed craters either a) initially erodes into

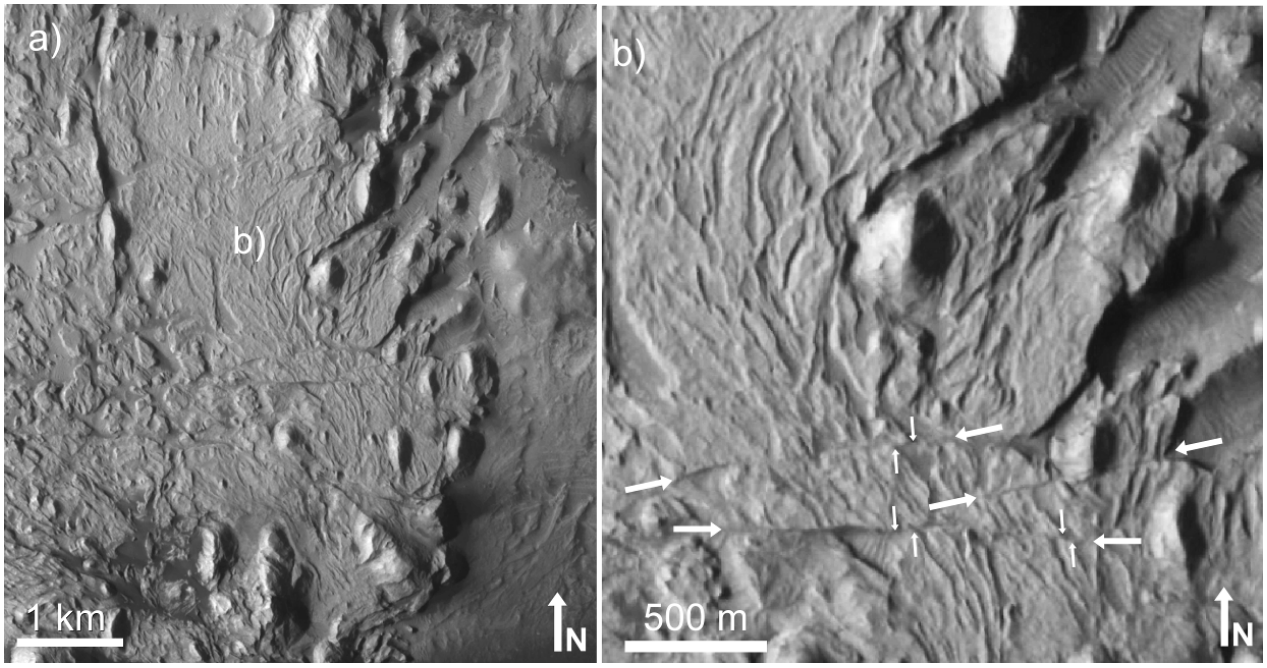

Figure 46. a) Closer view of the high thermal inertia portion of the fan-shaped lobate unit. **b)** Inset of a), showing the unusual streamlined texture of this portion of the fan-shaped lobate unit. Arrows mark the location of linear features that may be faults. Small vertical arrows mark examples of features that appear to be offset. CTX image ID: P04_002464_1746_XI_05S221W. Illumination is from the left. Location: 4.588°S 138.013°E (figure46.jpg)

particles small enough to be carried out of the crater in suspension, or b) that particles generated by erosion continue to break down until they are small enough to be carried away in suspension. The latter possibility is consistent with the elevated saltation velocities of sand grains on Mars (*e.g.*, Sagan 1977; Bridges et al. 2004) and the "Kamikaze" sand grain effect proposed by Sagan et al. (1977). In addition, other erosional processes such as fluvial erosion, could contribute to the breakdown of larger particles until they are susceptible to aeolian suspension.

Implications for MSL landing site selection

The selection of a landing site for MSL is driven by four primary criteria: diversity, context, habitability, and preservation potential (Grotzinger et al. 2009). As shown above, Gale Crater presents a location in which the rover could land and explore numerous distinct units distinguishable by their geomorphology, visible and infrared spectral characteristics, and thermal properties. The MSL payload could test hypotheses about each of the units discussed, as well as hypotheses regarding the relationship between units. The variety of units and the layering within the mound units suggests changing conditions at the time of deposition. This is shown most clearly by the detection of phyllosilicates and hydrated sulfates that correlate with the phyllosilicate-bearing trough and dark-toned layered yardang units, respectively.

Malin and Edgett (2000) have argued that the sedimentary rocks at Gale Crater can be placed into a global context, based on similarities between sedimentary deposits across the planet. Gale Crater is one of many large craters on Mars that shows evidence of filling and exhumation, and therefore discoveries made by MSL at Gale Crater could be extrapolated to global processes. In particular, determining the nature of the layered deposits and numerous units at Gale would allow inferences to be made for deposits elsewhere on Mars with similar properties.

If lacustrine deposits were confirmed, then sedimentary outcrops in craters of similar age could likewise be due to aqueous deposition. If a crater as deep as Gale Crater were shown to have never hosted a lake, this would have significant implications for the understanding of early Mars. If the Gale Crater layered rocks are primarily aeolian or volcaniclastic, that would confirm that those processes have been very important in shaping the martian surface. In addition, the presence of both sulfates and phyllosilicates exposed in the stratigraphic section at Gale Crater could provide insight into a key transition in the global weathering environment on Mars. (Milliken et al. 2010)

The MSL mission is focused on determining the habitability of Mars, and therefore the potential for preservation of chemical and geologic evidence for past habitability is paramount in the selection of a landing site. Habitability as currently understood (through terrestrial analogy) requires water, an energy source, and carbon (Grotzinger et al. 2009). Numerous fluvial channels and inverted channels provide the best evidence for aqueous activity at Gale. Some (but perhaps not all) fan-shaped units may also be associated with fluvial activity, as in the case of the large fan-shaped feature in the landing ellipse

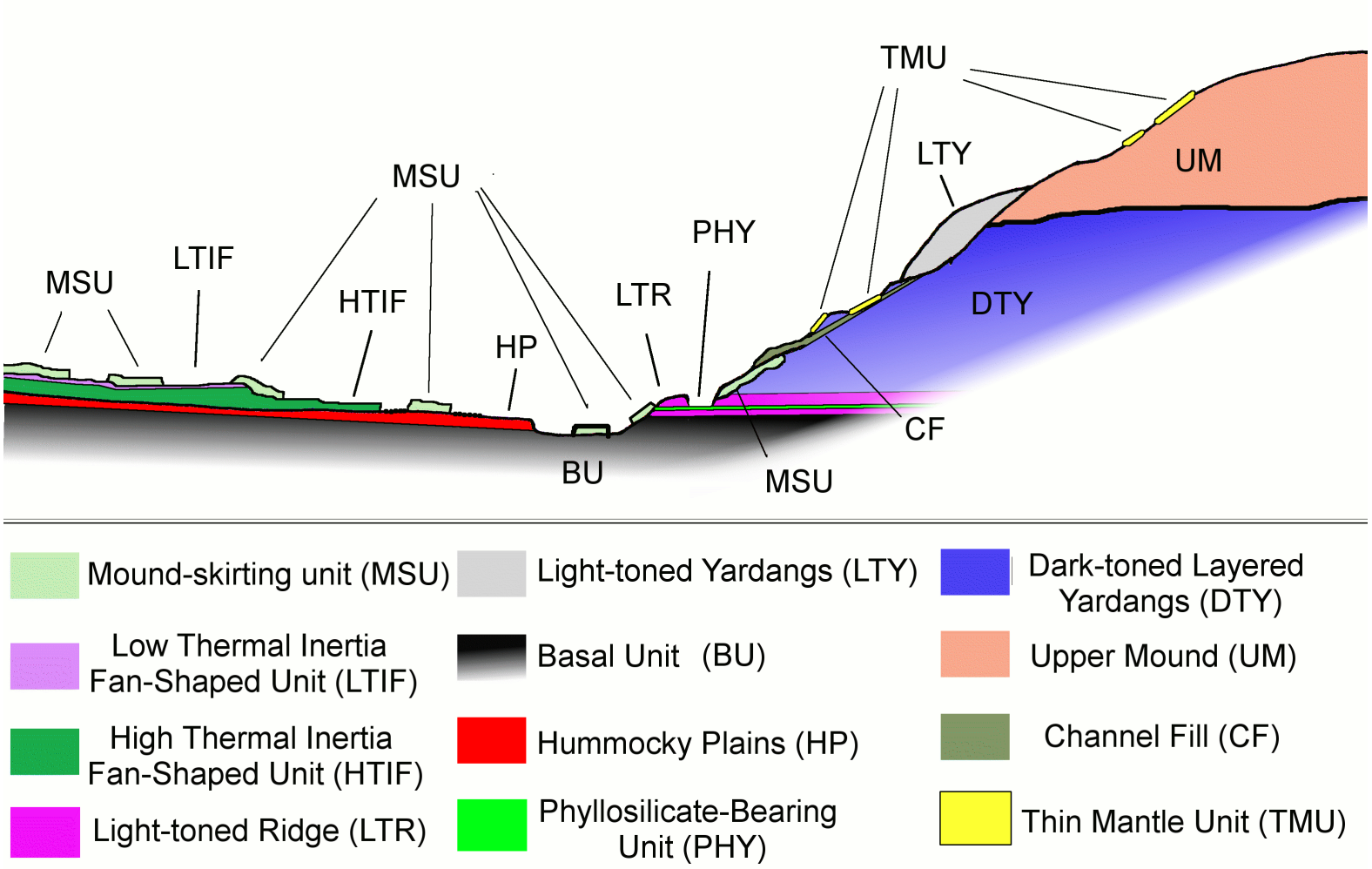

Figure 47. A cartoon of the inferred stratigraphy of the proposed Gale crater landing site and traverse region. This cartoon is not to scale, and is significantly simplified, but it does show the primary units discussed in the previous sections. (figure47.gif)

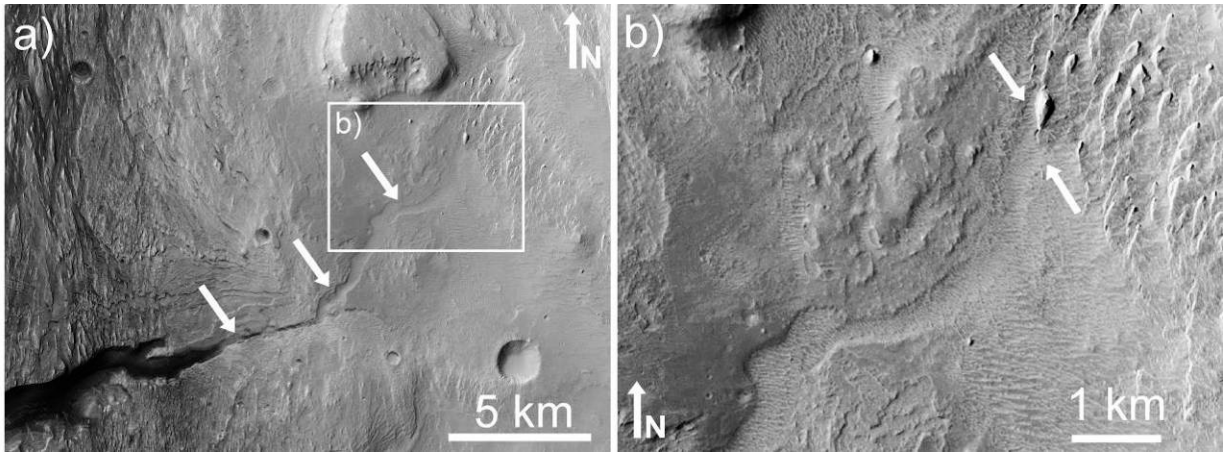

Figure 48. a) The largest canyon in the western mound becomes a shallower channel (marked by arrows) before disappearing beneath the layers of the upper mound, as shown in **b)**. An outcrop of upper mound material lies in the trough at the end of the channel, marking an unconformity between the surface into which the channel was carved and the overlying upper mound layers. Refer to Table 1 for CTX Image IDs. Illumination is from the left. (figure48.jpg)

that begins at the end of a branching channel. The presence of hydrated minerals on the mound, and particularly the detection of nontronite, which forms at a moderate pH, suggests a potentially habitable environment in which water was present (Milliken et al. 2009). Furthermore, if the layers of the mound are lacustrine in origin, they could represent the preserved remains of a once-habitable environment. Alternate origins (*e.g.*, aeolian, lava flow, pyroclastic) are less favorable for habitability, but the erosion-resistant ridges on the mound may indicate alteration and/or cementation of mound materials by water (Figure 22; Thomson and Bridges 2008), and therefore could be evidence of a habitable post-depositional environment.

Preservation of biological material in rocks depends on the deposition and subsequent history of those rocks. Based on studies of biomarker preservation on Earth, organic material is most likely to be concentrated in sediments deposited in aqueous environments and would likely be preserved in association with high surface-area minerals such as phyllosilicates (Bordovskiy 1965; Hedges et al. 1995; Summons 2008; Kennedy et al. 2002) Evaporites and silica deposits are also favorable for biomarker preservation and microfossil formation because organics can be entombed as minerals precipitate out of solution. (Summons 2008; Walter and Des Marais 1993; Martin 1999). The inverted channels on the crater floor preserve geomorphic evidence of liquid water, but may only be favorable for preservation in cases where the features suggest a low-energy depositional environment. If the layers of the Gale Crater mound are lacustrine sediments, then they would be favorable for preservation of organic biomarkers. An intermittent lake setting would also be favorable due to the formation of evaporite minerals, which can trap organic material due to rapid crystallization. An aeolian or volcanic origin for the layers would be less favorable, although post-depositional alteration could provide evidence of later habitability. The erosion-resistant ridges on the mound may represent a habitable environment, with preservation potential depending on the chemistry of the rocks and the fluid involved. Organic material can be preserved in contact with chemically reducing fluid, but if the rocks are composed of oxidized material or have oxidizing fluid flowing through them, then organics are unlikely to be preserved (Sumner 2004). Post-depositional contact with water can also contribute to biomarker degradation by facilitating aqueous chemical reactions, participating in hydrolysis reactions, and promoting microbial activity (Eglinton et al. 1991).

Smectite phyllosilicates are effective at preserving organic molecules due to their low permeability after deposition, their large surface area, and their ability to bind organics between the layers of the mineral structure (Sumner 2004; Kennedy et al. 2002). Therefore the detection of smectites at Gale (Milliken et al. 2009) is significant for biomarker preservation potential. Sulfate minerals have also been shown to preserve organic molecules such as amino acids (Aubrey et al. 2006). The presence of both sulfates and phyllosilicates at Gale Crater therefore provides multiple locations with biomarker preservation potential.

Gale Crater shows relatively few impact craters on its exposed surfaces, suggesting that the exposures of sedimentary material are relatively fresh. This is also a favorable characteristic for preserving evidence of habitability because exposure to radiation and oxidation can destroy biomarkers (Aubrey et al. 2006; Kminek 2003; Sumner 2004).

Conclusions

We used a variety of visible (CTX, HiRISE, MOC), infrared (THEMIS, CRISM, OMEGA) and topographic (MOLA, HRSC, CTX) datasets to conduct a study of Gale Crater, with a particular focus on the region

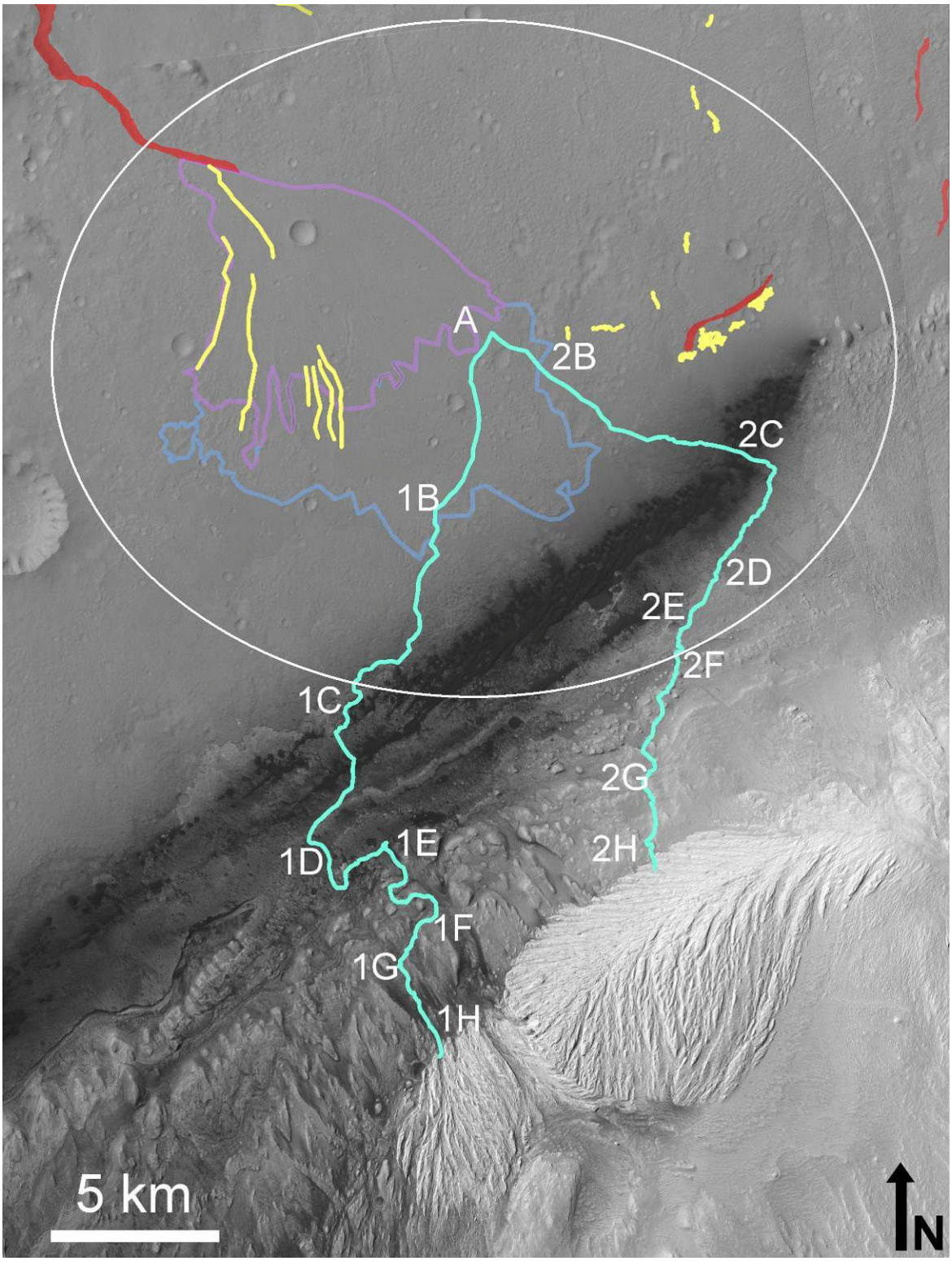

Figure 49. Two proposed MSL traverses, starting at the center of the landing ellipse and proceeding toward the two breaks in the line of dunes that provide access to the mound. See text for discussion. Refer to Table 1 for CTX image IDs. Illumination is from the left. (figure49.jpg)

surrounding the proposed MSL landing site. We found evidence of aqueous activity, including numerous fluvial channels and inverted fluvial channels, fan-shaped deposits, erosion-resistant fractures, and hydrated minerals. We have described the major geomorphic units in the proposed MSL landing site and on the western and northern mound and crater floor, and constructed a simplified stratigraphic section of the mound along the nominal MSL traverse (Figure 47). The high-elevation upper mound exhibits apparent large-scale cross-beds (Figure 30), suggesting an origin as aeolian dunes. At the lower elevations accessible to MSL, for example in the dark-toned layered yardang unit, the presence of layers traceable for tens of kilometers appears to preclude a spring mound origin, but an aeolian or lacustrine origin both remain as possible depositional processes. Pyroclastic materials are likely present in the mound, but probably do not represent the bulk of the material. Due to the great thickness of the stratigraphic column at Gale, it is likely that the mound formed through a combination of processes. Both aeolian and fluvial erosion appear to have played a role in exhuming the sedimentary layers of the Gale mound, but the only process that seems capable of explaining the transport of such a significant amount of material out of the crater without breaching the crater rim is aeolian suspension.

We identified two possible traverses from the center of the proposed MSL landing ellipse up onto the mound of layered sediments. The preferred traverse would access the mound in a well-exposed and therefore well-studied location. The alternate traverse comes closer to one or more of the inverted fluvial features within the ellipse before accessing the mound through a gap in the line of dunes at its base. It would climb a portion of the mound that is partially obscured by the thin mantle unit, but layered outcrops would still provide access to the stratigraphy.

Gale Crater's geomorphic diversity, thick stratigraphic sequence, similarity to other filled craters on Mars, and morphological and spectral evidence for an aqueous history make it a highly desirable landing site for MSL, and a target for substantial future orbital remote sensing studies.

Directory of supporting data

root directory
anderson_mars_2010_0004.pdf
- Fig. 1 figure1.jpg
- Fig. 2 figure2.jpg
- Fig. 3 figure3.jpg
- Fig. 4 figure4.jpg
- Fig. 5 figure5.jpg
- Fig. 6 figure6.jpg
- Fig. 7 figure7.jpg
- Fig. 8 figure8.jpg
- Fig. 9 figure9.jpg
- Fig. 10 figure10.jpg
- Fig. 11 figure11.jpg
- Fig. 12 figure12.jpg
- Fig. 13 figure13.jpg
- Fig. 14 figure14.jpg
- Fig. 15 figure15.jpg
- Fig. 16 figure16.jpg
- Fig. 17 figure17.jpg
- Fig. 18 figure18.jpg
- Fig. 19 figure19.jpg
- Fig. 20 figure20.jpg
- Fig. 21 figure21.jpg
- Fig. 22 figure22.jpg
- Fig. 23 figure23.jpg
- Fig. 24 figure24.jpg
- Fig. 25 figure25.jpg
- Fig. 26 figure26.jpg
- Fig. 27 figure27.jpg
- Fig. 28 figure28.jpg
- Fig. 29 figure29.jpg
- Fig. 30 figure30.jpg
- Fig. 31 figure31.jpg
- Fig. 32 figure32.jpg
- Fig. 33 figure33.jpg
- Fig. 34 figure34.jpg
- Fig. 35 figure35.gif
- Fig. 36 figure36.jpg
- Fig. 37 figure37.jpg
- Fig. 38 figure38.jpg
- Fig. 39 figure39.jpg
- Fig. 40 figure40.jpg
- Fig. 41 figure41.jpg
- Fig. 42 figure42.jpg
- Fig. 43 figure43.jpg
- Fig. 44 figure44.jpg
- Fig. 45 figure45.jpg
- Fig. 46 figure46.jpg
- Fig. 47 figure47.gif
- Fig. 48 figure48.jpg
- Fig. 49 figure49.jpg

Acknowledgements

We are indebted to our colleagues on the MSL Mastcam, MAHLI, and MARDI science team for stimulating discussions and insights about Gale Crater as a possible MSL landing site. We are also grateful to our many science and operations colleagues on the Mars Global Surveyor, Mars Odyssey, Mars Express, and Mars Reconnaissance Orbiter teams who have made remote sensing observations of Gale Crater rapidly available to the broader community as part of the MSL landing site selection process. We thank Larry Edwards for creating and providing the CTX DEM. We thank Ken Herkenhoff, Aileen Yingst and Ralph Milliken for useful comments on early drafts of this paper. We also thank Ken Edgett, Nathan Bridges and an anonymous reviewer for detailed reviews and helpful comments on the manuscript. This work was supported by NASA grants and contracts from the Mars Data Analysis Program and the Mars Science Laboratory Project.

References

Arvidson, R. E. et al. (2004) "Localization and physical properties experiments conducted by Spirit at Gusev Crater" Science 305, 821-824. doi:10.1126/science.1099922

Aubrey, A., H. J. Cleaves, J. H. Chalmers, A. M. Skelley, R. A. Mathies, F. J. Grunthaner, P. Erhenfreund and J. L. Bada (2006) "Sulfate minerals and organic compounds on Mars" Geology 34(5), 357-360. doi:10.1130/G22316.1

Bakalowicz, M. J., D. C. Ford, T. E. Miller, A. N. Palmer and M. V. Palmer (1987) "Thermal genesis of dissolution caves in the Black Hills, South Dakota" Geological Society of America Bulletin 99(6), 729-738. doi:10.1130/0016-7606(1987)99<729:TGODCI>2.0.CO;2

Bell III, J. F., K. S. Edgett, S. Rowland and M. C. Malin (2006) "The Gale Crater mound: A strong candidate landing site for the 2009 Mars Science Laboratory" First Mars Science Laboratory Landing Site Workshop, Pasadena.

Bibring, J.-P. et al. (2006) "Global mineralogical and aqueous Mars history derived from OMEGA/Mars Express data" Science 312, 400-404. doi:10.1126/science.1122659

Bibring, J.-P. et al. (2004) "OMEGA: Observatoire pour la Minéralogie, l'Eau, les Glaces et l'Activité" in Mars Express - The scientific payload (A. Wilson editor) 37–49, ESA Publications, Noordwijk.

Bordovskiy, O. K. (1965) "Accumulation of organic matter in bottom sediments" Marine Geology 3, 33-82. doi:10.1016/0025-3227(65)90004-6

Bridges, N. T. (2001) "Assessing layered materials in Gale Crater" First Landing Site Workshop for Mars Exploration Rovers, Abstract No. 9033, NASA Ames Research Center, Mountain View.

Bridges, N. T., J. E. Laity, R. Greeley, J. Phoreman and E. E. Eddlemon (2004) "Insights on rock abrasion and ventifact formation from laboratory and field analog studies with applications to Mars" Planetary and Space Science 52(1-3) special issue, 199-213. doi:10.1016/j.pss.2003.08.026

Bridges, N. T. (2006) "Studies of Martian sedimentological history through *in-situ* study of Gale and Oudemans Craters: Two landing site proposals for the Mars Science Laboratory" First Mars Science Laboratory Landing Site Workshop, Pasadena.

Bridges, N. T. et al. (2010) "Aeolian bedforms, yardangs, and indurated surfaces in the Tharsis Montes as seen by the HiRISE Camera: Evidence for dust aggregates" Icarus 205, 165-182. doi:10.1016/j.icarus.2009.05.017

Broxton, M. J. and L. J. Edwards (2008) "The Ames Stereo Pipeline: Automated 3D surface reconstruction from orbital imagery" Lunar and Planetary Science XXXIX, Abstract No. 2419, League City.

Cabrol, N. A., E. A. Grin, H. E. Newsom, R. Landheim and C. P. McKay (1999) "Hydrogeologic evolution of gale crater and its relevance to the exobiological exploration of Mars" Icarus 139, 235-245. doi:10.1006/icar.1999.6099

Christensen, P. R., N. S. Gorelick, G. L. Mehall and K. C. Murray (2006) THEMIS data collection. Planetary System node, Arizona State University.

Cutigni, M. et al. (2007) "Incoherent simulator for Mars surface applied to the analysis of SHARAD radar data" American Geophysical Union Fall Meeting, Abstract No. P11B-0546, San Francisco.

Degenhardt, J. J. and J. R. Giardino (2003) "Subsurface investigation of a rock glacier using ground-penetrating radar: Implications for locating stored water on Mars" Journal of Geophysical Research 108, 8036-8052. doi:10.1029/2002JE001888

Edgett, K. S. and P. R. Christensen (1994) "Mars aeolian sand: Regional variations among dark-hued crater floor features" Journal of Geophysical Research 99, 1997-2018. doi:10.1029/93JE03094

Edgett, K. S. and M. C. Malin (2001) "Rock stratigraphy in Gale Crater, Mars" Lunar and Planetary Science XXXII, Abstract No. 1005, Houston.

Edgett, K. S. (2005) "The sedimentary rocks of Sinus Meridiani: Five key observations from data acquired by the Mars Global Surveyor and Mars Odyssey orbiters" Mars 1, 5-58. doi:10.1555/mars.2005.0002

Edgett, K. S. and M. C. Malin (2005) "The sedimentary rocks of Mars: A global perspective" Geological Society of America Annual Meeting, Abstract No. 249-1, Salt Lake City.

Edgett, K. S. (2009) "MRO CTX and MGS MOC observations regarding small impact craters and substrate resistance to erosion on Mars" Bulletin of the American Astronomical Society 41(3).

Edwards, L. and M. Broxton (2006) "Automated 3D Surface Reconstruction from Orbital Imagery" AIAA, Space 2006, San Jose California, Sep. 19-21.

Eglinton, G., G. A. Logan, R. P. Ambler, J. J. Boon and W. R. K. Perizonius (1991) "Molecular Preservation" Philosophical Transactions: Biological Sciences 333(1268) 315-328.

Fergason, R. L., P. R. Christensen and H. H. Keiffer (2006) "High-resolution thermal inertia derived from the Thermal Emission Imaging System (THEMIS): Thermal model and applications" Journal of Geophysical Research 111, E12004. doi:10.1029/2006JE002735

Francis, P. W., M. Gardeweg, C. F. Ramirez and D. A. Rothery (1985) "Catastrophic debris avalanche deposit of Socompa volcano, northern Chile" Geology 13(9), 600-603. doi:10.1130/0091-7613(1985)13<600:CDADOS>2.0.CO;2

Garvin, J. B., S. E. H. Sakimoto and J. J. Frawley (2003) "Craters on Mars: Global Geometric Properties from Gridded MOLA Topography" Sixth International Conference on Mars, Abstract No. 3277, Pasadena.

Gillespie, A. R., A. B. Kahle and R. E. Walker (1986) "Color enhancement of highly correlated images. I. Decorrelation and HIS contrast stretches" Remote Sensing of Environment 20(3), 209-235. doi:10.1016/0034-4257(86)90044-1

Golombek, M. P. et al. (2003) "Selection of the Mars Exploration Rover landing sites" Journal of Geophysical Research 13, 8072. doi:10.1029/2003JE002074

Golombek, M., J. Grant, A. R. Vasavada, J. Grotzinger, M. Watkins, D. Kipp, E. Noe Dobrea, J. Griffes and T. Parker (2009) "Selection of four landing sites for the Mars Science Laboratory" Lunar and Planetary Science XL, Abstract No. 1404, The Woodlands.

Grant, J. A., R. P. Irwin III, J. P. Grotzinger, R. E. Milliken, L. L. Tornabene, A. S. McEwen, C. M. Weitz, S. W. Squyres, T. D. Glotch and B. J. Thomson (2008) "HiRISE imaging of impact megabreccia and sub-meter aqueous strata in Holden Crater, Mars" Geology 36, 195-198. doi:10.1130/G24340A.1

Greeley, R. and J. E. Guest (1987) "Geologic map of the eastern equatorial region of Mars" United States Geological Survey Miscellaneous Investigations Series, Map I-1802-B, scale 1:15,000,000.

Grotzinger, J. (2009) "Beyond water on Mars" Nature Geoscience 2(4) 231-233. doi:10.1038/ngeo480

Hamilton, V. E., M. M. Osterloo and B. S. McGrane (2007) "THEMIS decorrelation stretched infrared mosaics for compositional evaluation of candidate 2009 Mars Science Laboratory landing sites" Lunar and Planetary Science XXXVIII, Abstract No. 1725, League City.

Hartmann, W. K. and G. Neukum (2001) "Cratering chronology and the evolution of Mars" Space Science Reviews 96(1/4) 165-194. doi:10.1023/A:1011945222010

Hedges, J. and R. Keil (1995) "Sedimentary organic matter preservation: an assessment and speculative synthesis" Marine Chemistry 49(2-3), 81-115. doi:10.1016/0304-4203(95)00012-G

Holt, J. W. et al. (2008) "Radar sounding evidence for buried glaciers in the southern mid-latitudes of Mars" Science 322, 1235-1238. doi:10.1126/science.1164246

Hynek, B. M., R. J. Phillips, R. E. Arvidson (2003) "Explosive volcanism in the Tharsis region: Global evidence in the Martian geologic record" Journal of Geophysical Research 108, 5111-5126. doi:10.1029/2003JE002062

Kargel, J. S. and R. G. Strom (1992) "Ancient glaciation on Mars" Geology 20(1), 3.

Kennedy, M., D. R. Pevear and R. J. Hill (2002) "Mineral surface control of organic carbon in black shale" Science 295, 657-660. doi:10.1126/science.1066611

Kerber, L. and J. W. Head (2010) "The age of the Medusae Fossae Formation: Evidence of Hesperian emplacement from crater morphology, stratigraphy, and ancient lava contacts" Icarus 206, 669-684. doi:10.1016/j.icarus.2009.10.001

Kminek, G. (2003) "The effect of ionising radiation on amino acids and bacterial spores in different geo- and cosmochemical environments" Ph.D. Thesis, Scripps Institution of Oceanography, University of California, San Diego.

Maizels, J. (1990) "Raised channel systems as indicators of palaeohydrologic change: a case study from Oman" Palaeogeography, Palaeoclimatology, Palaeoecology 76(3-4), 241-277. doi:10.1016/0031-0182(90)90115-N

Malin, M. C. and K. S. Edgett (2000) "Sedimentary rocks of early Mars" Science 290, 1927-1937. doi:10.1126/science.290.5498.1927

Malin, M. C. and K. S. Edgett (2001) "Mars Global Surveyor Mars Orbiter Camera: Interplanetary cruise through primary mission" Journal of Geophysical Research 106, 23429-23570. doi:10.1029/2000JE001455

Malin, M. C. et al. (2007) "Context Camera investigation on board the Mars Reconnaissance Orbiter" Journal of Geophysical Research 112, E05S04 doi:10.1029/2006JE002808

Malin, M. C., K. S. Edgett, B. A. Cantor, M. A. Caplinger, G. E. Danielson, E. H. Jensen, M. A. Ravine, J. L. Sandoval and K. D. Supulver (2010) "An overview of the 1985-2006 Mars Orbiter Camera science investigation" Mars 5, 1-60. doi:10.1555/mars.2010.0001

Martin, H. and W. Whalley (1987) "Rock glaciers: Part 1: Rock glacier morphology: Classification and distribution" Progress in Physical Geography 11(2), 260-282. doi:10.1177/030913338701100205

Martin, R. (1999) Taphonomy: A process approach, Cambridge University Press, Cambridge.

Masson, D., Q. J. Huggett and D. Brundsen (1993) "The surface texture of the Saharan Debris Flow deposit and some speculations on submarine debris flow processes" Sedimentology 40(3) 583-598. doi:10.1111/j.1365-3091.1993.tb01351.x

McCauley, J. F. (1974) "White Rock: A Martian enigma" NASA Special Publication 329, 170–171.

McEwen, A. S. et al. (2007) "Mars Reconnaissance Orbiter's High Resolution Imaging Science Experiment (HiRISE)" Journal of Geophysical Research 112, E05S02. doi:10.1029/2005JE002605

Milliken, R. (2008) "THEMIS, TES and CRISM data of Gale" Third Mars Science Laboratory Landing Site Workshop, Monrovia.

Milliken, R. E., K. S. Edgett, G. Swayze, R. N. Clark, B. J. Thomson, R. Anderson and J. F. Bell III (2009) "Clay and sulfate-bearing rocks in a stratigraphic sequence in Gale Crater" Lunar and Planetary Science XL, Abstract No. 1479, Lunar and Planetary Institute, Houston.

Milliken, R. E., J. P. Grotzinger and B. J. Thomson (2010) "Paleoclimate of Mars as captured by the stratigraphic record in Gale Crater" Geophysical Research Letters 37, L04201. doi:10.1029/2009GL041870

Murchie, S. et al. (2007) "Compact Reconnaissance Imaging Spectrometer for Mars (CRISM) on Mars Reconnaissance Orbiter (MRO)" Journal of Geophysical Research 112, E05S03. doi:10.1029/2006JE002682

Neukum, G. and R. Jaumann (2004) "HRSC: the High Resolution Stereo Camera of Mars Express" in Mars Express - The scientific payload (A. Wilson editor) 17–35, ESA Publications, Noordwijk.

Neuendorf, K. K. E., J. P. Mehl Jr. and J. A. Jackson (2005) Glossary of Geology 5th Edition, American Geological Institute, Alexandria.

Okubo, C. H. and A. S. McEwen (2007) "Fracture-controlled paleo-fluid flow in Candor Chasma, Mars" Science 315, 983-985. doi:10.1126/science.1136855

Pain, C. F., J. D. A. Clarke and M. Thomas (2007) "Inversion of relief on Mars" Icarus 190(2), 478-491. doi:10.1016/j.icarus.2007.03.017

Pelkey, S. M. and B. M. Jakosky (2002) "Surficial geologic surveys of Gale Crater and Melas Chasma, Mars: Integration of remote-sensing data" Icarus 160, 228-257. doi:10.1006/icar.2002.6978

Pelkey, S. M., B. M. Jakosky and P. R. Christensen (2004) "Surficial properties in Gale Crater, Mars, from Mars Odyssey THEMIS data" Icarus 167, 244-270. doi:10.1016/j.icarus.2003.09.013

Pelkey, S. M. et al. (2007) "CRISM multispectral summary products: Parameterizing mineral diversity on Mars from reflectance" Journal of Geophysical Research 112, E08S14. doi:10.1029/2006JE002831

Pike, R. J. et al. (1980) "Gravity and target strength: controls on the morphologic transition from simple to complex impact craters" Reports of Planetary Geology Program 1980, 108-110.

Rogers, A. D. and J. L. Bandfield (2009) "Mineralogical characterization of Mars Science Laboratory candidate landing sites from THEMIS and TES data" Icarus 203(2), 437-453. doi:10.1016/j.icarus.2009.04.020

Rossi, A. P., G. Neukum, M. Pondrelli, S. van Gasselt, T. Zegers, E. Hauber, A. Chicarro and B. Foing (2008) "Large-scale spring deposits on Mars?" Journal of Geophysical Research 113, E08016. doi:10.1029/2007JE003062

Rubin, D. M. and C. L. Carter (2006) "Bedforms and Cross-Bedding in Animation" SEPM Atlas Series No. 2., United States Geological Survey, Santa Cruz.

Ruff, S. W. et al. (2001) "Mars' `White Rock' feature lacks evidence of an aqueous origin: Results from Mars Global Surveyor" Journal of Geophysical Research 106, 23921-23927. doi:10.1029/2000JE001329

Sagan, C., D. Pieri, P. Fox, R. E. Arvidson and E. A. Guinness (1977) "Particle motion on Mars inferred from the Viking lander cameras" Journal of Geophysical Research 82, 4430-4438. doi:10.1029/JS082i028p04430

Scott, D. H. and M. G. Chapman (1995) "Geologic and topographic maps of the Elysium paleolake basin, Mars" United States Geological Survey Series, Map I-2397, scale 1:5,000,000.

Scott, D. H., E. C. Morris and M. N. West (1978) "Geologic map of the Aeolis quadrangle of Mars" United States Geological Survey Miscellaneous Investigations Series, Map I-1111, scale 1:5,000,000.

Smith, D. E. et al. (1999) "The global topography of Mars and implications for surface evolution" Science 284, 1495-1503. doi:10.1126/science.284.5419.1495

Sullivan, R. et al. (2008) "Wind-driven particle mobility on Mars: Insights from Mars Exploration Rover observations at `El Dorado' and surroundings at Gusev Crater" Journal of Geophysical Research 113, E06S07. doi:10.1029/2008JE003101

Summons, R. (2008) "Preservation of organic biomarkers on Earth" Third Mars Science Laboratory Landing Site Workshop, Monrovia.

Sumner, D. Y. (2004) "Poor preservation potential of organics in Meridiani Planum hematite-bearing sedimentary rocks" Journal of Geophysical Research 109, E12007. doi:10.1029/2004JE002321

Thomson, B. and N. Bridges (2008) "Gale Crater: Context and layer diversity from HiRISE images" Third MSL Landing Site Workshop, Monrovia.

Thomson, B., N. Bridges, J. Bell, R. Milliken and W. Calvin (2007) "Gale Crater layered mound: A closed hydrologic system" Second Mars Science Laboratory Landing Site Workshop, Pasadena.

Thomson, B. J., N. T. Bridges, R. Milliken, J. F. Bell III, W. C. Calvin and C. M. Weitz (2008) "New constraints on the origin and evolution of the layered deposits in Gale Crater, Mars" Lunar and Planetary Science XXXIX, Abstract No. 1456.

Walter, M. R. and D. J. Des Marais (1993) "Preservation of biological information in thermal spring deposits: Developing a strategy for the search for fossil life on Mars" Icarus 101(1), 129-143. doi:10.1006/icar.1993.1011

Whalley, W. B. and F. Azizi (2003) "Rock glaciers and protalus landforms: Analogous forms and ice sources on Earth and Mars" Journal of Geophysical Research 108, 8032-8048. doi:10.1029/2002JE001864

Williams, R. M. E., R. P. Irwin III and J. R. Zimbelman (2009) "Evaluation of paleohydrologic models for terrestrial inverted channels: Implications for application to martian sinuous ridges" Geomorphology 107(3-4), 300-315. doi:10.1016/j.geomorph.2008.12.015

Wilson, L. and J. W. Head (2007) "Explosive volcanic eruptions on Mars: Tephra and accretionary lapilli formation, dispersal and recognition in the geologic record" Journal of Volcanology and Geothermal Research 163(1-4), 83-97. doi:10.1016/j.jvolgeores.2007.03.007

Wilson, L. and J. W. Head (2009) "Tephra deposition on glaciers and ice sheets on Mars: Influence on ice survival, debris content and flow behavior" Journal of Volcanology and Geothermal Research 185(4), 290–297. doi:10.1016/j.jvolgeores.2008.10.003

Zimbelman, J. R. (2010) "Geologic Mapping of the MC-23 NW quadrangle: Emplacement and erosion of the lower member of the Medusae Fossae Formation on Mars" Lunar and Planetary Science XLI, Abstract No. 1157, The Woodlands.

Zuber, M. T., D. E. Smith, S. C. Solomon, D. O. Muhleman, J. W. Head, J. B. Garvin, J. B. Abshire and J. L. Bufton (1992) "The Mars Observer laser altimeter investigation" Journal of Geophysical Research 97, 7781-7797. http://dx.doi.org/10.1029/92JE00341